

X-ray spectral variability of LINERs selected from the Palomar sample

Hernández-García, L.¹; González-Martín, O.^{2,3}; Masegosa, J.¹; Márquez, I.¹

¹ Instituto de Astrofísica de Andalucía, CSIC, Glorieta de la Astronomía, s/n, 18008 Granada, Spain
e-mail: lorena@iaa.es

² Instituto de Astrofísica de Canarias (IAC), C/ Vía Lactea, s/n, 38205 La Laguna, Tenerife, Spain

³ Departamento de Astrofísica, Universidad de La Laguna (ULL), 38205 La Laguna, Tenerife, Spain

Received XXXX; accepted YYYY

ABSTRACT

Context. Variability is a general property of active galactic nuclei (AGN). At X-rays, the way in which these changes occur is not yet clear. In the particular case of low ionisation nuclear emission line region (LINER) nuclei, variations on months/years timescales have been found for some objects, but the main driver of these changes is still an open question.

Aims. The main purpose of this work is to investigate the X-ray variability in LINERs, including the main driver of such variations, and to search for eventual differences between type 1 and 2 objects.

Methods. We use the 18 LINERs in the Palomar sample with data retrieved from *Chandra* and/or *XMM-Newton* archives corresponding to observations gathered at different epochs. All the spectra for the same object are simultaneously fitted in order to study long term variations. The nature of the variability patterns are studied allowing different parameters to vary during the spectral fit. Whenever possible, short term variations from the analysis of the light curves and UV variability are studied.

Results. Short term variations are not reported in X-rays. Three LINERs are classified as non-AGN candidates in X-rays, all of them being *Compton-thick* candidates; none of them show variations at these frequencies and two of them vary in the UV. Long term X-ray variations can be analysed in 12 out of 15 AGN candidates, about half of them showing variability (7 out of the 12). At UV frequencies, most of the AGN candidates with available data are variable (five out of six). Thus, 13 AGN candidates are analysed at UV and/or X-rays, ten of them variable at least in one energy band. None of the three objects that do not vary in X-rays have UV available data. Therefore, long timescale variability is very common in LINERs. The main driver of these X-ray variations is related to changes in the nuclear power, while changes in absorptions are found only for NGC 1052. We do not find any difference between type 1 and 2 LINERs, nor in the number of variable cases (three out of five type 1s and four out of seven type 2s) nor in the nature of the variability pattern. We find indications of an anticorrelation between the slope of the power law, Γ , and the Eddington ratio.

Conclusions.

Key words. Galaxies: active – X-rays: galaxies – Ultraviolet: galaxies

1. Introduction

Active galactic nuclei (AGN) are divided into two classes depending on the width of optical Balmer permitted spectral lines, which can be broad (type 1) or narrow (type 2). From the viewpoint of the unified model (UM) of AGN (Antonucci 1993; Urry & Padovani 1995), the difference between type 1 and 2 objects is due to orientation effects relative to the obscuring medium, where a direct view into the black hole (type 1) or a view through the absorbing material (type 2) give rise to a variety of subtypes between both classes. In the case of low luminosity nuclear emission line regions (LINER), it is tempting to view them as a scaled-down version of Seyfert galaxies. However, different physical properties (e.g., black hole masses or luminosities) have been inferred (Eracleous et al. 2010a; Masegosa et al. 2011), and the way to introduce them in the UM is still controversial (Ho 2008). Ho et al. (1997) optically classified a variety of LINERs as 1.9 or 2.0 types, while pure type 1 like Seyfert 1–1.5 objects have not been found.

X-ray data offer the most reliable probe of the high-energy spectrum, providing many AGN signatures (D’Onofrio et al. 2012). AGN are detected as a point-like source at hard X-rays. This method was applied for LINERs in a number

of publications (e.g., Satyapal et al. 2004, 2005; Dudik et al. 2005; Ho 2008). The most extensive work was carried out by González-Martín et al. (2009b). They analyzed 82 LINERs with *Chandra* and/or *XMM-Newton* data and found that 60% of the sample show a compact nuclear source in the 4.5–8 keV band; a multiwavelength analysis resulted in about 80% of the nuclei showing evidence of AGN-related properties. Moreover, their result is a low limit since *Compton-thick* (CT) objects (i.e., $N_H > 1.5 \times 10^{24} \text{cm}^{-2}$) were not taken into account.

Variability is one of the main properties characterizing AGN (Peterson 1997). In the case of LINERs, the first clear evidence showing variability was the work by Maoz et al. (2005) at UV frequencies. In X-rays, the study of variability can be accomplished by the comparison of spectra at different epochs, what can account for long term variations. This was done for LINERs by different authors. Pian et al. (2010) and Younes et al. (2011) showed that long term variability is common in type 1 LINERs. González-Martín et al. (2011a) studied a type 2 LINER also showing long term variations. In a previous paper, we studied long term spectral variability in six type 1 and 2 LINERs, where spectral and flux variations were found at long timescales in four objects (Hernández-García et al. 2013, hereinafter HG13).

Table 1: General properties of the sample galaxies.

Name	RA (J2000)	DEC (J2000)	Dist. ¹ (Mpc)	N_{Gal} (10^{20} cm^{-2})	m_B	Morph. Type	Optical class.	X-ray class.	Jet	Ref. ²
(1)	(2)	(3)	(4)	(5)	(6)	(7)	(8)	(9)	(10)	(11)
NGC 315	00 57 48.88	+00 21 08.8	59.60	5.88	12.20	E	L1.9	AGN	Y	(1)
NGC 1052	02 41 04.80	+08 15 20.8	19.48	3.07	11.44	E	L1.9	AGN	Y	(2)
NGC 1961	05 42 04.6	+69 22 42	56.20	8.28	11.01	SAB(rs)c	L2	AGN	Y	(3)
NGC 2681	08 53 32.73	+51 18 49.3	15.25	2.45	11.15	S0-a(s)	L1.9	AGN*	N	(1)
NGC 2787	09 19 18.56	+69 12 12.0	10.24	4.32	11.60	S0-a(sr)	L1.9	AGN	N	(1)
NGC 2841	09 22 02.63	+50 58 35.5	16.62	1.45	10.06	Sb(r)	L2	AGN	N	(1)
NGC 3226 ³	10 23 27.01	+19 53 54.7	29.84	2.14	12.34	E	L1.9	AGN	N	(1)
NGC 3608	11 16 58.96	+18 08 54.9	24.27	1.49	11.57	E	L2/S2:	Non-AGN*	N	(1)
NGC 3718	11 32 34.8	+53 04 05	17.00	1.08	11.19	SB(s)a	L1.9	AGN	Y	(1)
NGC 4261	12 19 23.22	+05 49 30.8	31.32	1.55	11.35	E	L2	AGN	Y	(4)
NGC 4278	12 20 06.83	+29 16 50.7	15.83	1.77	11.04	E	L1.9	AGN	Y	(5)
NGC 4374	12 25 03.74	+12 53 13.1	17.18	2.60	10.11	E	L2	AGN*	Y	(6)
NGC 4494	12 31 24.03	+25 46 29.9	13.84	1.52	10.68	E	L2::	AGN	N	(1)
NGC 4636	12 42 49.87	+02 41 16.0	16.24	1.81	10.43	E	L1.9	Non-AGN*	Y	(7)
NGC 4736	12 50 53.06	+41 07 13.6	5.02	1.44	8.71	Sab(r)	L2	AGN	N	(1)
NGC 5195	13 29 59.6	+47 15 58	7.91	1.56	10.38	IA	L2:	AGN	N	(8)
NGC 5813	15 01 11.26	+01 42 07.1	30.15	4.21	11.48	E	L2:	Non-AGN*	Y	(9)
NGC 5982	15 38 39.8	+59 21 21	41.22	1.82	12.05	E	L2::	AGN	N	(10)

(Col. 1) Name, (Col. 2) right ascension, (Col. 3) declination, (Col. 4) distance, (Col. 5) galactic absorption, (Col. 6) apparent magnitude in the Johnson filter B from Ho et al. (1997), (Col. 7) galaxy morphological type from González-Martín et al. (2009a), (Col. 8) optical classification from Ho et al. (1997), (Col. 9) X-ray classification from González-Martín et al. (2009b), where the * represent *Compton*-thick candidates from González-Martín et al. (2009a), (Col. 10) evidence of radio jet, and (Col. 11) references for radio data.

¹All distances are taken from NED and correspond to the average redshift-independent distance estimates. ²References: (1) Nagar et al. (2005); (2) Vermeulen et al. (2003); (3) Krips et al. (2007); (4) Birkinshaw & Davies (1985); (5) Giroletti et al. (2005); (6) Xu et al. (2000); (7) Giacintucci et al. (2011); (8) Ho & Ulvestad (2001); (9) Randall et al. (2011); (10) Vrtillek et al. (2013). ³We rejected the long term variability analysis (i.e., comparison of spectra at different epochs) of NGC 3226 because *XMM*-Newton data may be contaminated by emission from NGC 3227 (see HG13), whereas we have maintained the UV and short term analyses (i.e., light curves).

These spectral variations may be related to the soft excess, the absorber, and/or the nuclear power.

For one epoch observation, when high signal to noise data are available, short timescale variations can be investigated through the power spectral density (PSD) analysis of the light curve (Lawrence et al. 1987; González-Martín & Vaughan 2012). Using PSDs, González-Martín & Vaughan (2012) found that variable LINERs amount to 14%, in comparison to the 79% found for Seyfert galaxies.

On the other hand, the normalised excess variance, σ_{NXS}^2 , is the most straightforward method to search for short term variations (Nandra et al. 1997; Vaughan et al. 2003). This quantity can be understood as a proxy of the area below the PSD shape, and can be used to search for short term variations, with the advantage that high quality data are not required for its calculation. In HG13 we did not find short timescale variations in six LINERs.

The aim of this paper is to study the main driver of the X-ray variability in LINERs. We analyzed the X-ray variability in the largest sample of LINERs studied for this purpose. This paper is organized as follows: the sample and the data are presented in Sect. 2. The reduction of the data is explained in Sect. 3. A review of the methodology is described in Sect. 4, where individual and simultaneous spectral fittings, comparisons of different apertures, flux variability at X-ray and UV frequencies, and short term variability are explained. The results from this analysis are given in Sect. 5, which are discussed in Sect. 6. Finally, our main results are summarized in Sect. 7.

2. Sample and data

We used the Palomar Sample (Ho et al. 1997), which is the largest sample of nearby galaxies with optical spectra, containing HII nuclei, Seyferts, LINERs, and transition objects. It includes measurements of the spectroscopic parameters for 418 emission-line nuclei. Since we are interested in LINERs, objects classified as L1, L1:, L1::, L2, L2:, L2:: and L/S⁴ were taken into account. This sample contains 89 LINERs, 22 type 1 and 67 type 2. Note that along this paper, we divide the objects into two groups, type 1 (1.9) and type 2 (2.0), in accordance with the classification by Ho et al. (1997).

We made use of all the publicly available *XMM*-Newton and *Chandra* data up to October 2013. Initially, 63 objects had either *Chandra* or *XMM*-Newton observations by the date of the sample selection. LINERs with only one available observation were rejected from the sample (28 objects). Objects affected by a pileup fraction of 10% or more were excluded (four objects, and one observation of another object). The pileup fractions were estimated using the simulation software *PIMMS*⁵ version 4.6. We used the 0.5–2 keV and 2–10 keV fluxes, the best fit model, and the redshift to evaluate its importance. Only two objects in the final sample are affected by a pileup fraction of 6% (obsID. 2079 of NGC 4494, and obsID. 5908 of NGC 4374). As shown later in the results (see Sect. 5.1), this does not have consequences in the variability studies. To guarantee a proper spectral fitting, observations with less than 400 number counts were also excluded

⁴ Quality ratings as described by Ho et al. (1997) are given by “:” and “::” for uncertain and highly uncertain classification, respectively.

⁵ <http://heasarc.gsfc.nasa.gov/docs/software/tools/pimms.html>

(12 objects, and 18 observations). ObsID 011119010 and 13814 of NGC 4636 and NGC 5195, respectively, met these criteria but a visual inspection showed low number counts in the hard band and were rejected from the sample. Finally, NGC 4486 was rejected because it is well known that this source is dominated by the jet emission (Harris et al. 2003, 2006, 2009, 2011).

The final sample of LINERs contains 18 objects, eight type 1 and 10 type 2. Table 1 shows the general properties of the galaxies. This sample covers the same range in total apparent blue magnitudes than all LINERs in Ho et al. (1997) sample, with B_T from 8.7 to 12.3, included in Col. 6. The X-ray classification from González-Martín et al. (2009b) divides the objects into AGN candidates (when a point-like source is detected in the 4.5–8.0 keV energy band) and non-AGN candidates (otherwise). Evidence of jet structure at radio frequencies is provided in Col. 10. Table A.1 shows the log of the valid observations, where the observational identification (Col. 3), dates (Col. 4), extraction radius (Col. 5), and the net exposure time (Col. 6) are presented. Number of counts and hardness ratios, defined as $HR = (H-S)/(H+S)$ ⁶ are also included in Cols. 7 and 8, respectively. Finally, UV luminosities from the optical monitor (OM) and its corresponding filter are given in Cols. 9 and 10.

3. Data reduction

3.1. Chandra data

Chandra observations were obtained with the ACIS instrument (Garmire et al. 2003). The data reduction and analysis were carried out in a systematic, uniform way using CXC *Chandra* Interactive Analysis of Observations (CIAO⁷), version 4.3. Level 2 event data were extracted with the ACIS-PROCESS-EVENTS task. We first cleaned the data from background flares (i.e., periods of high background) using the LC_CLEAN_SL⁸ task, which removes periods of anomalously low (or high) count rates from light curves from source-free background regions of the CCD. This routine calculates a mean rate from which it deduces a minimum and maximum valid count rate, and creates a file with the periods that are considered by the algorithm to be good.

Nuclear spectra were extracted from a circular region centered on the positions given by NED⁹. These positions were visually inspected to make sure that the coordinates match the X-ray source position. We chose circular radii, aiming to include all possible photons, while excluding other sources or background effects. The radii are in the range between $r_{Chandra} = 1.5\text{--}5.0''$ (or 3–10 pixels, see Table A.1). The background selection was made taking circular regions between 5–10'' apertures free of sources in the same chip as the target and close to the source to minimize effects related to the spatial variations of the CCD response. We used the DMEXTRACT task to extract the spectra of the source and the background regions. The response matrix file (RMF) and ancillary reference file (ARF) were generated for each source region using the MKACISRMF and MKWARF tasks, respectively. The spectra were binned to have a minimum of 20 counts per spectral bin, to be able the use of the χ^2 -statistics, that was made with the GRPPHA task included in FTOOLS.

⁶ H is the number of counts in the hard (2–10 keV) band and S is the number of counts in the soft (0.5–2 keV) band

⁷ <http://cxc.harvard.edu/ciao4.4/>

⁸ http://cxc.harvard.edu/ciao/ahelp/lc_clean.html

⁹ <http://ned.ipac.caltech.edu/>

3.2. XMM–Newton data

All XMM–Newton observations were obtained from the EPIC pn camera (Strüder et al. 2001). The data were reduced in a systematic, uniform way using the Science Analysis Software (SAS¹⁰), version 11.0.0. Before extracting the spectra, good-time intervals were selected (i.e., flares were excluded). The method we used for this purpose maximizes the signal to noise ratio of the net source spectrum by applying a different constant count rate threshold on the single-events, $E > 10$ keV field-of-view background light curve. The nuclear positions were taken from NED and visually inspected to check that they match the X-ray nuclear positions. As a sanity check, the EREGIONANALYSE task was used to compare whether our visual selection deviates from this selection. This task was applied to three objects with low number counts in the sample (namely NGC 1961, NGC 3608, and NGC 5982) and relative differences $< 1\%$ were obtained. The extraction region was determined through circles of $r_{XMM} = 15\text{--}35''$ (i.e., 300–700 px) radius and the background has been determined with an algorithm that selects the best circular region around the source, that is free of other sources and as close as possible to the nucleus. This automatic selection was checked manually to ensure the best selection for the backgrounds.

We extracted the source and background regions with the EVSELECT task. RMFs were generated using the RMFGEN task, and the ARFs were generated using the ARFGEN task. We then grouped the spectra to obtain at least 20 counts per spectral bin using the GRPPHA task, as is required to use the χ^2 -statistics.

3.3. Light curves

Light curves in the 0.5–10 keV, 0.5–2.0 keV and 2.0–10.0 keV energy bands of the source and background were extracted using the DMEXTRACT and EVSELECT tasks for XMM–Newton and *Chandra*, respectively, with a 1000s bin. We studied only those light curves with exposure times longer than 30 ksec. For light curves with longer exposure times, we divided them in segments of 40 ksec. Thus, in some cases more than one segment are obtained from the same light curve. The light curve from the source was manually screened for high background and flaring activity, i.e., when the background light curve showed flare-like events and/or prominent decreasing/increasing trends. After this process the total useful observation time is usually lower, thus only light curves with more than a total of 30 ksec are used for the analysis. The light curves are shown in Appendix D, where the solid line represents the mean value of the count rate and the dashed lines represent 1σ standard deviation. Note that these values will not be used for the variability analysis, but for a visual inspection of the data.

4. Methodology

The methodology is explained in HG13, whereas it differs in the treatment of the short-term variability (see Sect. 4.4). For clarity, we recall the procedure in the following.

4.1. Individual spectral analysis

An individual spectral analysis allowed us to select the best fit model for each data set. We used XSPEC¹¹ version 12.7.0 to fit the data with five different models:

¹⁰ <http://xmm.esa.int/sas/>

¹¹ <http://heasarc.nasa.gov/xanadu/xspec/>

- ME : $e^{N_{Gal}\sigma(E)} \cdot e^{N_H\sigma(E(1+z))} [N_H] \cdot MEKAL[kT, Norm]$
- PL : $e^{N_{Gal}\sigma(E)} \cdot e^{N_H\sigma(E(1+z))} [N_H] \cdot Norm e^{-\Gamma} [\Gamma, Norm]$
- 2PL : $e^{N_{Gal}\sigma(E)} \left(e^{N_{H1}\sigma(E(1+z))} [N_{H1}] \cdot Norm_1 e^{-\Gamma} [\Gamma, Norm_1] + e^{N_{H2}\sigma(E(1+z))} [N_{H2}] \cdot Norm_2 e^{-\Gamma} [\Gamma, Norm_2] \right)$
- MEPL : $e^{N_{Gal}\sigma(E)} \left(e^{N_{H1}\sigma(E(1+z))} [N_{H1}] \cdot MEKAL[kT, Norm_1] + e^{N_{H2}\sigma(E(1+z))} [N_{H2}] \cdot Norm_2 e^{-\Gamma} [\Gamma, Norm_2] \right)$
- ME2PL : $e^{N_{Gal}\sigma(E)} \left(e^{N_{H1}\sigma(E(1+z))} [N_{H1}] \cdot Norm_1 e^{-\Gamma} [\Gamma, Norm_1] + MEKAL[kT] + e^{N_{H2}\sigma(E(1+z))} [N_{H2}] \cdot Norm_2 e^{-\Gamma} [\Gamma, Norm_2] \right)$

where $\sigma(E)$ is the photo-electric cross-section, z is the redshift, and $Norm_i$ are the normalizations of the power law or the thermal component (i.e., $Norm_1$ and $Norm_2$). For each model, the parameters varying are written in brackets. The Galactic absorption, N_{Gal} , is included in each model and fixed to the predicted value (Col. 5 in Table 1) using the `NH` tool within `FROOTS` (Dickey & Lockman 1990; Kalberla et al. 2005).

The $\chi^2/d.o.f$ and F-test were used to select the simplest model which better represents the data.

4.2. Simultaneous spectral analysis

We simultaneously fitted the spectra for each object with the same model. The baseline model was obtained from the individual fittings. For each galaxy, the initial values for the parameters were set to those obtained for the spectrum with the largest number counts.

The simultaneous fit was done in three steps:

0. SMF0 (Simultaneous fit 0) : The same model was used with all parameters linked to the same value to fit every spectra of the same object, i.e., the non-variable case.
1. SMF1 : Using SMF0 as the baseline for this step, we let the parameters N_{H1} , N_{H2} , Γ , $Norm_1$, $Norm_2$, and kT vary individually. The best fit was selected for χ_r^2 closest to unity that improved SMF0 (using the F-test).
2. SMF2 : Using SMF1 as the baseline for this step (in case SMF1 did not fit the data well), we let two parameters vary, the one that varied in SMF1 along with any of the other parameters of the fit. χ_r^2 and F-test were again used to confirm an improvement of the fit.

Whenever possible, this method was applied to the data coming from the two instruments separately. When data from *Chandra* and *XMM-Newton* were used together, an additional analysis was performed to make sure the sources included in the larger aperture did not produce the observed variability. A spectrum of an annular region was then extracted from *Chandra* data, with $r_{ext} = r_{XMM}$ and $r_{int} = r_{Chandra}$. We recall that the PSF of *Chandra* is energy dependent and therefore the annular region might be affected by contamination from the source photons at high energies. We have estimate this contribution by simulating the PSF of the sources in our sample using `ChaRT`¹² and `MARX`¹³. A monochromatic energy of 8 keV was used and the ray density was obtained for each observation individually. We find that the highest contribution from the source photons at 8 keV is 7%. Note that this contribution is at high energies (i.e., the contribution is lower at lower energies) and does not affect our

results (see Sect. 5.1). The data used for comparisons are marked with c in Table A.1. When the contamination by the annular region to the *Chandra* data with the r_{XMM} aperture emission was higher than 50% in the 0.5-10.0 keV energy band, we did not consider the joint analysis since the accuracy of the derived parameters could be seriously affected. For lower contamination levels, we considered that *Chandra* data can be used to estimate the contribution of the annular region to the *XMM-Newton* spectrum. The ring from *Chandra* data was fitted with the five models explained above. The resulting model was incorporated (with its parameters frozen) in the fit of the *XMM-Newton* nuclear spectrum, so we were able to extract the parameters of the nuclear emission. When multiple observations of the same object and instrument were available, we compared the data with similar dates (see Table A.1).

4.3. Flux variability

X-ray luminosities for the individual and simultaneous fits were computed using `XSPEC` for the soft and hard bands. Distances were taken from NED and correspond to the average redshift-independent distance estimate for each object when available (or to the redshift estimated distance otherwise) and are listed in Table 1.

UV luminosities were obtained (when available) from the optical monitor (OM) onboard *XMM-Newton* simultaneously to X-ray data. Whenever possible, measurements from different filters were retrieved. We recall that UVW2 is centered at 1894 Å (1805-2454) Å, UVM2 at 2205 Å (1970-2675) Å, and UVW1 at 2675 Å (2410-3565) Å. In the case of NGC 4736 we used data from the U filter (centered at 3275 Å (3030-3890) Å) because measures from other filters were not available. We used the OM observation FITS source lists (OBSMLI)¹⁴ to obtain the photometry. When OM data were not available, we searched for UV information in the literature. It is worth to notice that in this case the X-ray and UV data might not be simultaneous (see Appendix B).

We assumed an object to be variable when:

$$L_{max} - L_{min} > 3 \times \sqrt{(errL_{max})^2 + (errL_{min})^2} \quad (1)$$

where L_{max} and L_{min} are the maximum and minimum luminosities of an object and $errL_{max}$ and $errL_{min}$ the errors of the measurements. We notice that this relation is used to determine if an object is variable, and not as an error estimation.

4.4. Short timescale variability

Assuming a constant count rate for the whole observation in the 0.5–10 keV energy band, we calculated $\chi^2/d.o.f$ as a proxy to the variations. We considered the source to be variable if the count rate differed from the average above 3σ (or 99.7% probability).

To compare the variability amplitude of the light curves between observations, we calculated the normalized excess variance, σ_{NXS}^2 , for each light curve segment with 30-40 ksec. This magnitude is related to the area below the power spectral density (PSD) shape. We followed the prescriptions given by Vaughan et al. (2003) to estimate σ_{NXS}^2 and its error, $err(\sigma_{NXS}^2)$ (see also González-Martín et al. 2011b):

$$\sigma_{NXS}^2 = \frac{S^2 - \langle \sigma_{err}^2 \rangle}{\langle x \rangle^2} \quad (2)$$

¹² <http://cxc.harvard.edu/chart/>

¹³ <http://space.mit.edu/ASC/MARX/>

¹⁴ <ftp://xmm2.esac.esa.int/pub/odf/data/docs/XMM-SOC-GEN-ICD-0024.pdf>

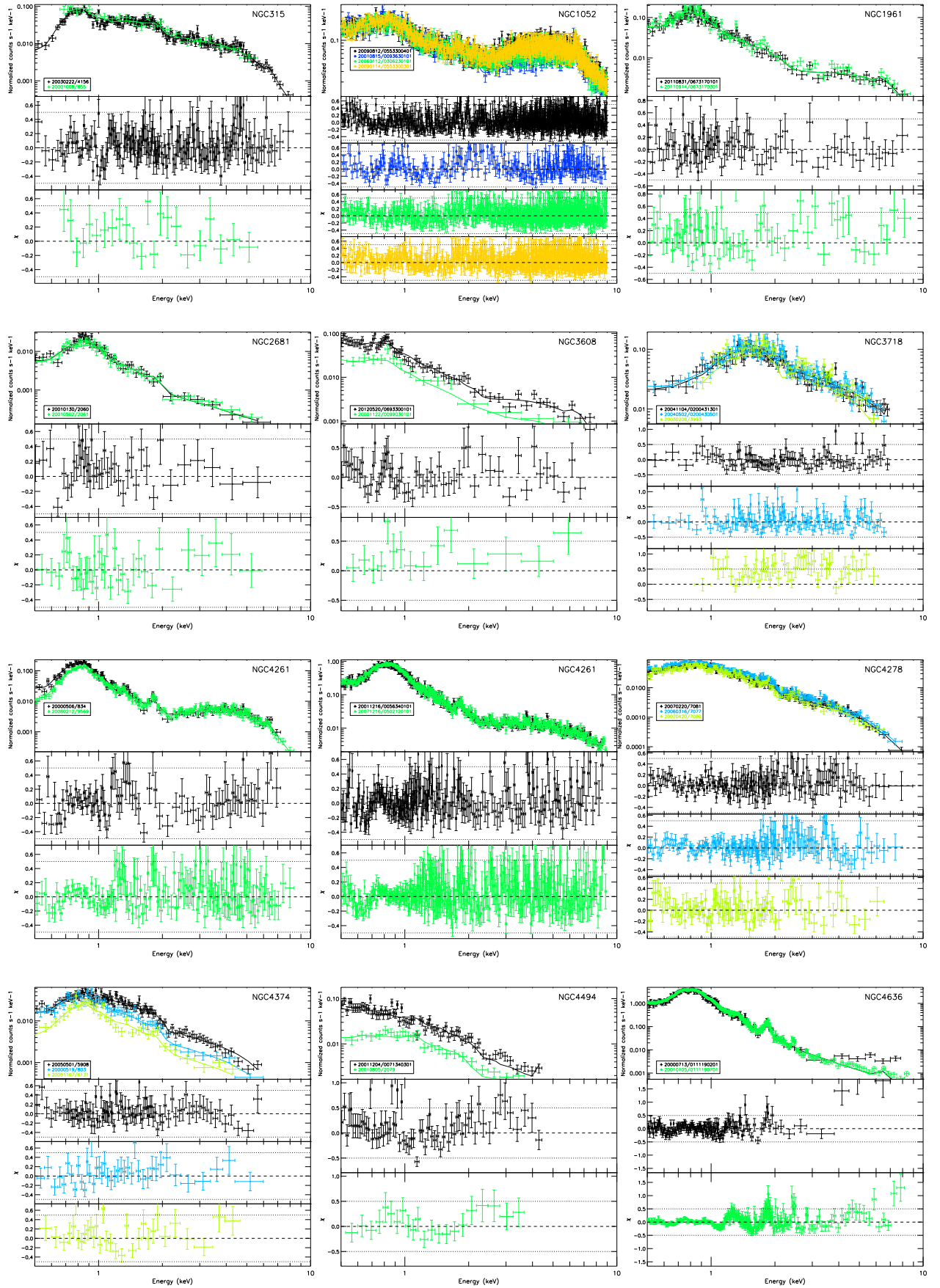


Fig. 1: For each object, (top): simultaneous fit of X-ray spectra; (from second row on): residuals. The legends contain the date (in the format yyymmdd) and the obsID. Details are given in Table A.1.

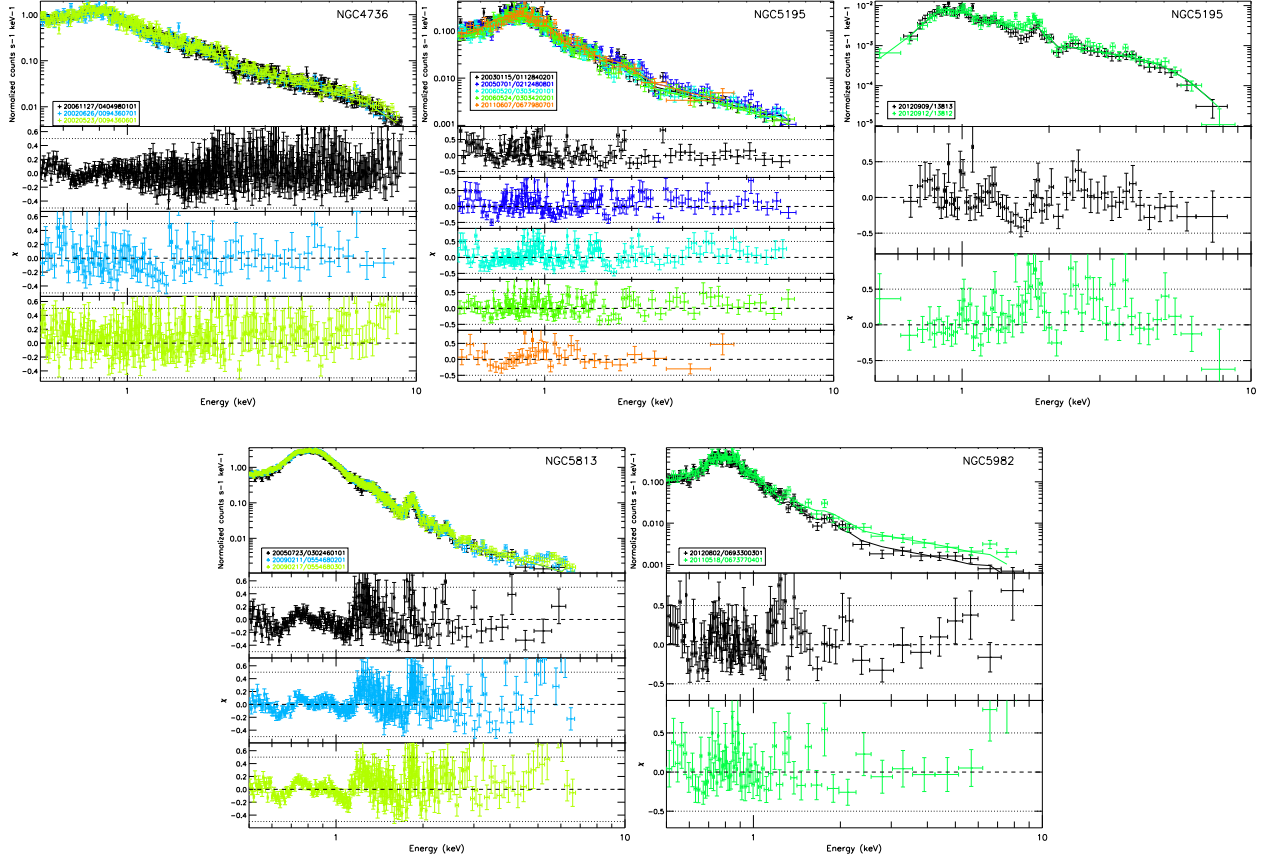


Fig. 1: (Cont.)

$$err(\sigma_{NXS}^2) = \sqrt{\frac{2}{N} \left(\frac{\langle \sigma_{err}^2 \rangle}{\langle x \rangle^2} \right)^2 + \frac{\langle \sigma_{err}^2 \rangle}{N} \frac{4\sigma_{NXS}^2}{\langle x \rangle^2}}, \quad (3)$$

where x , σ_{err}^2 and N are the count rate, its error and the number of points in the light curve, respectively, and S^2 is the variance of the light curve:

$$S^2 = \frac{1}{N-1} \sum_{i=1}^N (x_i - \langle x \rangle)^2. \quad (4)$$

When σ_{NXS}^2 was negative or compatible with zero within the errors, we estimated the 90% upper limits using Table 1 in Vaughan et al. (2003). We assumed a PSD slope of -1, the upper limit from Vaughan et al. (2003) and we added the value of $1.282err(\sigma_{NXS}^2)$ (to take into account the uncertainty due to the experimental Poisson fluctuations) to the limit. For a number of segments, N , obtained from an individual light curve, an upper limit for the normalised excess variance was calculated as:

$$\sigma_{NXS}^2 = \frac{\sqrt{\sum_{i=1}^N \sigma_{NXS_i}^2}}{N} \quad (5)$$

In case N segments were obtained for the same light curve and at least one was consistent with being variable, we calculated the normalised weighted mean and its error as the weighted variance.

5. Results

In this section we present the results on the variability in LINERs of all the sources individually (Sect. 5.1) and the general results (Sects. 5.2, 5.3, and 5.4). This includes short and long term variations in X rays and long term variations at UV frequencies. The summary of the results obtained for the variability is given in Table 2. Notes and comparisons with previous works for individual objects are included in Appendix B.

5.1. Individual objects

To be concise, we stand out the peculiarities of each source. For details on the data and results, we refer the reader to the following tables and figures: the observations used in the analysis (Table A.1), variations of the hardness ratio, HR, only compared for data from the same instrument (Col. 8 in Table A.1), UV luminosities when simultaneous data from the OM monitor were available in more than one date (Col. 9 in Table A.1 and Fig. 2), individual and simultaneous best fit and the parameters varying in the model (Table A.2 and Fig. 1), X-ray flux variations (Table A.3 and Fig. 3), the analysis of the annular region when data from *Chandra* and *XMM-Newton* are used together (Table A.4), and the simultaneous fittings of these observations (Table A.5), and short-term variability from the analysis of the light curves (Table A.6 and Appendix D). When short term variations are not detected, upper limits of σ_{NXS}^2 are calculated.

- **NGC 315:** From the simultaneous analysis of *Chandra* data, variations are not found (i.e., SMF0) in a three years pe-

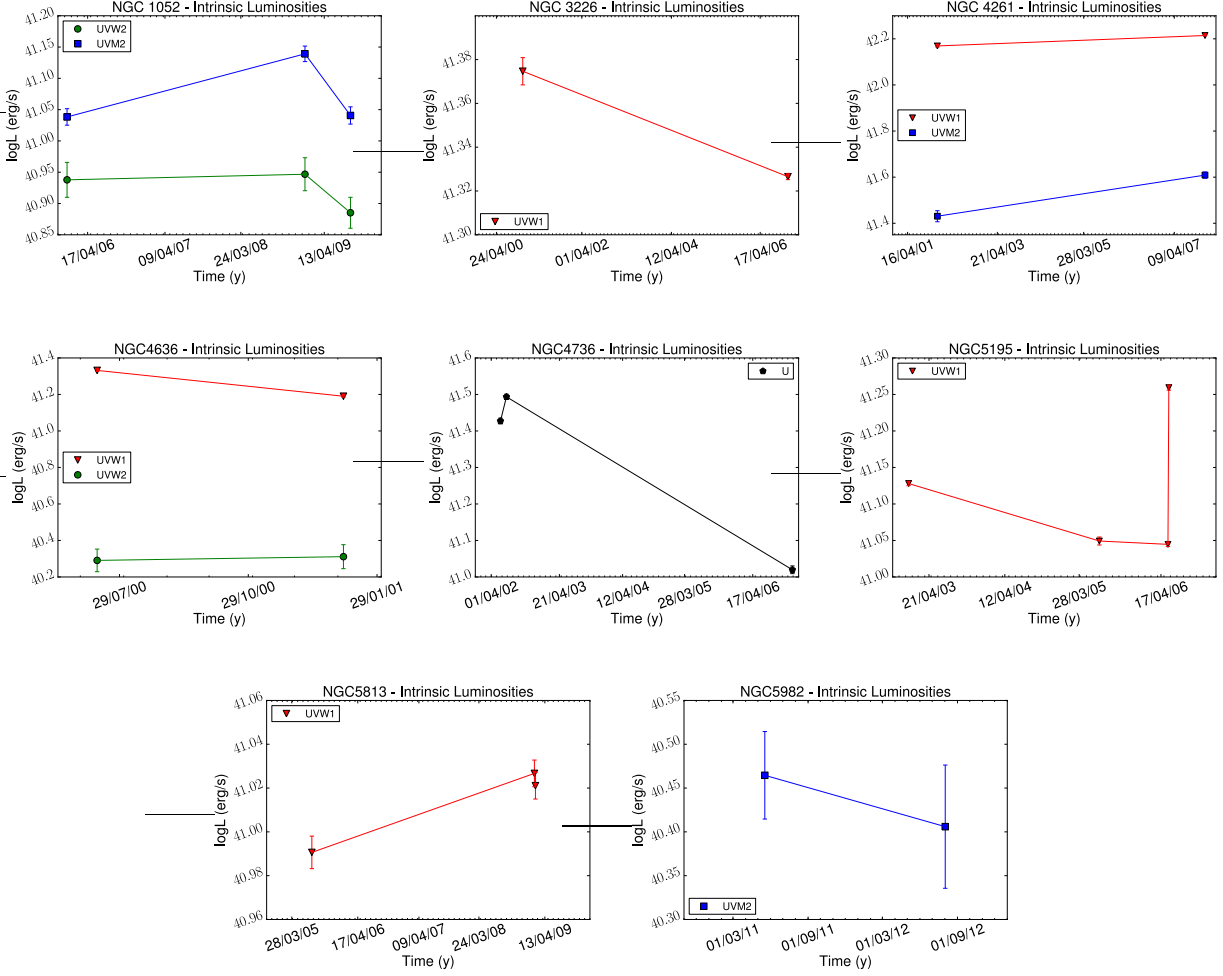


Fig. 2: UV luminosities obtained from the data with the OM camera onboard *XMM–Newton*, when available. Different filters have been used; UVW1 (red triangles), UVW2 (green circles), UVM2 (blue squares), U (black pentagons).

riod. The annular region contributes with 3% in *Chandra* data. When comparing with *XMM–Newton* data, variations of the parameters do not improve the fit within the five years period. The analysis from one of the *Chandra* light curves shows variations in the hard band at 1.6 σ confidence level.

- **NGC 1052:** SMF2 is used to fit its *XMM–Newton* data, with variations of $Norm_2$ (49%) and N_{H2} (31%) over a period of eight years. Flux variations of 20% are obtained for soft and hard energies in the same period. Since the annular region contributes with 10% in *Chandra* data, *Chandra* and *XMM–Newton* data are compared, without changes in one year period. Short term variations are not detected. UV variations from the UVW2 (13%) and UVM2 (21%) are found.
- **NGC 1961:** *XMM–Newton* data do not show variations in one month period (i.e., SMF0). UV data are available, but the nucleus of the galaxy is not detected.
- **NGC 2681:** The SMF0 results for *Chandra* data with no improvement when vary the parameters. Thus, the object do not vary in a period of four months. Short term variations are not detected.
- **NGC 2787:** One observation per instrument is available. When they are compared, the emission from the annular region contributes with 53% in *Chandra* data. Thus, we do not perform a simultaneous fit and we can not use this object to

discuss long term variations. Short term variations are not detected.

- **NGC 2841:** One observation per instrument is available. When they are compared, the emission from the annular region contributes with 60% in *Chandra* data. Thus, we do not perform a simultaneous fit and we can not use this object to discuss long term variations. In this case *Chandra* image reveals at least three X-ray sources within the annular region (see Appendix C).
- **NGC 3226:** Long-term X-ray variations from this source are not taken into account due to possible contamination from NGC 3227. We refer the reader to HG13 for details. The analysis from the *Chandra* light curve shows variations in the soft and total bands below 2 σ confidence level. UV variations amounts to 11% in the UVW1 filter.
- **NGC 3608:** SMF0 is used to fit the *XMM–Newton* data, with no variations in a 12 years period.
- **NGC 3718:** We jointly fit *Chandra* and *XMM–Newton* data since emission from the annular region is negligible. The best representation of the data needs $Norm_2$ vary (37%), i.e., SMF1 is used. This implies a change in luminosity of 35% (29%) at soft (hard) energy in one years period. In the UV data, the nucleus of the galaxy is not detected.

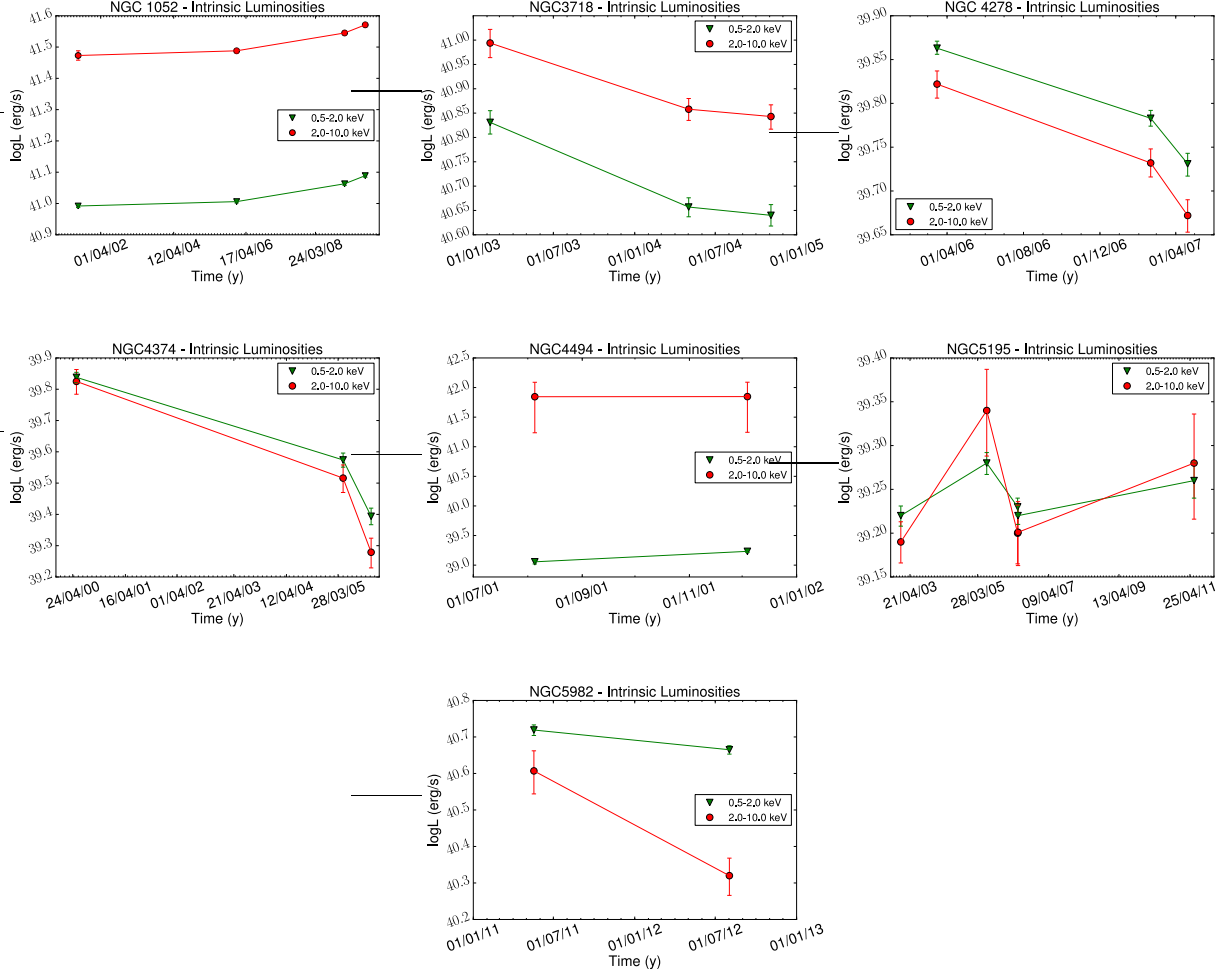


Fig. 3: Intrinsic luminosities calculated for the soft (0.5-2.0 keV, green triangles) and hard (2.0-10.0 keV, red circles) energies in the simultaneous fitting, only for the variable objects.

- **NGC 4261:** The simultaneous fit without allowing to vary any parameter (i.e., SMF0) results in a good fit both in *Chandra* and *XMM-Newton* data over a period of eight and six years, respectively. Simultaneous fit of *Chandra* and *XMM-Newton* (the annular region contributes 37% in *Chandra* data) do not show changes. Short term variations are not detected. Considering the UV range, variations amount to 9% in the UVW1 filter and 34% in the UVM2 filter.
- **NGC 4278:** The best fit for *Chandra* data is SMF1 with $Norm_2$ varying (30%) in a one year period. An X-ray intrinsic luminosity variation at soft (hard) energy of 26% (29%) is found. The contribution of the annular region in *Chandra* data amounts to 38%. When comparing *XMM-Newton* and *Chandra* data, a variation in the normalization of the PL (15%) along two years is found. Short term variations are not detected.
- **NGC 4374:** SMF1 is used for the simultaneous fit with *Chandra* data, with variations of $Norm_2$ (73%) in a period of five years. Flux variation of 64% (71%) in the soft (hard) band during the same period are found. Data from different instruments are not compared because the annular region contributes 84% in *Chandra* data. Short term variations in the soft and total bands are found from one *Chandra* observation below 2σ confidence level.
- **NGC 4494:** The simultaneous fit is jointly performed for *Chandra* and *XMM-Newton* data (the contribution of the annular region is 21% in *Chandra* data) up to 4.5 keV, because *Chandra* data show a low count-rate at harder energies. We use SMF1, obtaining the best representation of the data set when $Norm$ varies (33%). Flux variation of 31% (35%) is obtained for the soft (hard) energy in four months period.
- **NGC 4636:** SMF0 is used to fit *XMM-Newton* data, i.e., variations are not found over six months period. Note that $\chi_r^2 \sim 2$. Unfortunately, none of the proposed models are good enough to improve the final fit. From the analysis of the light curves, short term variations in the hard band are obtained from one *XMM-Newton* observation at 1.4σ confidence level. In the UV, variations of 28% are obtained from the UVW1 filter.
- **NGC 4736:** Variations are not found from *XMM-Newton* data, i.e., SMF0 is used in a period of four years. *Chandra* and *XMM-Newton* data are not compared since the emission from the annular region contributes with 84% in *Chandra* data. From the analysis of the light curves, variations in the soft, hard, and total bands are obtained below 2σ confidence

- level in all cases. At UV frequencies, a variation of 66% is obtained from the U filter.
- NGC 5195: SMF1 is used for *XMM*–Newton data, where the best representation let $Norm_2$ vary (20%). A flux variation of 9% (19%) in the soft (hard) energy band is found in a period of eight years. In the case of *Chandra* data, no variations are found from the simultaneous fit (i.e., SMF0) in a three days period. The annular region contributes with 74% in *Chandra* data, so the data from the two instruments are not compared. The analysis of one *Chandra* light curve reveals short term variations in the soft and total bands below 2σ confidence level. At UV frequencies, variation of 16% are found with the UVW1 filter.
 - NGC 5813: For *Chandra* data we make the simultaneous analysis up to 4 keV because of the low count rate at harder energies. For both *Chandra* and *XMM*–Newton data SMF0 is used, with no improvement of the fit when varying the parameters in a period of six and four years, respectively. Note that $\chi_r^2 \sim 2$ in *XMM*–Newton data. Unfortunately, none of the proposed models are good enough to improve the final fit. The data from the two instruments are not compared since the annular region contributes with 100% in *Chandra* data. Short term variations are not detected. In the UV, OM observations with the UVW1 filter are used, which show variations of 8% in a period of four years.
 - NGC 5982: SMF1 is used to fit *XMM*–Newton data, with the best representation being when varying $Norm_2$ (50%). Flux variations of 11% (49%) in the soft (hard) band are obtained in a period of one year. UV variations are not found.

Table 2: Results of the variability analysis.

Name	Type	$\log(L_{soft})$ (0.5-2 keV)	$\log(L_{hard})$ (2-10 keV)	$\log(M_{BH})$	$\log(R_{Edd})$	Variability			T (Years)	HR
						SMF0 (7)	SMF1 (8)	SMF2 (9)		
NGC 315 (C)	AGN L1.9	41.38 0%	41.58 0%	8.65	-3.67	MEPL	-	-	3	8%
NGC 1052 (X)	AGN L1.9	41.04 20%	41.52 20%	8.07	-3.14	ME2PL	$Norm_2$ 49%	N_{H2} 31%	8	33%
NGC 1961 (X)	AGN L2	41.20 0%	41.23 0%	8.67	-4.03	ME2PL	-	-	0.08	0%
NGC 2681* (C)	AGN L1.9	39.02 0%	38.93 0%	7.07	-4.73	MEPL	-	-	0.4	4%
NGC 3608* (X)	Non-AGN L2/S2:	40.32 0%	40.24 0%	8.06	-4.41	ME2PL	-	-	12	4%
NGC 3718 (C+X)	AGN L1.9	40.76 35%	40.99 29%	7.85	-3.60	2PL	$Norm_2$ 37%	-	1	14%
NGC 4261 (X)	AGN L2	40.98 0%	41.02 0%	8.96	-4.54	ME2PL	-	-	8	0%
(C)		0%	0%			ME2PL	-	-	6	19%
NGC 4278 (C)	AGN L1.9	39.80 26%	39.75 29%	8.46	-5.30	MEPL	$Norm_2$ 30%	-	1	4%
NGC 4374* (C)	AGN L2	39.64 64%	39.59 71%	8.74	-5.79	MEPL	$Norm_2$ 73%	-	5	12%
NGC 4494 (X,C)	AGN L2::	39.13 31%	39.37 35%	7.64	-4.84	PL	$Norm$ 33%	-	0.3	
NGC 4636* (X)	Non-AGN L1.9	40.86 0%	39.81 0%	8.16	-5.00	MEPL	-	-	0.5	14%
NGC 4736 (X)	AGN L2	39.61 0%	39.73 0%	6.98	-3.84	MEPL	-	-	4	5%
NGC 5195 (X)	AGN L2:	39.24 9%	39.25 19%	7.59	-4.86	MEPL	$Norm_2$ 20%	-	8	3%
(C)		38.56 0%	38.61 0%			MEPL	-	-	0	2%
NGC 5813* (X)	Non-AGN L2:	41.33 0%	40.30 0%	8.42	-4.72	MEPL	-	-	4	1%
(C)		39.68 0%	39.07 0%	8.42	-5.95	MEPL	-	-	6	5%
NGC 5982 (X)	AGN L2::	40.70 11%	40.49 49%	8.44	-4.71	MEPL	$Norm_2$ 50%	-	1	10%

Notes. (Col. 1) Name (the asterisks represent *Compton*-thick objects), and the instrument (C: *Chandra* and/or X: *XMM*-Newton) in parenthesis, (Col. 2) X-ray and optical types, (Col. 3 and 4) logarithm of the soft (0.5-2 keV) and hard (2-10 keV) X-ray luminosities, where the mean was calculated for objects showing variability, and percentages in flux variations, (Col. 5) black-hole mass in logarithmical scale, determined using the correlation between stellar velocity dispersion (from HyperLeda) and black hole mass (Tremaine et al. 2002), (Col. 6) Eddington ratio, L_{bol}/L_{Edd} , calculated from Eracleous et al. (2010a) using $L_{bol} = 33L_{2-10keV}$, (Col. 7) best fit for SMF0, (Col. 8) parameter varying in SMF1, with the percentage of variation, (Col. 9) parameter varying in SMF2, with the percentage of variation, (Col. 10) the sampling timescale, and (Col. 11) variations in the hardness ratios.

5.2. Long term X-ray spectral variability

A first approximation to the spectral variations can be estimated from the hardness ratios (HR). Following the results in HG13, an object can be considered as variable when HR varies more than 20%. One out of the 14 objects in our sample is variable according to this criterium using the HR measurements with the same instrument (namely NGC 1052). Since we are mainly doubling the sample number, we conclude that the result obtained in HG13 is a consequence of low number statistics. However, no clear relation can be invoked between variable objects and a minimum in HR variations (see Table 2).

Chandra and *XMM*–Newton data are available together for the same object in 12 cases. We recall that comparison of the data from the two instruments is done only when the emission from the annular region with $r_{ext} = r_{XMM}$ and $r_{int} = r_{Chandra}$ contributes less than 50% in *Chandra* data with the r_{XMM} aperture. In the case of NGC 3718 the extranuclear contamination is null, so the simultaneous analysis is performed without any prior analysis of the extended emission. In six cases a simultaneous fit with data from the two instruments is not conducted. In five objects (NGC 315, NGC 1052, NGC 4261, NGC 4278, and NGC 4494) the extranuclear contamination is taken into account for the simultaneous fit following the methodology described in Sect. 4.2.

None of the three non-AGN candidates show variations (one type 1 and two type 2). Seven out of the 12 AGN candidates (three out of five type 1, and four out of seven type 2) show spectral variations. We find no variations in the spectral index, Γ , in any of the objects in the sample. In all cases $Norm_2$ is responsible for these variations (between 20-73%). In one case (NGC 1052, type 1) variation in N_{H2} (31%) is required along with variations in $Norm_2$. These variations are found irrespectively of the LINER type (see Table 2).

5.3. UV and X-ray long term flux variability

Since variations in $Norm_2$ naturally imply changes in the flux, at X-ray frequencies all the objects showing spectral variations also show flux variability (see Sect. 5.2). This means that none of the non-AGN candidates show flux variations, whereas seven out of the 12 AGN candidates do. Variations from 9 to 64% (19 to 71%) are obtained in the soft (hard) band (see Table 2). Soft and hard X-ray luminosities are listed in Table A.3, and presented in Fig. 3 for objects with flux variations.

In eight out of the 18 cases, data at UV frequencies are provided by the OM onboard *XMM*–Newton at different epochs (simultaneously with X-ray data). Two of them are non-AGN candidates (the type 1 NGC 4636 and the type 2 NGC 5813). Both show variations in the UVW1 filter, while NGC 4636 does not vary in the UVW2 filter. Five out of the six AGN candidates show UV variability in at least one filter (except NGC 5982, type 2). Two variable objects are type 1 (NGC 1052 varies about 20% in the UVM2 and UVW2 filters, and NGC 3226¹⁵ shows 11% variation in the UVW1 filter), and three are type 2 (NGC 4261 shows 10% (33%) variations in the UVW1 (UVM2) filter, NGC 4736 varies 66% in the U filter, and NGC 5195 varies 51% in the UVW1 filter). In summary, three out of four type 1 and the two type 2 AGN candidates are variable objects at UV frequencies. Their UV luminosities are presented in Table A.1 and Fig. 2.

¹⁵ We recall that NGC 3226 varies at UV frequencies, but long term variations in X-rays were rejected for the analysis.

Comparing X-ray and UV flux variations, two non-AGN candidates show UV variations but do not show X-ray variations (one type 1 and one type 2). From the AGN candidates, three show X-ray and UV flux variations (two type 1 and one type 2), and three type 2s show variations only in one of the frequencies (two in the UV, and one in X-rays).

Taking into account UV and/or X-ray variations, ten out of 13 AGN candidates are variable (four out of six type 1, and six out of seven type 2). We note that the three objects showing no variations at X-ray frequencies (NGC 315, NGC 2681, and NGC 1961) do not have UV data in more than one epoch.

5.4. Short term variability

According to the values of σ_{NXS}^2 , four objects show positive values within the errors in the soft and total bands, one type 1 (NGC 3226), and three type 2 (NGC 4374, NGC 4736, NGC 5195). We obtain σ_{NXS}^2 values above zero for three objects in the hard band, two type 1 (NGC 315, and NGC 4636), and one type 2 (NGC 4736). However, all the measurements are consistent with zero at 2σ level. For the remaining light curves we estimate upper limits for the normalised excess variance. Therefore, we can not confirm short term variability in our sample. The light curves are in Appendix D, and their statistics in Table A.6.

6. Discussion

6.1. Long term variations

We analysed three non-AGN candidates (one type 1 and two type 2), and none of them show X-ray spectral nor flux variations. An additional source, NGC 5846 (type 2), was studied in HG13, that does not show variations either. All of them are classified as CT candidates by González-Martín et al. (2009a). In these objects, the nuclear obscuration is such that X-ray emission can not be directly observed, i.e., the view of their nuclear emission is suppressed below ~ 10 keV (Maiolino et al. 1998). If this is the case, spectral variations might not be detected, in accordance with our results. Indications to classify objects as an AGN candidate can be found at other frequencies, for example with radio data. At these frequencies, a compact, flat spectrum nuclear source can be considered as AGN signature (Nagar et al. 2002, 2005). González-Martín et al. (2009b) collected multiwavelength properties of 82 LINERs. In their sample, 18 objects are classified in X-rays as non-AGN candidates and have nuclear radio cores detected. From these, 14 are classified as CT candidates. Thus, it might be possible that the AGN in CT objects are not seen at X-ray frequencies (and therefore its X-ray classification is non-AGN), whereas at radio frequencies the AGN can be detected. In the four non-AGN candidates studied in HG13 and this work, radio cores are detected in three objects and, in fact, evidence of jet structures are reported in the literature (NGC 4636, Giacintucci et al. 2011; NGC 5813, Randall et al. 2011; NGC 5846, Filho et al. 2004), suggesting their AGN nature. Moreover, in this work UV variability is found for NGC 4636 and NGC 5813, whereas UV data is not available to study long term variations in the other two cases. A nuclear counterpart was not detected for NGC 3608 with *VLA* by Nagar et al. (2005). Therefore, the X-ray variable nature of CT objects can not be dismissed, but variability analyses at higher energies should be performed.

Among the 12 AGN candidates in our sample, two objects are proposed to be CT candidates (NGC 2681 and NGC 4374, González-Martín et al. 2009a). In these objects a point-like

source at hard energies is detected, what might indicate that part of the AGN continuum is still contributing below 10 keV. Hence, variations in the nuclear continuum may be observed, as is the case of NGC 4374. An example of a confirmed CT type 2 Seyfert that shows spectral variations with *XMM*-Newton data is Mrk 3 (Guainazzi et al. 2012).

Only in one case (NGC 1052) variations in N_{H2} are needed along with those in $Norm_2$ (see below). Variations in the column density have been extensively observed in type 1 Seyferts (e.g., NGC 1365, Risaliti et al. 2007; NGC 4151, Puccetti et al. 2007; Mrk 766, Risaliti et al. 2011; Swift J2127.4+5654, Sanfrutos et al. 2013). Brenneman et al. (2009) studied a 101 ksec observation of NGC 1052 from *Suzaku* data and did not find short-term variations. NGC 1052 also shows variations at UV frequencies, as shown by Maoz et al. (2005) and we confirm in this work. However, the LINER nature of this source has been discussed in the literature; Pogge et al. (2000) studied 14 LINERs with *HST* data and only NGC 1052 shows clear evidence for an ionization cone, analogous to those seen in Seyferts. From a study where artificial neural networks (ANN) were used to classify X-ray spectra, NGC 1052 seems to be associated to type 1 Seyfert galaxies in X-rays (Gonzalez-Martin et al. 2014). The fact that the observed variations in NGC 1052 are similar to those seen in type 1 Seyfert galaxies agrees well with this galaxy resembling Seyferts at X-ray frequencies.

Spectral variations do not necessarily imply flux variations. For example, if variations in the column density, N_H , were found alone, flux variations would not be present. However, all the results reported in the literature for LINERs show spectral variations related to flux variability. Variations in the normalisation of the power law, i.e. $Norm_2$, are found in all the variable sources in our sample. Variations of other components, as the soft emission (NGC 4102, González-Martín et al. 2011a; NGC 4552, HG13) or the slope of the power law (NGC 7213, Emmanoulopoulos et al. 2012) are reported in the literature. The variations in Γ found by Emmanoulopoulos et al. (2012) are small and were obtained on average every two days from 2006 to 2009. On the contrary, the observations we use in the present analysis were obtained with separations of months, and therefore it might be that if these variations occur in LINERs we are not able to detect them. The most natural explanation for the variations in $Norm_2$ is that the AGN continuum is changing with time. The first conclusion derived from this result is that the X-ray emission in these variable LINERs is AGN-like. Moreover, these kind of variations are common in other AGN (e.g., Turner et al. 1997). Thus, even if the sample is not large enough to be conclusive, from the point of view of the X-ray variability, LINERs are similar to more powerful AGN. This is confirmed by the characteristic timescales derived from our analysis (see Sect. 6.2).

Our results show that UV and X-ray variations are not simultaneous (see Sect. 5.3). This means that some X-ray variable sources are not UV variable, and vice versa. The most illustrative case is NGC 5195, that changes 39% at UV frequencies but do not vary in X-rays in the same period (see Tables A.1 and A.3, and Figures 2 and 3). The most accepted scenario assumes that the X-ray emission is produced by a disc-corona system, where UV photons from the inner parts of the accretion disc are thermally Comptonized and scattered into the X-rays by a hot corona surrounding the accretion disc (Haardt & Maraschi 1991). In this case we expect that X-ray and UV emissions reach us at different times, due to the time that light takes to travel from one place to another. These time lags will depend on the sizes of the BH, the disc and the corona, so that at larger sizes, the greater the time lags we expect. For example, Degenaar et al.

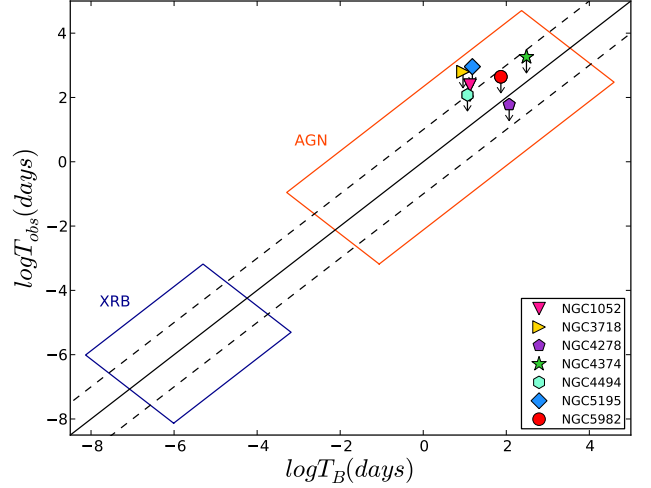


Fig. 4: Observed variability timescale, T_{obs} , against the predicted value, T_B , from González-Martín & Vaughan (2012). The solid line represents the 1:1 relationship, and the dashed lines the errors. Only variable objects are represented. The big orange rectangle represents the location of AGN, and the small blue rectangle the location of XRB as in McHardy et al. (2006).

(2014) conducted a multi-wavelength study of the X-ray binary (XRB) Swift J1910.2-0546 and find time lags between X-ray and UV frequencies of ~ 8 days. They argue that the changes may be related to the accretion morphology, perhaps due to a jet or a hot flow. LINERs have larger sizes than XRBs and, therefore, larger time lags are expected. Thus, the mismatch between UV and X-ray variabilities might be due to these time lags. Simultaneous X-ray and UV studies monitoring the sources would be useful to measure these time lags, and also to calculate the sizes of the variable regions.

6.2. Variability timescales

Short variability timescales (\sim few days) are found in the literature. Pian et al. (2010) and Younes et al. (2011) from their analysis of type 1 LINERs find short term variations in two objects, i.e., four in total. Two objects are common with our sample (NGC 3226 and NGC 4278). However, in HG13 we did not find short term variations, nor in these two nor in the other objects in the sample. González-Martín & Vaughan (2012) reported two out of 14 variable LINERs, one of them common with those reported by Pian et al. (2010). In the present paper, we study short term variability from the analysis of the light curves for a total of 12 objects in three energy bands (soft, hard, total). Six objects show $\sigma_{NXS}^2 > 0$ in at least one of the three bands. However, we note that these variations are below 2σ confidence level. None of the objects show a value consistent with being greater than zero above 3σ , and therefore we can not confirm short term variations.

McHardy et al. (2006) reported a relation between the bend timescale for variations (i.e., the predicted timescale, T_B), black hole mass and bolometric luminosity. This T_B corresponds to a characteristic frequency, ν_B , of the power spectral density (PSD), happening when the spectral index of the power law bends from

~ 1 to ~ 2 . González-Martín & Vaughan (2012) updated this relation as:

$$\log(T_B) = A\log(M_{BH}) + B\log(L_{bol}) + C \quad (6)$$

where $A = 1.34^{+0.36}$, $B = -0.24^{+0.28}$, $C = -1.88^{+0.36}$, and T_B , M_{BH} , and L_{bol} are in units of *days*, $10^6 M_\odot$, and 10^{44}erg/s , respectively. Using Eq. 6 we plot the observed timescales of the variability, T_{obs} , against the predicted timescales, T_B , for the sources showing variations in our sample (Fig. 4). The observed timescales are computed from the shortest periods in which variations are observed, and are represented as upper limits. It is important to note that the timescales between the observations probably differs from the predicted timescales. This is obvious since the observations were obtained randomly at different epochs. All the variable objects are compatible with the 1:1 relation (represented by a solid line, and dashed lines are the errors), although most of them have larger T_{obs} than predicted. In Fig. 4, we also plot the location of AGN (big orange rectangle) and X-ray binaries (XRB, small blue rectangle) as in McHardy et al. (2006). It can be observed that LINERs are located in the upper part of the relation together with the most massive AGN, due to the strong dependence of T_B with the M_{BH} . Note here that while T_B represents the bending frequency of the PSD, T_{obs} is a direct measure of changes in the spectral shape. This implies that the variability timescales are often shorter than the timescales between the observations (except for NGC 4278) for our sample. All the variable objects are then consistent with the relation reported by González-Martín & Vaughan (2012).

On the other hand, five objects in our sample do not show variations (and are not represented in Fig. 4). For these (NGC 315, NGC 1961, NGC 2681, NGC 4261, and NGC 4494), we obtain T_B (T_{obs}) ~ 77 (873), 100 (14), 3 (92), 273 (2830), and 12 (120) days, respectively. In the case of NGC 1961, $T_B > T_{obs}$, so variations between the observations are not expected. Under Eq. 6, we would expect variations from the other sources. It could be possible that we do not detect variations because observations were taken at random. However, it could also be possible that these objects do not follow Eq. 6.

Our results are consistent with the scaling relation found by McHardy et al. (2006) and González-Martín & Vaughan (2012) because, according to the BH mass and accretion rates of LINERs, variations of the intrinsic continuum are expected to be of large scales. Therefore, LINERs would follow the same relation than other AGN and XRBs (see Fig. 4). We recall that T_B has a strong dependence on M_{BH} , while the dependence with L_{bol} (and with the accretion rate) is much lower (McHardy 2010), and hence it prevents us to obtain useful information related to accretion physics.

Despite LINERs and more powerful AGN are located in the same plane, different authors have pointed out that the accretion mechanism in LINERs could be different from that happening in more powerful AGN (e.g., Gu & Cao 2009; Younes et al. 2011). When a source accretes at a very low Eddington rate ($R_{Edd} < 10^{-3}$), the accretion is dominated by radiatively inefficient accretion flows (RIAF, Narayan & Yi 1994; Quataert 2004). Such flows are though to be present in XRB, which are closer accreting black holes that can be easily studied. It is well known that XRB show different X-ray emission states which are differentiated by their spectral properties (e.g., Remillard & McClintock 2006). In comparison to XRB, LINERs should be in the “low/hard” state or, if the Eddington ratio is too low, in the “quiescent” state, while more powerful AGN should be in the “high/soft” state.

An anticorrelation between the slope of the power law, Γ , and the Eddington ratio, R_{Edd} , is expected from RIAF models. Qiao & Liu (2013) theoretically investigated this correlation for XRB and found that advection dominated accretion flow (ADAF)¹⁶ models can reproduce it well. In these models the X-ray emission is produced by Comptonization of the synchrotron and bremsstrahlung photons. Later, they studied low luminosity AGN (LLAGN) in the framework of a disc evaporation model (inner ADAF plus an outer truncated accretion disc) and found that it can also reproduce the anticorrelation (Qiao et al. 2013).

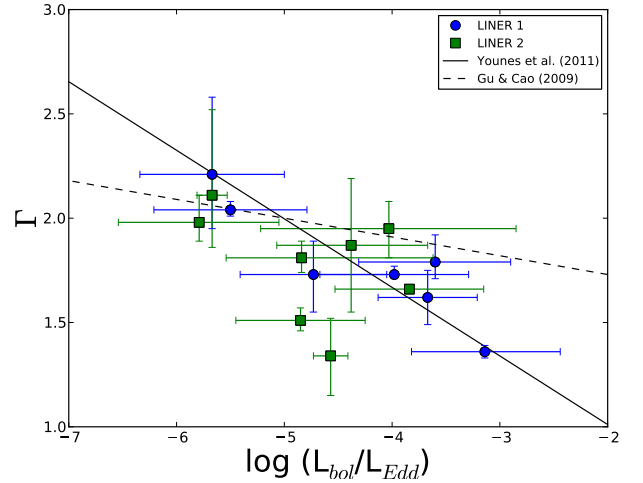


Fig. 5: Spectral index, Γ , versus the Eddington ratio, $R_{Edd} = \log(L_{bol}/L_{Edd})$. Type 1 (blue circles) and type 2 (green squares) LINERs are distinguished. The solid and dashed lines represent the relations given by Younes et al. (2011) and Gu & Cao (2009), respectively, shifted to the same bolometric correction (see text).

Some efforts have been done to observationally investigate that relationship for LLAGN. Gu & Cao (2009) used a sample of 55 LLAGN (including 27 LINERs and 28 Seyferts) and found a regular anticorrelation between Γ and R_{Edd} . However, when LINERs were considered alone, they did not find a strong correlation. Later, Younes et al. (2011) studied a sample of type 1 LINERs and found a statistically significant anticorrelation. In HG13 we found that the seven LINERs studied in the sample fitted well in the relation given by Younes et al. (2011). Here we plot the same relation in Fig. 5, where the values of Γ and $L_{2-10keV}$ were obtained from the simultaneous fittings, since Γ did not vary in any of the objects (see Table 2). In the cases of NGC 2787 and NGC 2841 the individual fit from *Chandra* data was used because the simultaneous fit can not be performed (see Sect. 5.1). R_{Edd} were calculated following the formulation given in Eracleous et al. (2010b), assuming $L_{bol} = 33L_{2-10keV}$. The solid and dashed lines in Fig. 5 are the relations given by Younes et al. (2011) and Gu & Cao (2009), respectively, corrected to our L_{bol} . The coefficient of the Pearson correlation is $r = -0.66$, with a coefficient of determination of $p = 0.008$. This might suggest that RIAF models apply to LINERs, indicating an inefficient accretion disc, in contrast to the efficient accretion discs found for more powerful AGN. A larger sample of LINERs would be useful to be conclusive.

¹⁶ The RIAF model is an updated version of the ADAF model.

6.3. Type 1/Type 2 variable AGN candidates

Some studies at X-ray frequencies have shown the variable nature of LINERs. Type 1 LINERs were studied by Pian et al. (2010), Younes et al. (2011), Emmanoulopoulos et al. (2012), and HG13. Pian et al. (2010) studied four sources with *Swift* and find variations in two of them. Younes et al. (2011) detected long term variations in seven out of the nine sources in their sample from *XMM-Newton* and *Chandra* data. Emmanoulopoulos et al. (2012) studied one object with Rossi X-ray Timing Explorer (RXTE) and find a ‘harder when brighter’ behaviour. In HG13 we analysed three AGN candidates using *Chandra* and/or *XMM-Newton* data and find variations in all the three.

In the present analysis our sample contains five type 1 AGN candidates, three of them consistent with being variable. From the sample by Younes et al. (2011), five objects are in common with our sample, four of them with similar results and only differing in the case of NGC 315 (see Appendix B for notes and comparisons).

Type 2 objects were studied by González-Martín et al. (2011a) and HG13. González-Martín et al. (2011a) used *Suzaku*, *Chandra* and *Swift* data to study one object and find variations in the thermal component. In HG13 we reported long term variations in one of the two AGN candidates.

In the present analysis our sample contains seven type 2 AGN candidates, four of them consistent with being variable.

Taking into account the present analysis and the studies listed above from the literature, 14 out of 22 LINERs are X-ray variable objects (eight out of 13 type 1, and six out of nine type 2). Therefore, there is no significant difference in the proportion of variable objects in X-rays in terms of the optical type1/type2 classification. Given that the observed variations are intrinsic to the sources, similar proportions were expected in view of the UM, in good agreement with our results.

Similar behaviour is found at UV frequencies. Maoz et al. (2005) were the first authors to show that UV variability is common in LINERs, and to demonstrate the presence of a nonstellar component at these frequencies. From their sample of 17 LINERs, only three do not show neither short-term (<1 yr) nor long-term (>1 yr) variability. From these, all the seven type 1s and seven out of 10 type 2 objects show variations.

When data from the OM onboard *XMM-Newton* are available, we searched for UV variability. Taking into account only AGN candidates, five out of six objects show variations (two type 1 and three type 2). This gives strength to the variable nature of LINERs. In common to our sample, Maoz et al. (2005) already showed the variable nature of NGC 1052 and NGC 4736. Thus, taking into account the present analysis and the study by Maoz et al. (2005), 17 out of 21 LINERs are variable at UV frequencies (the eight type 1, and nine out of 13 type 2). As previously noted by Maoz et al. (2005), the fact that type 2 LINERs show variations at UV frequencies suggests that the UM may not always apply to LINERs. It has been suggested that the broad line region (BLR) and the torus, responsible for obscuring the continuum that is visible in type 1 AGN, disappear at low luminosities (Elitzur & Shlosman 2006; Elitzur & Ho 2009). The disappearance of the torus could in principle explain why type 2 LINERs do vary in the UV, because the naked AGN is directly seen at these frequencies.

We find that some objects show variations in X-rays but do not vary at UV frequencies, or vice versa. This means that the percentage of variable objects is higher if we take into account different frequencies. From all the 34 studied LINERs at UV and X-ray frequencies in the present and other works, 27 LINERs

show variations in at least one energy band (13 out of 16 type 1, and 14 out of 18 type 2). Thus, the percentage of type 1 and 2 variable objects is similar. Consequently, variability is very common in LINER nuclei, a property that share with other AGN.

7. Conclusions

Using *Chandra* and *XMM-Newton* public archives we performed a spectral and flux, short and long term variability analysis of 18 LINERs in the Palomar sample. The main results of this study can be summarized as follows:

1. Seven out of 12 AGN candidate LINERs show long term spectral variability, while the three non-AGN candidates do not. In two cases the simultaneous fit was not possible due to strong external contamination, and in one case the long term analysis was rejected due to possible contamination of a companion galaxy.
2. No significant difference in the proportion of X-ray variable nuclei (type 1 or 2) are found.
3. The main driver of the spectral variations is the change in the normalization of the power law, $Norm_2$; only for NGC 1052 this is accompanied by variations in the column density, N_{H2} .
4. UV variations are found in five out of six AGN candidates. The two non-AGN candidates also show variations.
5. Short term variations are not found.

From X-ray and UV data, we find that ten out of 13 LINERs in our sample show evidence of long term variability in at least one energy band. Hence, variability is very common in LINERs.

We find that X-ray variations are due to changes in the continuum of the AGN. These results agree well with the expected variations according to their BH masses and accretion rates. In this sense, LINERs would be in the same plane than more powerful AGN and XRB. However, we find an anticorrelation between the slope of the power law, Γ , and the Eddington ratio, that may suggest a different accretion mechanism in LINERs, more similar to the hard state of XRB.

On the other hand, the result that some type 2 LINERs eventually vary at UV frequencies may suggest that a naked AGN can be observed at these wavelengths, what could be explained in the scenario where the torus disappears at low luminosities.

Acknowledgements. We thank the anonymous referee for his/her helpful comments that helped to improve the paper, and the AGN group at the IAA for helpful comments during this work. This work was financed by MINECO grant AYA 2010-15169, Junta de Andalucía TIC114 and Proyecto de Excelencia de la Junta de Andalucía P08-TIC-03531. LHG acknowledges financial support from the Ministerio de Economía y Competitividad through the Spanish grant FPI BES-2011-043319. OGM thanks Spanish MINECO through a Juan de la Cierva Fellowship. This research made use of data obtained from the *Chandra* Data Archive provided by the *Chandra* X-ray Center (CXC). This research made use of data obtained from the *XMM-Newton* Data Archive provided by the *XMM-Newton* Science Archive (XSA). This research made use of the NASA/IPAC extragalactic database (NED), which is operated by the Jet Propulsion Laboratory under contract with the National Aeronautics and Space Administration. We acknowledge the usage of the HyperLeda database (<http://leda.univ-lyon1.fr>).

References

- Antonucci, R. 1993, *ARA&A*, 31, 473
 Birkinshaw, M. & Davies, R. L. 1985, *ApJ*, 291, 32
 Brassington, N. J., Fabbiano, G., Kim, D.-W., et al. 2009, *ApJS*, 181, 605
 Brenneman, L. W., Weaver, K. A., Kadler, M., et al. 2009, *ApJ*, 698, 528
 Brightman, M. & Nandra, K. 2011, *MNRAS*, 413, 1206
 Cappellari, M., Renzini, A., Greggio, L., et al. 1999, *ApJ*, 519, 117
 Cardullo, A., Corsini, E. M., Beifiori, A., Pizzella, A., & Buson, L. M. 2008, in *Astronomical Society of the Pacific Conference Series*, Vol. 396, *Formation and Evolution of Galaxy Disks*, ed. J. G. Funes & E. M. Corsini, 53

- Carollo, C. M., Franx, M., Illingworth, G. D., & Forbes, D. A. 1997, *ApJ*, 481, 710
- de Vaucouleurs, G. 1975, *Social Studies of Science*, 9, 557
- Degenaar, N., Maitra, D., Cackett, E. M., et al. 2014, *ArXiv e-prints*
- Dickey, J. M. & Lockman, F. J. 1990, *ARA&A*, 28, 215
- D’Onofrio, M., Marziani, P., & Sulentic, J. W. 2012, *Fifty Years of Quasars: Current Impressions and Future Perspectives*, ed. M. D’Onofrio, P. Marziani, & J. W. Sulentic, 549
- Dudik, R. P., Satyapal, S., Gliozzi, M., & Sambruna, R. M. 2005, *ApJ*, 620, 113
- Elitzur, M. & Ho, L. C. 2009, *ApJ*, 701, L91
- Elitzur, M. & Shlosman, I. 2006, *ApJ*, 648, L101
- Emmanoulopoulos, D., Papadakis, I. E., McHardy, I. M., et al. 2012, *MNRAS*, 424, 1327
- Eracleous, M., Hwang, J. A., & Flohic, H. M. L. G. 2010a, *ApJ*, 711, 796
- Eracleous, M., Hwang, J. A., & Flohic, H. M. L. G. 2010b, *ApJS*, 187, 135
- Eracleous, M., Shields, J. C., Chartas, G., & Moran, E. C. 2002, *ApJ*, 565, 108
- Ferrarese, L., Ford, H. C., & Jaffe, W. 1996, *ApJ*, 470, 444
- Filho, M. E., Fraternali, F., Markoff, S., et al. 2004, *A&A*, 418, 429
- Garcia, A. M. 1993, *A&AS*, 100, 47
- Garmire, G. P., Bautz, M. W., Ford, P. G., Nousek, J. A., & Ricker, J. G. R. 2003, in *Society of Photo-Optical Instrumentation Engineers (SPIE) Conference Series*, Vol. 4851, *Society of Photo-Optical Instrumentation Engineers (SPIE) Conference Series*, ed. J. E. Truemper & H. D. Tananbaum, 28–44
- Giacintucci, S., O’Sullivan, E., Vrtilek, J., et al. 2011, *ApJ*, 732, 95
- Giroletti, M., Taylor, G. B., & Giovannini, G. 2005, *ApJ*, 622, 178
- González-Martín, O., Diaz-Gonzalez, D., Acosta-Pulido, J. A., et al. 2014, *ArXiv e-prints*
- González-Martín, O., Masegosa, J., Márquez, I., & Guainazzi, M. 2009a, *ApJ*, 704, 1570
- González-Martín, O., Masegosa, J., Márquez, I., Guainazzi, M., & Jiménez-Bailón, E. 2009b, *A&A*, 506, 1107
- González-Martín, O., Papadakis, I., Braito, V., et al. 2011a, *A&A*, 527, A142
- González-Martín, O., Papadakis, I., Reig, P., & Zezas, A. 2011b, *A&A*, 526, A132
- González-Martín, O. & Vaughan, S. 2012, *A&A*, 544, A80
- Gu, M. & Cao, X. 2009, *MNRAS*, 399, 349
- Guainazzi, M., La Parola, V., Miniutti, G., Segreto, A., & Longinotti, A. L. 2012, *A&A*, 547, A31
- Guainazzi, M., Oosterbroek, T., Antonelli, L. A., & Matt, G. 2000, *A&A*, 364, L80
- Haardt, F. & Maraschi, L. 1991, *ApJ*, 380, L51
- Harris, D. E., Biretta, J. A., Junor, W., et al. 2003, *ApJ*, 586, L41
- Harris, D. E., Cheung, C. C., Biretta, J. A., et al. 2006, *ApJ*, 640, 211
- Harris, D. E., Cheung, C. C., Stawarz, Ł., Biretta, J. A., & Perlman, E. S. 2009, *ApJ*, 699, 305
- Harris, D. E., Massaro, F., Cheung, C. C., et al. 2011, *ApJ*, 743, 177
- Heckman, T. M. 1980, *A&A*, 87, 152
- Hernández-García, L., González-Martín, O., Márquez, I., & Masegosa, J. 2013, *A&A*, 556, A47
- Ho, L. C. 2008, *ARA&A*, 46, 475
- Ho, L. C., Filippenko, A. V., Sargent, W. L. W., & Peng, C. Y. 1997, *ApJS*, 112, 391
- Ho, L. C. & Ulvestad, J. S. 2001, *ApJS*, 133, 77
- Ishwara-Chandra, C. H. & Saikia, D. J. 1999, *MNRAS*, 309, 100
- Kalberla, P. M. W., Burton, W. B., Hartmann, D., et al. 2005, *A&A*, 440, 775
- Krips, M., Eckart, A., Krichbaum, T. P., et al. 2007, *A&A*, 464, 553
- Lawrence, A., Watson, M. G., Pounds, K. A., & Elvis, M. 1987, *Nature*, 325, 694
- Maiolino, R., Salvati, M., Bassani, L., et al. 1998, *A&A*, 338, 781
- Maoz, D., Nagar, N. M., Falcke, H., & Wilson, A. S. 2005, *ApJ*, 625, 699
- Masegosa, J., Márquez, I., Ramirez, A., & González-Martín, O. 2011, *A&A*, 527, A23
- McHardy, I. 2010, in *Lecture Notes in Physics*, Berlin Springer Verlag, Vol. 794, *Lecture Notes in Physics*, Berlin Springer Verlag, ed. T. Belloni, 203
- McHardy, I. M., Koerding, E., Knigge, C., Uttley, P., & Fender, R. P. 2006, *Nature*, 444, 730
- Nagar, N. M., Falcke, H., & Wilson, A. S. 2005, *A&A*, 435, 521
- Nagar, N. M., Falcke, H., Wilson, A. S., & Ulvestad, J. S. 2002, *A&A*, 392, 53
- Nandra, K., George, I. M., Mushotzky, R. F., Turner, T. J., & Yaqoob, T. 1997, *ApJ*, 476, 70
- Narayan, R. & Yi, I. 1994, *ApJ*, 428, L13
- O’Sullivan, E., Vrtilek, J. M., & Kempner, J. C. 2005, *ApJ*, 624, L77
- Pellegrini, S., Fabbiano, G., Fiore, F., Trinchieri, G., & Antonelli, A. 2002, *A&A*, 383, 1
- Pellegrini, S., Wang, J., Fabbiano, G., et al. 2012, *ApJ*, 758, 94
- Peterson, B. M. 1997, *An Introduction to Active Galactic Nuclei*, ed. Peterson, B. M.
- Pian, E., Romano, P., Maoz, D., et al. 2010, *MNRAS*, 401, 677
- Pogge, R. W., Maoz, D., Ho, L. C., & Eracleous, M. 2000, *ApJ*, 532, 323
- Puccetti, S., Fiore, F., Risaliti, G., et al. 2007, *MNRAS*, 377, 607
- Qiao, E. & Liu, B. F. 2013, *ApJ*, 764, 2
- Qiao, E., Liu, B. F., Panessa, F., & Liu, J. Y. 2013, *ApJ*, 777, 102
- Quataert, E. 2004, in *Astronomical Society of the Pacific Conference Series*, Vol. 311, *AGN Physics with the Sloan Digital Sky Survey*, ed. G. T. Richards & P. B. Hall, 131
- Randall, S. W., Forman, W. R., Giacintucci, S., et al. 2011, *ApJ*, 726, 86
- Remillard, R. A. & McClintock, J. E. 2006, *ARA&A*, 44, 49
- Risaliti, G., Elvis, M., Fabbiano, G., et al. 2007, *ApJ*, 659, L111
- Risaliti, G., Nardini, E., Salvati, M., et al. 2011, *MNRAS*, 410, 1027
- Rubin, V. C., Ford, W. K. J., & Roberts, M. S. 1979, *ApJ*, 230, 35
- Sambruna, R. M., Gliozzi, M., Eracleous, M., Brandt, W. N., & Mushotzky, R. 2003, *ApJ*, 586, L37
- Sanfrutos, M., Miniutti, G., Agís-González, B., et al. 2013, *MNRAS*, 436, 1588
- Satyapal, S., Dudik, R. P., O’Halloran, B., & Gliozzi, M. 2005, *ApJ*, 633, 86
- Satyapal, S., Sambruna, R. M., & Dudik, R. P. 2004, *A&A*, 414, 825
- Strüder, L., Briel, U., Dennerl, K., et al. 2001, *A&A*, 365, L18
- Terashima, Y. & Wilson, A. S. 2003, *ApJ*, 583, 145
- Terashima, Y. & Wilson, A. S. 2004, *ApJ*, 601, 735
- Tremaine, S., Gebhardt, K., Bender, R., et al. 2002, *ApJ*, 574, 740
- Turner, T. J., George, I. M., Nandra, K., & Mushotzky, R. F. 1997, *ApJS*, 113, 23
- Urry, C. M. & Padovani, P. 1995, *PASP*, 107, 803
- Vaughan, S., Edelson, R., Warwick, R. S., & Uttley, P. 2003, *MNRAS*, 345, 1271
- Venturi, T., Giovannini, G., Feretti, L., Comoretto, G., & Wehrle, A. E. 1993, *ApJ*, 408, 81
- Vermeulen, R. C., Ros, E., Kellermann, K. I., et al. 2003, *A&A*, 401, 113
- Vrtilek, J. M., O’Sullivan, E., David, L. P., et al. 2013, in *AAS/High Energy Astrophysics Division*, Vol. 13, *AAS/High Energy Astrophysics Division*, #116.06
- Xu, C., Baum, S. A., O’Dea, C. P., Wrobel, J. M., & Condon, J. J. 2000, *AJ*, 120, 2950
- Younes, G., Porquet, D., Sabra, B., et al. 2010, *A&A*, 517, A33
- Younes, G., Porquet, D., Sabra, B., & Reeves, J. N. 2011, *A&A*, 530, A149
- Younes, G., Porquet, D., Sabra, B., Reeves, J. N., & Grosso, N. 2012, *A&A*, 539, A104

Appendix A: Tables

Table A.1. Observational details.

Name	Instrument	ObsID	Date	R ('')	Net Exptime (ksec)	Counts	HR	$\log(L_{UV})$ (erg/s)	Filter
(1)	(2)	(3)	(4)	(5)	(6)	(7)	(8)	(9)	(10)
NGC 315	<i>XMM-Newton</i> ^c	0305290201	2005-07-02	25	14	5799	-0.55 ± 0.01	41.75 ± 0.05	UVM2
	<i>Chandra</i>	855	2000-10-08	3	5	501	-0.27 ± 0.13	-	
	<i>Chandra</i> ^c	4156	2003-02-22	3	55	5550	-0.23 ± 0.05	-	
NGC 1052	<i>XMM-Newton</i> ^c	0093630101	2001-08-15	25	11.2	5818	0.28 ± 0.06	-	
	<i>XMM-Newton</i>	0306230101	2006-01-12	25	44.8	25565	0.34 ± 0.03	41.04 ± 0.01	UVM2
								40.94 ± 0.03	UVW2
	<i>XMM-Newton</i>	0553300301	2009-01-14	25	42.4	27367	0.39 ± 0.02	41.14 ± 0.01	UVM2
								40.95 ± 0.03	UVW2
	<i>XMM-Newton</i>	0553300401	2009-08-12	25	46.8	30643	0.42 ± 0.02	41.04 ± 0.01	UVM2
								40.89 ± 0.03	UVW2
	<i>Chandra</i> ^c	5910	2000-08-29	3	59.2	6549	0.40 ± 0.04	-	
NGC 1961	<i>XMM-Newton</i>	0673170101	2011-08-31	35	17	1934	-0.54 ± 0.02	Not detected	
	<i>XMM-Newton</i>	0673170301	2011-09-14	35	14	1680	-0.54 ± 0.02	Not detected	
NGC 2681	<i>Chandra</i>	2060	2001-01-30	3	81	1126	-0.76 ± 0.01	-	
	<i>Chandra</i>	2061	2001-05-02	3	79	1018	-0.73 ± 0.01	-	
NGC 2787	<i>XMM-Newton</i> ^c	0200250101	2004-10-10	25	25	2557	-0.37 ± 0.04	-	
	<i>Chandra</i> ^c	4689	2004-05-18	3	31	527	-0.59 ± 0.03	-	
NGC 2841	<i>XMM-Newton</i> ^c	0201440101	2004-11-09	30	9	1712	-0.57 ± 0.02	41.28 ± 0.03	UVW2
	<i>Chandra</i> ^c	6096	2004-12-18	5	28	486	-0.81 ± 0.01	-	
NGC 3226	<i>XMM-Newton</i>	0101040301	2000-11-28	-	-	-	-	41.38 ± 0.01	UVW1
	<i>XMM-Newton</i>	0400270101	2006-12-03	-	-	-	-	41.33 ± 0.01	UVW1
	<i>Chandra</i>	860	1999-12-30	3	46.6	476	0.53 ± 0.12	-	
NGC 3608	<i>XMM-Newton</i>	0099030101	2000-11-22	20	12	454	-0.48 ± 0.06	-	
	<i>XMM-Newton</i>	0693300101	2012-05-20	20	23	1749	-0.46 ± 0.03	41.01 ± 0.07	UVM2
NGC 3718	<i>XMM-Newton</i> ^c	0200430501	2004-05-02	25	10	2473	0.12 ± 0.19	Not detected	
	<i>XMM-Newton</i> ^c	0200431301	2004-11-04	25	8	1734	0.14 ± 0.20	Not detected	
	<i>Chandra</i> ^c	3993	2003-02-08	3	5	1143	0.11 ± 0.29	-	
NGC 4261	<i>Chandra</i>	834	2000-05-06	3	34.4	3465	-0.58 ± 0.01	-	
	<i>Chandra</i> ^c	9569	2008-02-12	3	100.9	7757	-0.47 ± 0.01	-	
	<i>XMM-Newton</i>	0056340101	2001-12-16	25	21.3	10730	-0.68 ± 0.01	41.43 ± 0.02	UVM2
								42.17 ± 0.01	UVW1
	<i>XMM-Newton</i> ^c	0502120101	2007-12-16	25	63.0	32156	-0.68 ± 0.01	41.61 ± 0.01	UVM2
								42.21 ± 0.01	UVW1
NGC 4278	<i>Chandra</i> ^c	7077	2006-03-16	3	110.3	9182	-0.66 ± 0.01	-	
	<i>Chandra</i>	7081	2007-02-20	3	110.7	7591	-0.66 ± 0.01	-	
	<i>Chandra</i>	7080	2007-04-20	3	55.8	3379	-0.69 ± 0.01	-	
	<i>XMM-Newton</i> ^c	0205010101	2004-05-23	25	20.8	34516	-0.60 ± 0.01	40.90 ± 0.02	UVW1
NGC 4374	<i>XMM-Newton</i> ^c	0673310101	2011-06-01	25	25	19788	-0.87 ± 0.01	41.48 ± 0.01	UVM2
	<i>Chandra</i>	803	2000-05-19	2	28	1010	-0.67 ± 0.02	-	
	<i>Chandra</i>	5908	2005-05-01	2	46	2401	-0.60 ± 0.01	-	
	<i>Chandra</i> ^c	6131	2005-11-07	2	41	812	-0.68 ± 0.02	-	
NGC 4494	<i>XMM-Newton</i> ^c	0071340301	2001-12-04	20	24	2116	-0.46 ± 0.04	41.99 ± 0.01	UVW1
	<i>Chandra</i> ^c	2079	2001-08-05	3	25	580	-0.57 ± 0.03	-	
NGC 4636	<i>XMM-Newton</i>	0111190201	2000-07-13	25	6	9889	-0.95 ± 0.01	40.62 ± 0.06	UVW2
								41.66 ± 0.01	UVW1
	<i>XMM-Newton</i>	0111190701	2001-01-05	25	51	91789	-0.97 ± 0.01	40.64 ± 0.07	UVW2
								41.52 ± 0.01	UVW1
NGC 4736	<i>XMM-Newton</i> ^c	0094360601	2002-05-23	20	8	11041	-0.59 ± 0.01	40.69 ± 0.01	U
	<i>XMM-Newton</i>	0094360701	2002-06-26	20	3	3010	-0.62 ± 0.01	40.76 ± 0.01	U
	<i>XMM-Newton</i>	0404980101	2006-11-27	20	33	42048	-0.60 ± 0.01	40.29 ± 0.01	U

Table A.1. (Cont.)

Name	Instrument	ObsID	Date	R (")	Net Exptime (ksec)	Counts	HR	$\log(L_{UV})$ (erg/s)	Filter
(1)	(2)	(3)	(4)	(5)	(6)	(7)	(8)	(9)	(10)
	<i>Chandra</i> ^c	808	2000-05-13	1.5	47	2986	-0.73 ± 0.01	-	
NGC 5195	<i>XMM-Newton</i>	0112840201	2003-01-15	20	17	2976	-0.77 ± 0.01	40.98 ± 0.01	UVW1
	<i>XMM-Newton</i>	0212480801	2005-07-01	20	22	3756	-0.68 ± 0.01	40.80 ± 0.01	UVW1
	<i>XMM-Newton</i>	0303420101	2006-05-20	20	27	4297	-0.69 ± 0.01	40.89 ± 0.01	UVW1
	<i>XMM-Newton</i>	0303420201	2006-05-24	20	21	3312	-0.70 ± 0.01	41.11 ± 0.01	UVW1
	<i>XMM-Newton</i> ^c	0677980701	2011-06-07	20	5	888	-0.79 ± 0.01	-	
	<i>Chandra</i> ^c	13813	2012-09-09	3	179	1340	-0.43 ± 0.04	-	
	<i>Chandra</i>	13812	2012-09-12	3	157	1359	-0.42 ± 0.04	-	
NGC 5813	<i>XMM-Newton</i>	0302460101	2005-07-23	30	20	25419	-0.96 ± 0.01	42.01 ± 0.01	UVW1
	<i>XMM-Newton</i>	0554680201	2009-02-11	30	43	58821	-0.95 ± 0.01	42.04 ± 0.01	UVW1
	<i>XMM-Newton</i> ^c	0554680301	2009-02-17	30	43	58175	-0.95 ± 0.01	42.04 ± 0.01	UVW1
	<i>Chandra</i>	5907	2005-04-02	3	48	518	-0.92 ± 0.01	-	
	<i>Chandra</i> ^c	9517	2008-06-05	3	99	1181	-0.90 ± 0.01	-	
	<i>Chandra</i>	12951	2011-03-28	3	74	714	-0.95 ± 0.01	-	
	<i>Chandra</i>	12952	2011-04-05	3	143	1451	-0.90 ± 0.01	-	
	<i>Chandra</i>	13253	2011-04-08	3	118	1295	-0.91 ± 0.01	-	
	<i>Chandra</i>	13255	2011-04-10	3	43	465	-0.92 ± 0.01	-	
NGC 5982	<i>XMM-Newton</i>	0673770401	2011-05-18	25	9	1932	-0.78 ± 0.01	41.71 ± 0.05	UVM2
	<i>XMM-Newton</i>	0693300301	2012-08-02	25	21	4235	-0.87 ± 0.01	41.65 ± 0.07	UVM2

Notes. (Col. 1) name, (Col. 2) instrument, obsID (Col. 3) obsID, (Col. 4) date, (Col. 5) aperture radius for the nuclear extraction, (Col. 6) net exposure time, (Col. 7) number of counts in the 0.5-10 keV band, (Col. 8) hardness ratio, (Cols. 9 and 10) UV luminosity from the optical monitor and filter. The *c* represents data from different instruments that were compared as explained in Sect. 4.2.

Table A.2. Final compilation of the best-fit models for the sample, including the individual best-fit model for each observation, and the simultaneous best-fit model with the varying parameters.

Analysis	ObsID	Model	N_{H1}	N_{H2}	kT keV	Γ	$Norm_1$ (10^{-4})	$Norm_2$ (10^{-4})	$\chi^2/d.o.f$ F-test
(1)	(2)	(3)	(4)	(5)	(6)	(7)	(8)	(9)	(10)
NGC 315									
Ind	0305290201	MEPL	-	$0.17^{0.25}_{0.11}$	$0.56^{0.58}_{0.54}$	$1.59^{1.69}_{1.50}$	$1.20^{1.29}_{1.11}$	$1.58^{1.77}_{1.41}$	197.97/198
Ind	855	MEPL	-	$0.35^{0.87}_{0.00}$	$0.33^{0.55}_{0.17}$	$1.53^{2.01}_{1.10}$	$0.52^{0.87}_{0.25}$	$1.66^{3.27}_{1.01}$	15.16/17
Ind (3")	4156*	MEPL	$0.00^{0.02}_{0.00}$	$0.77^{0.92}_{0.62}$	$0.52^{0.55}_{0.49}$	$1.61^{1.76}_{1.49}$	$0.40^{0.43}_{0.37}$	$2.04^{2.44}_{1.71}$	190.43/172
Ind (25")	4156	MEPL	-	$0.16^{0.23}_{0.12}$	$0.56^{0.57}_{0.55}$	$1.30^{1.38}_{1.22}$	$1.17^{1.25}_{1.11}$	$1.51^{1.67}_{1.39}$	258.47/206
SMF0	All	MEPL	-	$0.75^{0.90}_{0.61}$	$0.52^{0.55}_{0.49}$	$1.62^{1.75}_{1.49}$	$0.40^{0.43}_{0.39}$	$2.02^{2.40}_{1.70}$	209.89/195
NGC 1052									
Ind	093630101	ME2PL	-	$13.77^{15.78}_{11.95}$	$0.62^{0.69}_{0.51}$	$1.24^{1.35}_{1.11}$	$1.05^{1.13}_{0.97}$	$6.09^{4.55}_{4.79}$	269.16/234
Ind	306230101	ME2PL	-	$9.30^{9.82}_{8.79}$	$0.50^{0.55}_{0.45}$	$1.30^{1.36}_{1.24}$	$1.05^{1.09}_{1.01}$	$7.20^{8.14}_{6.34}$	799.19/822
Ind	553300301	ME2PL	-	$8.96^{9.39}_{8.54}$	$0.61^{0.64}_{0.57}$	$1.38^{1.43}_{1.32}$	$1.09^{1.14}_{1.06}$	$10.16^{11.31}_{9.10}$	923.38/869
Ind	553300401*	ME2PL	-	$9.47^{9.86}_{9.09}$	$0.53^{0.61}_{0.48}$	$1.43^{1.48}_{1.38}$	$1.10^{1.14}_{1.06}$	$12.02^{13.32}_{10.82}$	1006.47/937
Ind (3")	5910	ME2PL	-	$5.33^{6.86}_{3.84}$	$0.64^{0.69}_{0.58}$	$1.21^{1.46}_{1.05}$	$0.37^{0.47}_{0.37}$	$0.57^{1.06}_{0.35}$	261.04/226
Ind (25")	5910	ME2PL	-	$8.13^{11.49}_{5.36}$	$0.61^{0.65}_{0.57}$	$1.25^{1.50}_{1.00}$	$0.49^{0.66}_{0.49}$	$0.61^{1.21}_{0.19}$	319.40/269
SMF2	093630101	ME2PL	-	$14.14^{15.77}_{12.66}$	$0.59^{0.61}_{0.57}$	$1.36^{1.39}_{1.33}$	$1.09^{1.11}_{1.06}$	$8.06^{8.89}_{7.31}$	3043.69/2886
	306230101			$9.80^{10.26}_{9.36}$				$8.38^{8.97}_{7.82}$	1.0e-24
	553300301			$8.75^{9.11}_{8.40}$				$9.74^{10.40}_{9.11}$	
	553300401			$9.21^{9.55}_{8.88}$				$10.41^{11.11}_{9.75}$	

Table A.2. (Cont.)

Analysis	ObsID	Model	N_{H1}	N_{H2}	kT	Γ	$Norm_1$	$Norm_2$	$\chi^2/d.o.f$
(1)	(2)	(3)	(4)	(5)	keV	(7)	(10 ⁻⁴)	(10 ⁻⁴)	F-test
(1)	(2)	(3)	(4)	(5)	(6)	(7)	(8)	(9)	(10)
NGC 1961									
Ind	0673170101*	ME2PL	0.00 ^{0.08} _{0.00}	20.83 ^{33.49} _{13.41}	0.63 ^{0.67} _{0.58}	2.00 ^{2.50} _{1.89}	0.34 ^{0.52} _{0.34}	1.44 ^{3.96} _{0.84}	69.32/70
Ind	0673170301	ME2PL	0.00 ^{0.05} _{0.00}	9.88 ^{18.23} _{5.67}	0.56 ^{0.61} _{0.49}	1.84 ^{2.27} _{1.60}	0.31 ^{0.41} _{0.31}	0.80 ^{1.43} _{0.35}	85.39/62
SMF0	All	ME2PL	-	15.60 ^{22.74} _{10.82}	0.60 ^{0.63} _{0.56}	1.95 ^{2.08} _{1.81}	0.37 ^{0.40} _{0.34}	1.07 ^{1.55} _{0.71}	165.72/142
NGC 2681									
Ind	2060*	MEPL	0.11 ^{0.26} _{0.00}	-	0.64 ^{0.71} _{0.56}	1.67 ^{1.86} _{1.45}	0.12 ^{0.18} _{0.07}	0.07 ^{0.08} _{0.06}	43.34/36
Ind	2061	MEPL	0.00 ^{0.16} _{0.00}	-	0.63 ^{0.68} _{0.56}	1.61 ^{1.78} _{1.41}	0.06 ^{0.07} _{0.06}	0.07 ^{0.08} _{0.06}	29.71/33
SMF0	All	MEPL	0.07 ^{0.19} _{0.00}	-	0.64 ^{0.69} _{0.58}	1.73 ^{1.89} _{1.55}	0.09 ^{0.12} _{0.06}	0.07 ^{0.08} _{0.06}	81.23/72
NGC 2787									
Ind (25'')	0200250101	PL	-	-	-	1.61 ^{1.66} _{1.55}	-	-	146.28/98
Ind (3'')	4689	PL	0.09 ^{0.18} _{0.03}	-	-	2.21 ^{2.58} _{1.95}	-	-	20.72/21
Ind (25'')	4689	PL	0.01 ^{0.07} _{0.00}	-	-	1.70 ^{1.98} _{1.59}	-	-	42.31/48
NGC 2841									
Ind	0201440101	MEPL	0.82 ^{0.95} _{0.68}	-	0.29 ^{0.34} _{0.25}	1.76 ^{1.97} _{1.60}	3327.57 ^{7082.60} _{368.14}	0.49 ^{0.57} _{0.43}	71.15/50
Ind (5'')	6096	MEPL	0.00 ^{0.68} _{0.00}	-	0.63 ^{0.74} _{0.44}	2.09 ^{2.52} _{1.86}	0.08 ^{0.27} _{0.06}	0.13 ^{0.16} _{0.11}	3.52/13
Ind (30'')	6096	MEPL	0.00 ^{0.45} _{0.00}	-	0.48 ^{0.61} _{0.25}	1.57 ^{1.75} _{1.43}	0.16 ^{0.21} _{0.12}	0.49 ^{0.55} _{0.43}	54.51/57
NGC 3608									
Ind	0099030101	ME2PL	-	9.69 ^{36.25} _{2.76}	0.60 ^{0.80} _{0.36}	2.13 ^{2.56} _{1.79}	0.21 ^{0.33} _{0.21}	0.92 ^{2.90} _{0.23}	6.30/8
Ind	0693300101*	ME2PL	-	13.77 ^{23.33} _{8.17}	0.40 ^{0.59} _{0.28}	2.11 ^{2.32} _{1.79}	0.21 ^{0.26} _{0.21}	0.95 ^{1.60} _{0.32}	89.32/55
SMF0	All	ME2PL	-	10.02 ^{15.64} _{6.26}	0.51 ^{0.60} _{0.35}	2.21 ^{2.38} _{2.03}	0.24 ^{0.26} _{0.22}	0.95 ^{1.40} _{0.62}	88.67/70
NGC 3718									
Ind	0200430501	2PL	1.02 ^{1.35} _{0.91}	0.01 ^{0.22} _{0.00}	-	1.76 ^{1.97} _{1.71}	0.21 ^{0.62} _{0.13}	5.56 ^{6.78} _{4.60}	129.94/104
Ind	0200431301*	2PL	0.08 ^{0.36} _{0.00}	0.96 ^{1.59} _{0.77}	-	1.67 ^{1.93} _{1.49}	0.31 ^{1.46} _{0.12}	4.23 ^{5.67} _{3.25}	56.16/71
Ind	3993	PL	0.95 ^{1.12} _{0.79}	-	-	1.73 ^{1.92} _{1.54}	-	-	51.98/48
Ind		2PL	3.08 ^{5.04} _{0.00}	0.87 ^{1.19} _{0.00}	-	2.15 ^{3.01} _{1.69}	8.74 ^{44.58} _{0.61}	6.77 ^{13.37} _{0.08}	49.04/43
SMF1	0200431301	2PL	0.09 ^{0.22} _{0.00}	1.10 ^{1.32} _{0.97}	-	1.79 ^{1.92} _{1.71}	0.32 ^{0.67} _{0.17}	5.11 ^{6.24} _{4.45}	237.70/224
	0200430501							5.31 ^{6.48} _{4.61}	1.0e-17
	3993							8.06 ^{9.92} _{7.02}	
NGC 4261									
Ind	834	ME2PL	0.18 ^{0.47} _{0.06}	11.89 ^{16.01} _{9.31}	0.58 ^{0.60} _{0.56}	2.11 ^{3.07} _{1.52}	0.29 ^{0.55} _{0.19}	4.72 ^{25.76} _{1.60}	110.82/80
Ind (3'')	9569*	ME2PL	0.18 ^{0.47} _{0.08}	8.40 ^{10.20} _{6.90}	0.57 ^{0.58} _{0.56}	1.24 ^{1.51} _{1.07}	0.26 ^{0.37} _{0.20}	2.13 ^{4.57} _{1.18}	198.74/157
Ind (25'')	9569	ME2PL	-	9.03 ^{12.90} _{6.55}	0.61 ^{0.62} _{0.60}	1.16 ^{1.39} _{0.89}	0.35 ^{0.47} _{0.35}	0.64 ^{1.11} _{0.29}	382.42/218
SMF0	All	ME2PL	0.18 ^{0.31} _{0.09}	9.38 ^{10.84} _{7.96}	0.57 ^{0.58} _{0.56}	1.87 ^{2.19} _{1.55}	0.27 ^{0.34} _{0.21}	2.70 ^{4.86} _{1.49}	312.57/247
Ind	0056340101	ME2PL	0.08 ^{0.15} _{0.01}	11.97 ^{14.73} _{9.31}	0.63 ^{0.64} _{0.61}	1.84 ^{2.22} _{1.45}	0.72 ^{0.94} _{0.54}	2.82 ^{6.30} _{1.11}	278.12/255
Ind	0502120101*	ME2PL	0.04 ^{0.07} _{0.00}	9.71 ^{11.14} _{8.30}	0.64 ^{0.65} _{0.64}	1.75 ^{1.97} _{1.54}	0.64 ^{0.74} _{0.55}	2.30 ^{3.65} _{1.40}	563.80/461
SMF0	All	ME2PL	0.04 ^{0.08} _{0.01}	10.28 ^{11.56} _{9.02}	0.64 ^{0.65} _{0.63}	1.76 ^{1.95} _{1.57}	0.67 ^{0.76} _{0.58}	2.36 ^{3.54} _{1.53}	855.28/726
NGC 4278									
Ind (3'')	7077*	MEPL	0.31 ^{0.58} _{0.05}	0.01 ^{0.03} _{0.00}	0.27 ^{0.38} _{0.19}	2.06 ^{2.15} _{1.99}	0.80 ^{6.21} _{0.18}	0.98 ^{1.06} _{0.90}	144.23/158
Ind (25'')	7077	MEPL	0.16 ^{0.45} _{0.01}	-	0.30 ^{0.37} _{0.21}	1.88 ^{1.95} _{1.83}	0.81 ^{3.96} _{0.28}	1.32 ^{1.39} _{1.27}	250.15/210
Ind	7081	MEPL	-	-	0.63 ^{0.68} _{0.57}	2.03 ^{2.10} _{1.99}	0.12 ^{0.14} _{0.09}	0.77 ^{0.82} _{0.75}	155.54/145
Ind	7080	MEPL	0.22 ^{0.71} _{0.00}	-	0.47 ^{0.61} _{0.18}	2.10 ^{2.25} _{2.03}	0.24 ^{13.76} _{0.07}	0.69 ^{0.79} _{0.65}	102.53/96
Ind	0205010101	PL	0.02 ^{0.03} _{0.02}	-	-	2.04 ^{2.08} _{2.01}	-	-	562.25/529
SMF1	7077	MEPL	-	-	0.58 ^{0.62} _{0.48}	2.05 ^{2.11} _{2.03}	0.11 ^{0.12} _{0.10}	0.97 ^{1.02} _{0.82}	414.71/415
	7081							0.78 ^{0.82} _{0.77}	6.7e-46
	7080							0.68 ^{0.72} _{0.65}	
NGC 4374									
Ind	0673310101	ME2PL	0.01 ^{0.02} _{0.00}	269.73 ^{462.21} _{79.23}	0.62 ^{0.63} _{0.61}	2.02 ^{2.08} _{1.93}	1.06 ^{1.23} _{1.06}	20.74 ^{1161.27} _{1.99}	283.99/282
Ind	803	MEPL	0.45 ^{0.79} _{0.00}	0.17 ^{0.28} _{0.10}	0.30 ^{0.60} _{0.18}	2.06 ^{2.42} _{1.79}	0.87 ^{10.78} _{0.06}	0.45 ^{0.61} _{0.34}	35.48/36
Ind	5908*	PL	0.10 ^{0.13} _{0.07}	-	-	2.18 ^{2.32} _{2.13}	-	-	78.73/87
		MEPL	0.00 ^{0.39} _{0.00}	0.10 ^{0.13} _{0.06}	0.54 ^{0.71} _{0.21}	2.07 ^{2.22} _{1.93}	0.06 ^{0.53} _{0.03}	0.83 ^{0.95} _{0.72}	67.73/81

Table A.2. (Cont.)

Analysis	ObsID	Model	N_{H1}	N_{H2}	kT keV	Γ	$Norm_1$ (10^{-4})	$Norm_2$ (10^{-4})	$\chi^2/d.o.f$ F-test
(1)	(2)	(3)	(4)	(5)	(6)	(7)	(8)	(9)	(10)
Ind (2'')	6131	MEPL	0.00 ^{0.20} _{0.00}	0.00 ^{0.09} _{0.00}	0.60 ^{0.66} _{0.54}	1.48 ^{1.81} _{1.32}	0.11 ^{0.13} _{0.09}	0.14 ^{0.18} _{0.12}	33.27/28
Ind (25'')	6131	MEPL	-	-	0.55 ^{0.57} _{0.53}	1.95 ^{2.09} _{1.856}	2.07 ^{2.16} _{1.97}	0.90 ^{0.98} _{0.81}	160.27/114
SMF1	5908	MEPL	0.02 ^{0.14} _{0.00}	0.09 ^{0.15} _{0.08}	0.59 ^{0.64} _{0.51}	1.98 ^{2.11} _{1.89}	0.10 ^{0.13} _{0.07}	0.80 ^{0.88} _{0.73}	161.08/154
	803							0.39 ^{0.44} _{0.35}	3.02e-55
	6131							0.22 ^{0.25} _{0.20}	
NGC 4494									
Ind	0071340301*	PL	-	-	-	1.76 ^{1.83} _{1.68}	-	-	115.04/74
Ind (3'')	2079	PL	-	-	-	1.66 ^{1.94} _{1.51}	-	-	19.32/21
Ind (20'')	2079	PL	0.00 ^{0.03} _{0.00}	-	-	1.49 ^{1.68} _{1.38}	-	-	69.38/43
SMF1		0071340301	-			1.81 ^{1.89} _{1.74}	0.36 ^{0.38} _{0.35}		117.35/86
		2079					0.24 ^{0.27} _{0.23}		6.9e-09
NGC 4636									
Ind	0111190201*	MEPL	-	-	0.53 ^{0.55} _{0.52}	2.47 ^{2.74} _{2.27}	7.93 ^{8.13} _{7.64}	1.01 ^{1.20} _{0.88}	280.73/176
Ind	0111190701	MEPL	-	-	0.55 ^{0.55} _{0.54}	2.58 ^{2.64} _{2.52}	8.07 ^{8.15} _{7.99}	1.01 ^{1.06} _{0.96}	958.65/344
SMF0	All	MEPL	-	-	0.55 ^{0.55} _{0.54}	2.58 ^{2.64} _{2.52}	8.05 ^{8.13} _{7.98}	1.02 ^{1.07} _{0.97}	1260.17/529
NGC 4736									
Ind	0094360601	MEPL	0.00 ^{0.04} _{0.00}	-	0.48 ^{0.51} _{0.45}	1.66 ^{1.70} _{1.64}	1.59 ^{1.73} _{1.47}	4.27 ^{4.43} _{4.10}	337.72/297
Ind	0094360701	MEPL	0.01 ^{0.09} _{0.00}	0.00 ^{0.01} _{0.00}	0.43 ^{0.52} _{0.31}	1.70 ^{1.80} _{1.60}	1.51 ^{1.74} _{10.23}	4.00 ^{4.31} _{3.67}	100.34/100
Ind	0404980101*	MEPL	0.00 ^{0.01} _{0.00}	-	0.55 ^{0.57} _{0.54}	1.66 ^{1.68} _{1.64}	1.61 ^{1.68} _{1.55}	3.87 ^{3.95} _{3.79}	562.21/587
Ind (1.5'')	808	MEPL	0.33 ^{0.49} _{0.27}	0.04 ^{0.09} _{0.02}	0.55 ^{0.61} _{0.47}	2.00 ^{2.25} _{1.88}	0.32 ^{0.80} _{0.23}	0.53 ^{0.67} _{0.51}	66.80/86
Ind (20'')	808	MEPL	-	-	0.51 ^{0.53} _{0.49}	1.57 ^{1.60} _{1.55}	1.28 ^{1.34} _{1.21}	3.07 ^{3.14} _{2.99}	232.63/232
SMF0	All	MEPL	-	-	0.54 ^{0.55} _{0.52}	1.66 ^{1.68} _{1.65}	1.60 ^{1.66} _{1.55}	3.95 ^{4.01} _{3.88}	1051.57/1002
NGC 5195									
Ind	0112840201	MEPL	0.42 ^{0.51} _{0.31}	-	0.29 ^{0.34} _{0.25}	1.58 ^{1.70} _{1.45}	4.74 ^{8.95} _{2.34}	0.37 ^{0.42} _{0.32}	131.59/102
Ind	0212480801*	MEPL	0.03 ^{0.10} _{0.00}	0.00 ^{0.04} _{0.00}	0.58 ^{0.63} _{0.50}	1.49 ^{1.60} _{1.41}	0.57 ^{0.73} _{0.50}	0.53 ^{0.58} _{0.48}	174.79/126
Ind	0303420101	MEPL	0.48 ^{0.53} _{0.37}	-	0.28 ^{0.32} _{0.26}	1.41 ^{1.54} _{1.30}	6.17 ^{8.69} _{3.08}	0.35 ^{0.39} _{0.31}	249.19/143
Ind	0303420201	MEPL	0.39 ^{0.52} _{0.29}	-	0.31 ^{0.38} _{0.26}	1.39 ^{1.53} _{1.26}	3.70 ^{8.21} _{1.93}	0.34 ^{0.39} _{0.29}	177.87/111
Ind	0677980701	MEPL	0.63 ^{0.79} _{0.45}	0.00 ^{0.06} _{0.00}	0.25 ^{0.35} _{0.18}	1.68 ^{2.08} _{1.51}	12.14 ^{57.71} _{3.71}	0.46 ^{0.55} _{0.37}	34.82/30
SMF1	0112840201	MEPL	-	-	0.61 ^{0.63} _{0.60}	1.51 ^{1.57} _{1.46}	0.55 ^{0.61} _{0.53}	0.36 ^{0.39} _{0.33}	639.89/533
	0212480801							0.51 ^{0.55} _{0.48}	6.8e-12
	0303420101							0.38 ^{0.40} _{0.35}	
	0303420201							0.37 ^{0.40} _{0.34}	
	0677980701							0.45 ^{0.51} _{0.40}	
Ind (3'')	13813	MEPL	0.40 ^{0.65} _{0.16}	0.95 ^{2.83} _{0.00}	0.61 ^{0.67} _{0.53}	1.53 ^{2.95} _{1.01}	0.22 ^{0.36} _{0.08}	0.10 ^{0.95} _{0.04}	47.08/50
Ind (20'')	13813	MEPL	0.23 ^{0.31} _{0.14}	0.04 ^{0.17} _{0.00}	0.57 ^{0.60} _{0.52}	1.73 ^{2.09} _{1.47}	0.42 ^{0.57} _{0.31}	0.12 ^{0.17} _{0.09}	129.49/107
Ind	13812	MEPL	0.41 ^{0.63} _{0.00}	0.18 ^{0.73} _{0.08}	0.62 ^{0.83} _{0.48}	1.37 ^{1.79} _{1.19}	0.11 ^{0.25} _{0.03}	0.11 ^{0.21} _{0.08}	59.03/50
SFM0	All	MEPL	0.37 ^{0.49} _{0.19}	0.15 ^{0.69} _{0.06}	0.62 ^{0.67} _{0.57}	1.27 ^{1.61} _{1.11}	0.14 ^{0.21} _{0.08}	0.07 ^{0.12} _{0.06}	134.19/106
NGC 5813									
Ind	5907	MEPL	0.42 ^{0.63} _{0.26}	0.00 ^{2.33} _{0.00}	0.27 ^{0.35} _{0.21}	3.98 ⁰ ₀	0.52 ^{2.26} _{0.11}	0.04 ^{0.19} _{0.01}	19.61/20
Ind (3'')	9517	MEPL	0.00 ^{0.11} _{0.00}	-	0.56 ^{0.60} _{0.48}	2.05 ^{2.32} _{1.72}	0.13 ^{0.20} _{0.12}	0.05 ^{0.07} _{0.04}	50.12/39
Ind (25'')	9517	MEPL	0.09 ^{0.22} _{0.00}	0.00 ^{0.93} _{0.00}	0.54 ^{0.63} _{0.45}	2.04 ^{3.61} _{1.34}	0.10 ^{0.17} _{0.07}	0.03 ^{0.08} _{0.02}	27.74/16
Ind	12951	MEPL	0.08 ^{0.18} _{0.00}	0.00 ^{0.28} _{0.00}	0.64 ^{0.69} _{0.60}	3.92 ⁰ ₀	0.12 ^{0.21} _{0.10}	0.05 ^{0.17} _{0.04}	49.45/24
Ind	12952*	MEPL	0.10 ^{0.19} _{0.00}	-	0.60 ^{0.65} _{0.53}	2.35 ^{2.60} _{2.09}	0.14 ^{0.19} _{0.10}	0.06 ^{0.07} _{0.05}	53.22/48
Ind	13253	MEPL	0.00 ^{0.12} _{0.00}	0.18 ^{0.48} _{0.00}	0.62 ^{0.65} _{0.58}	2.44 ^{3.00} _{1.59}	0.13 ^{0.18} _{0.11}	0.08 ^{0.18} _{0.04}	59.76/43
Ind	13255	MEPL	0.29 ^{0.49} _{0.15}	1.71 ^{4.86} _{0.58}	0.33 ^{0.59} _{0.25}	2.60 ⁰ _{1.10}	0.63 ^{1.78} _{0.13}	0.20 ^{1.10} _{0.09}	21.43/15
SMF0	All	MEPL	0.01 ^{0.07} _{0.00}	0.06 ^{0.17} _{0.00}	0.60 ^{0.62} _{0.57}	2.40 ^{2.87} _{2.01}	0.12 ^{0.13} _{0.11}	0.07 ^{0.09} _{0.05}	260.993/213
Ind	0302460101	MEPL	0.01 ^{0.02} _{0.00}	0 ^{0.03} _{0.00}	0.58 ^{0.59} _{0.57}	2.10 ^{2.33} _{2.00}	7.12 ^{7.30} _{6.77}	0.53 ^{0.65} _{0.48}	436.83/251
Ind	0554680201	MEPL	0.01 ^{0.01} _{0.00}	0.00 ^{0.01} _{0.00}	0.60 ^{0.60} _{0.61}	1.88 ^{2.04} _{1.74}	7.28 ^{7.49} _{7.15}	0.47 ^{0.56} _{0.40}	687.18/329
Ind	0554680301*	MEPL	0.00 ^{0.01} _{0.00}	-	0.59 ^{0.60} _{0.59}	1.66 ^{1.77} _{1.48}	7.19 ^{7.31} _{7.11}	0.44 ^{0.50} _{0.35}	849.57/334

Table A.2. (Cont.)

Analysis	ObsID	Model	N_{H1}	N_{H2}	kT	Γ	$Norm_1$	$Norm_2$	$\chi^2/d.o.f$
(1)	(2)	(3)	(4)	(5)	keV	(7)	(10 ⁻⁴)	(10 ⁻⁴)	F-test
(1)	(2)	(3)	(4)	(5)	(6)	(7)	(8)	(9)	(10)
SMF0	All	MEPL	0.01 ^{0.01} _{0.00}	0.01 ^{0.01} _{0.00}	0.59 ^{0.60} _{0.59}	1.95 ^{2.01} _{1.91}	7.17 ^{7.28} _{7.07}	0.51 ^{0.58} _{0.49}	1937.02/918
NGC 5982									
Ind	0673770401	MEPL	-	-	0.53 ^{0.56} _{0.49}	1.28 ^{1.50} _{0.99}	0.81 ^{0.93} _{0.76}	0.23 ^{0.29} _{0.17}	65.24/64
Ind	0693300301*	MEPL	-	-	0.52 ^{0.54} _{0.50}	1.52 ^{1.78} _{1.21}	0.76 ^{0.80} _{0.72}	0.16 ^{0.20} _{0.11}	186.37/117
SMF1	0693300301	MEPL	-	-	0.52 ^{0.54} _{0.50}	1.34 ^{1.52} _{1.15}	0.79 ^{0.82} _{0.75}	0.13 ^{0.16} _{0.10}	260.60/189
	0673770401							0.26 ^{0.31} _{0.21}	3.3e-9

Notes. (Col. 1) kind of analysis performed, where Ind refers to the individual fitting of the observation, SMF0 is the simultaneous fit without varying parameters, SMF1 is the simultaneous fit varying one parameter and SMF2 is the simultaneous fit varying two parameters, (Col. 2) obsID, where the * represents the data that are used as a reference model for the simultaneous fit, (Col. 3) best-fit model, (Col. 4, 5, 6, 7, 8 and 9) parameters in the model, where N_H are in units of 10^{22} cm^{-2} , and (Col. 10) $\chi^2/d.o.f$ and in SMF x (where $x = 1, 2$) the result of the F-test is presented in the second line.

Table A.3. X-ray luminosities.

Name	Satellite	ObsID	Individual		Simultaneous	
			log(L(0.5-2 keV))	log(L(2-10 keV))	log(L(0.5-2 keV))	log(L(2-10 keV))
(1)	(2)	(3)	(4)	(5)	(6)	(7)
NGC 315	<i>XMM</i> -Newton	0305290201	41.46 ^{41.47} _{41.44}	41.55 ^{41.57} _{41.52}		
	<i>Chandra</i>	855	41.31 ^{41.43} _{41.15}	41.55 ^{41.63} _{41.47}	41.38 ^{41.40} _{41.37}	41.58 ^{41.61} _{41.55}
	<i>Chandra</i> (3'')	4156	41.38 ^{41.39} _{41.37}	41.58 ^{41.61} _{41.56}	41.38 ^{41.40} _{41.37}	41.58 ^{41.61} _{41.55}
	<i>Chandra</i> (25'')	4156	41.44 ^{41.45} _{41.44}	41.68 ^{41.700} _{41.66}		
NGC 1052	<i>XMM</i> -Newton	093630101	40.96 ^{40.97} _{40.94}	41.46 ^{41.47} _{41.45}	40.99 ^{41.00} _{40.99}	41.47 ^{41.49} _{41.46}
	<i>XMM</i> -Newton	306230101	40.96 ^{40.97} _{40.95}	41.48 ^{41.49} _{41.48}	41.01 ^{41.01} _{41.00}	41.49 ^{41.49} _{41.48}
	<i>XMM</i> -Newton	553300301	41.10 ^{41.11} _{41.10}	41.56 ^{41.56} _{41.55}	41.06 ^{41.07} _{41.06}	41.55 ^{41.55} _{41.54}
	<i>XMM</i> -Newton	553300401	41.12 ^{41.13} _{41.11}	41.55 ^{41.56} _{41.55}	41.09 ^{41.09} _{41.08}	41.57 ^{41.58} _{41.57}
	<i>Chandra</i> (3'')	5910	40.19 ^{40.20} _{40.17}	41.29 ^{41.29} _{41.27}	-	-
	<i>Chandra</i> (25'')	5910	40.29 ^{40.31} _{40.27}	41.34 ^{41.37} _{41.30}	-	-
NGC 1961	<i>XMM</i> -Newton	0673170101	41.20 ^{41.22} _{41.18}	41.27 ^{41.31} _{41.22}	41.20 ^{41.21} _{41.18}	41.23 ^{41.27} _{41.20}
	<i>XMM</i> -Newton	0673170301	41.42 ^{41.44} _{41.40}	41.01 ^{41.06} _{40.97}	41.20 ^{41.21} _{41.18}	41.23 ^{41.27} _{41.20}
NGC 2681	<i>Chandra</i>	2060	39.11 ^{39.13} _{39.08}	38.89 ^{38.97} _{38.80}	39.02 ^{39.04} _{38.99}	38.93 ^{38.99} _{38.87}
	<i>Chandra</i>	2061	38.95 ^{38.97} _{38.92}	38.95 ^{39.02} _{38.86}	39.02 ^{39.04} _{38.99}	38.93 ^{38.99} _{38.87}
NGC 2787	<i>XMM</i> -Newton	0200250101	39.13 ^{39.15} _{39.12}	39.49 ^{39.52} _{39.47}		
	<i>Chandra</i> (3'')	4689	38.95 ^{38.99} _{38.90}	38.86 ^{38.94} _{38.76}		
	<i>Chandra</i> (25'')	4689	39.15 ^{39.18} _{39.11}	39.34 ^{39.41} _{39.26}		
NGC 2841	<i>XMM</i> -Newton	0201440101	39.74 ^{39.76} _{39.72}	39.75 ^{39.79} _{39.71}		
	<i>Chandra</i> (5'')	6096	39.22 ^{39.27} _{39.17}	39.16 ^{39.29} _{38.98}		
	<i>Chandra</i> (30'')	6096	39.71 ^{39.73} _{39.68}	39.86 ^{39.92} _{39.78}		
NGC 3608	<i>XMM</i> -Newton	0099030101	39.65 ^{39.69} _{39.62}	40.37 ^{40.41} _{40.33}	40.32 ^{40.34} _{40.30}	40.24 ^{40.28} _{40.19}
	<i>XMM</i> -Newton	0693300101	40.33 ^{40.35} _{40.31}	40.31 ^{40.35} _{40.26}	40.32 ^{40.34} _{40.30}	40.24 ^{40.28} _{40.19}
NGC 3718	<i>XMM</i> -Newton	0200430501	40.65 ^{40.67} _{40.63}	40.84 ^{40.86} _{40.82}	40.66 ^{40.68} _{40.64}	40.86 ^{40.88} _{40.83}
	<i>XMM</i> -Newton	0200431301	40.42 ^{40.44} _{40.39}	40.85 ^{40.87} _{40.82}	40.64 ^{40.66} _{40.62}	40.84 ^{40.87} _{40.82}
	<i>Chandra</i> (3'')	3993	40.76 ^{40.79} _{40.72}	41.01 ^{41.14} _{40.84}	40.83 ^{40.86} _{40.81}	40.99 ^{41.02} _{40.97}
	<i>Chandra</i> (25'')	3993	40.75 ^{40.78} _{40.72}	41.02 ^{41.15} _{40.24}		
NGC 4261	<i>Chandra</i>	834	41.18 ^{41.20} _{41.16}	41.11 ^{41.27} _{40.86}	40.98 ^{40.98} _{40.97}	41.02 ^{41.06} _{40.97}
	<i>Chandra</i> (3'')	9569	40.92 ^{40.94} _{40.91}	41.00 ^{40.89} _{41.08}	40.98 ^{40.98} _{40.97}	41.02 ^{41.06} _{40.97}
	<i>Chandra</i> (25'')	9569	40.79 ^{40.81} _{40.78}	40.97 ^{40.99} _{40.94}		

Table A.3. (Cont.)

Name	Satellite	ObsID	Individual		Simultaneous	
			log(L(0.5-2 keV))	log(L(2-10 keV))	log(L(0.5-2 keV))	log(L(2-10 keV))
(1)	(2)	(3)	(4)	(5)	(6)	(7)
	<i>XMM</i> –Newton	0056340101	41.30 ^{41.31} _{41.29}	41.19 ^{41.21} _{41.17}	41.14 ^{41.15} _{41.14}	41.13 ^{41.15} _{41.11}
	<i>XMM</i> –Newton	0502120101	41.22 ^{41.23} _{41.22}	41.15 ^{41.16} _{41.14}	41.14 ^{41.15} _{41.14}	41.13 ^{41.15} _{41.11}
NGC 4278	<i>Chandra</i> (3'')	7077	39.87 ^{39.88} _{39.87}	39.76 ^{39.98} _{39.32}	39.86 ^{39.87} _{39.86}	39.82 ^{39.84} _{39.81}
	<i>Chandra</i> (25'')	7077	40.14 ^{40.17} _{40.10}	40.06 ^{40.08} _{40.04}	-	-
	<i>Chandra</i>	7081	39.31 ^{39.32} _{39.30}	39.27 ^{39.29} _{39.24}	39.78 ^{39.79} _{39.77}	39.73 ^{39.75} _{39.72}
	<i>Chandra</i>	7080	39.78 ^{39.81} _{39.74}	39.62 ^{40.73}	39.73 ^{39.74} _{39.72}	39.67 ^{39.69} _{39.65}
	<i>XMM</i> –Newton	0205010101	40.73 ^{40.74} _{40.73}	40.77 ^{40.78} _{40.76}	-	-
NGC 4374	<i>Chandra</i>	803	39.95 ^{40.02} _{39.86}	39.53 ^{39.60} _{39.44}	39.83 ^{39.85} _{39.82}	39.82 ^{39.86} _{39.78}
	<i>Chandra</i>	5908	39.83 ^{39.86} _{39.80}	39.80 ^{39.84} _{39.75}	39.57 ^{39.59} _{39.55}	39.51 ^{39.55} _{39.47}
	<i>Chandra</i>	6131	39.30 ^{39.35} _{39.24}	39.39 ^{39.46} _{39.30}	39.39 ^{39.42} _{39.36}	39.28 ^{39.32} _{39.23}
	<i>Chandra</i> (25'')	6131	40.39 ^{40.40} _{40.38}	39.98 ^{40.09} _{39.83}		
	<i>XMM</i> –Newton	0673310101	41.30 ^{41.30} _{41.29}	41.31 ^{41.33} _{41.28}		
NGC 4494	<i>XMM</i> –Newton	0071340301	39.29 ^{39.31} _{39.27}	39.50 ^{39.54} _{39.46}	39.26 ^{39.28} _{39.25}	39.48 ^{39.57} _{39.36}
	<i>Chandra</i> (3'')	2079	39.13 ^{39.19} _{39.06}	39.37 ^{39.46} _{39.25}	39.10 ^{39.14} _{39.07}	39.29 ^{39.41} _{39.13}
	<i>Chandra</i> (20'')	2079	39.29 ^{39.34} _{39.23}	39.65 ^{39.73} _{39.54}		
NGC 4636	<i>XMM</i> –Newton	0111190201	40.85 ^{40.86} _{40.84}	39.89 ^{39.94} _{39.85}	40.86 ^{40.86} _{40.86}	39.81 ^{39.83} _{39.80}
	<i>XMM</i> –Newton	0111190701	40.87 ^{40.87} _{40.86}	39.05 ^{39.05} _{39.04}	40.86 ^{40.86} _{40.86}	39.81 ^{39.83} _{39.80}
NGC 4736	<i>XMM</i> –Newton	0094360601	39.63 ^{39.64} _{39.63}	39.75 ^{39.77} _{39.73}	39.61 ^{39.61} _{39.61}	39.73 ^{39.74} _{39.72}
	<i>XMM</i> –Newton	0094360701	39.59 ^{39.61} _{39.58}	39.73 ^{39.76} _{39.69}	39.61 ^{39.61} _{39.61}	39.73 ^{39.74} _{39.72}
	<i>XMM</i> –Newton	0404980101	39.74 ^{39.75} _{39.74}	39.77 ^{39.78} _{39.76}	39.61 ^{39.61} _{39.61}	39.73 ^{39.74} _{39.72}
	<i>Chandra</i>	808	38.80 ^{38.84} _{38.76}	38.60 ^{38.64} _{38.54}		
	<i>Chandra</i> (20'')	808	39.50 ^{39.51} _{39.50}	39.66 ^{39.67} _{39.64}		
NGC5195	<i>XMM</i> –Newton	0112840201	39.86 ^{39.88} _{39.85}	39.17 ^{39.21} _{39.12}	39.22 ^{39.24} _{39.20}	39.19 ^{39.22} _{39.15}
	<i>XMM</i> –Newton	0212480801	39.29 ^{39.31} _{39.28}	39.39 ^{39.42} _{39.35}	39.28 ^{39.30} _{39.26}	39.34 ^{39.37} _{39.31}
	<i>XMM</i> –Newton	0303420101	39.44 ^{39.45} _{39.43}	39.39 ^{39.43} _{39.35}	39.23 ^{39.24} _{39.21}	39.20 ^{39.23} _{39.17}
	<i>XMM</i> –Newton	0303420201	39.76 ^{39.77} _{39.74}	39.23 ^{39.26} _{39.18}	39.22 ^{39.24} _{39.20}	39.20 ^{39.23} _{39.16}
	<i>XMM</i> –Newton	0677980701	40.19 ^{40.23} _{40.15}	39.19 ^{39.26} _{39.10}	39.26 ^{39.28} _{39.23}	39.28 ^{39.33} _{39.23}
	<i>Chandra</i> (3'')	13813	38.77 ^{38.83} _{38.71}	38.59 ^{38.66} _{38.49}	38.59 ^{38.61} _{38.56}	38.61 ^{38.64} _{38.57}
	<i>Chandra</i> (20'')	13813	39.00 ^{39.03} _{38.97}	38.55 ^{38.65} _{38.44}		
	<i>Chandra</i>	13812	38.60 ^{38.66} _{38.52}	38.66 ^{38.72} _{38.57}	38.59 ^{38.61} _{38.56}	38.61 ^{38.64} _{38.57}
NGC5813	<i>Chandra</i>	5907	40.09 ^{40.25} _{39.83}	39.32 ^{39.58} _{38.65}	39.68 ^{39.72} _{39.63}	39.07 ^{39.15} _{38.95}
	<i>Chandra</i> (3'')	9517	39.69 ^{39.72} _{39.66}	39.15 ^{39.24} _{39.02}	39.68 ^{39.72} _{39.63}	39.07 ^{39.16} _{38.95}
	<i>Chandra</i> (30'')	9517	39.53 ^{39.56} _{39.49}	39.03 ^{39.16} _{38.83}		
	<i>Chandra</i>	12951	39.67 ^{39.80} _{39.48}	39.02 ^{39.16} _{38.78}	39.68 ^{39.72} _{39.63}	39.07 ^{39.16} _{38.95}
	<i>Chandra</i>	12952	39.73 ^{39.76} _{39.69}	39.00 ^{39.10} _{38.88}	39.68 ^{39.72} _{39.63}	39.07 ^{39.16} _{38.95}
	<i>Chandra</i>	13253	39.74 ^{39.81} _{39.66}	39.09 ^{39.22} _{38.91}	39.68 ^{39.72} _{39.63}	39.07 ^{39.16} _{38.95}
	<i>Chandra</i>	13255	39.36 ^{39.43} _{39.29}	39.30 ^{39.42} _{39.14}	39.68 ^{39.72} _{39.63}	39.07 ^{39.16} _{38.95}
	<i>XMM</i> –Newton	0302460101	41.32 ^{41.33} _{41.32}	40.23 ^{40.26} _{40.19}	41.33 ^{41.33} _{41.32}	40.30 ^{40.32} _{40.28}
	<i>XMM</i> –Newton	0554680201	41.52 ^{41.52} _{41.51}	40.84 ^{40.87} _{40.82}	41.33 ^{41.33} _{41.32}	40.30 ^{40.32} _{40.28}
	<i>XMM</i> –Newton	0554680301	41.32 ^{41.33} _{41.32}	40.38 ^{40.40} _{40.35}	41.33 ^{41.33} _{41.32}	40.30 ^{40.32} _{40.28}
NGC 5892	<i>XMM</i> –Newton	0673770401	40.73 ^{40.75} _{40.71}	40.68 ^{40.73} _{40.61}	40.73 ^{40.73} _{40.70}	40.61 ^{40.66} _{40.54}
	<i>XMM</i> –Newton	0693300301	40.67 ^{40.68} _{40.66}	40.11 ^{40.17} _{40.05}	40.67 ^{40.68} _{40.65}	40.32 ^{40.37} _{40.27}

Notes. (Cols. 4 and 5) soft and hard intrinsic luminosities for individual fits, and (Cols. 6 and 7) soft and hard intrinsic luminosities for simultaneous fitting. Blanks mean observations that are not used for the simultaneous fittings.

Table A.4. Results for the best fit of the annular region (ring) in *Chandra* data, and the best fit obtained for the nucleus of *XMM*–Newton data when the contribution from the annular region was removed.

Name (obsID)	Region	Model	N_{H1} (10^{22} cm^{-2})	N_{H2} (10^{22} cm^{-2})	kT (keV)	Γ	χ^2_r	$\log(L_{\text{soft}})$ (0.5–2 keV)	$\log(L_{\text{hard}})$ (2–10 keV)	Cont. %
(1)	(2)	(3)	(4)	(5)	(6)	(7)	(8)	(9)	(10)	(11)
NGC 315 (4156)	Ring*	MEPL	-	-	$0.59^{0.61}_{0.57}$	$1.47^{1.63}_{1.31}$	1.49	41.13	40.88	3
NGC 315 (0305290201)	Nucleus**	MEPL	-	$0.77^{1.08}_{0.47}$	$0.53^{0.59}_{0.45}$	$1.96^{2.20}_{1.74}$	0.97	41.41	41.43	-
NGC 1052 (5910)	Ring*	ME2PL	-	$26.10^{38.14}_{16.93}$	$0.31^{0.39}_{0.28}$	$1.98^{2.23}_{1.71}$	1.47	40.185	40.563	10
NGC 1052 (093630101)	Nucleus**	ME2PL	-	$7.54^{9.98}_{5.20}$	$0.78^{0.89}_{0.68}$	$1.69^{1.86}_{1.50}$	1.13	39.875	41.235	-
NGC 2787 (4689)	Ring*	PL	$0.00^{0.05}_{0.00}$	-	-	$1.59^{1.92}_{1.43}$	1.05	38.82	39.23	53
NGC 2787 (0200250101)	Nucleus**	PL	-	-	-	$1.65^{1.77}_{1.54}$	1.49	39.12	39.47	-
NGC 2841 (6096)	Ring*	PL	$0.02^{0.11}_{0.00}$	-	-	$1.96^{2.45}_{1.72}$	1.09	39.54	39.60	60
NGC 2841 (0201440101)	Nucleus**	MEPL	$0.43^{0.51}_{0.00}$	-	$0.31^{0.60}_{0.19}$	$2.19^{2.34}_{1.93}$	1.41	39.73	39.77	-
NGC 4261 (9569)	Ring*	MEPL	$0.06^{0.11}_{0.03}$	$0.00^{0.04}_{0.00}$	$0.61^{0.62}_{0.59}$	$1.87^{2.07}_{1.70}$	2.07	40.663	40.252	37
NGC 4261 (0502120101)	Nucleus**	ME2PL	-	$8.29^{9.89}_{7.28}$	$0.67^{0.68}_{0.65}$	$1.56^{1.72}_{1.41}$	1.21	40.857	41.051	-
NGC 4278 (7077)	Ring*	MEPL	-	-	$0.29^{0.36}_{0.19}$	$1.61^{1.71}_{1.51}$	1.12	39.551	39.707	38
NGC 4278 (0205010101)	Nucleus**	PL	$0.02^{0.03}_{0.02}$	-	-	$2.05^{2.10}_{2.03}$	1.05	40.681	40.736	-
NGC 4374 (6131)	Ring*	MEPL	-	-	$0.54^{0.56}_{0.52}$	$2.11^{2.23}_{1.98}$	1.41	40.36	39.78	84
NGC 4374 (0673310101)	Nucleus**	MEPL	-	-	$0.71^{0.74}_{0.68}$	$1.57^{1.80}_{1.33}$	1.06	40.00	39.76	-
NGC 4494 (2079)	Ring*	ME	-	-	$4.00_{3.34}$	-	3.23	38.76	38.88	21
NGC 4494 (0071340301)	Nucleus**	PL	-	-	-	$1.76^{1.83}_{1.68}$	1.54	39.25	39.54	-
NGC 4736 (808)	Ring*	MEPL	-	-	$0.52^{0.54}_{0.49}$	$1.50^{1.54}_{1.47}$	1.12	39.41	39.60	84
NGC 4736 (0404980101)	Nucleus**	MEPL	-	-	$0.62^{0.65}_{0.59}$	$2.03^{2.10}_{1.97}$	0.93	39.15	39.04	-
NGC 5195 (13813)	Ring*	ME	$0.32^{0.37}_{0.27}$	-	$0.54^{0.58}_{0.50}$	-	1.35	39.00	37.18	74
NGC 5195 (0677980701)	Nucleus**	MEPL	$0.66^{0.90}_{0.41}$	-	$0.23^{0.36}_{0.14}$	$1.71^{1.95}_{1.46}$	1.11	39.17	39.14	-
NGC 5813 (9517)	Ring*	MEPL	-	-	$0.59^{0.60}_{0.58}$	$2.29^{2.47}_{2.10}$	1.55	41.08	40.22	100
NGC 5813 (0554680301)	Nucleus**	MEPL	-	-	$0.71^{0.72}_{0.70}$	$0.54^{2.15}_{0.00}$	1.78	40.85	40.05	-

Notes (Col. 1) name and obsID in parenthesis, (Col. 2) extracted region, (Col. 3) best-fit model, (Col. 4, 5, 6, 7 and 8) parameters of the best-fit model, (Col. 9 and 10) soft and hard intrinsic luminosities, and (Col. 11) the percentage of the contribution from the ring to the r_{ext} aperture *Chandra* data in the 0.5–10.0 keV band.

*Spectral parameters of the annular region in *Chandra* data.

**Spectral parameters of the nuclear region in *XMM*–Newton data when the spectral parameters of the ring from *Chandra* data are included in the fit.

Table A.5. Simultaneous fittings taking into account the contribution from the annular region given in Table A.4.

ObsID	N_{H1} (10^{22} cm^{-2})	N_{H2} (10^{22} cm^{-2})	kT (keV)	Γ	$Norm_1$ (10^{-4})	$Norm_2$ (10^{-4})	$\chi^2/d.o.f$	$\log(L_{\text{soft}})$ (0.5–2 keV)	$\log(L_{\text{hard}})$ (2–10 keV)
(1)	(2)	(3)	(4)	(5)	(6)	(7)	(8)	(9)	(10)
NGC 315									
0305290201	-	$0.86^{1.00}_{0.73}$	$0.52^{0.55}_{0.50}$	$1.85^{1.96}_{1.74}$	$0.42^{0.44}_{0.39}$	$2.38^{2.77}_{2.05}$	467.58/379	$41.44^{41.55}_{41.43}$	$41.54^{41.55}_{41.52}$
4156	-	-	-	-	-	-	-	$41.44^{41.55}_{41.43}$	$41.51^{41.53}_{41.49}$
NGC 1052									
0093630101	-	$6.11^{7.18}_{5.07}$	$0.68^{0.73}_{0.63}$	$1.58^{1.70}_{1.47}$	$0.48^{0.53}_{0.44}$	$1.28^{1.69}_{0.95}$	577.98/477	$40.35^{40.36}_{40.34}$	$41.33^{41.35}_{41.32}$
5910	-	-	-	-	-	-	-	$40.35^{40.36}_{40.34}$	$41.27^{41.28}_{41.26}$
NGC 4261									
0502120101	$0.03^{0.08}_{0.00}$	$7.64^{8.74}_{6.58}$	$0.60^{0.61}_{0.59}$	$1.55^{1.75}_{1.36}$	$0.22^{0.26}_{0.19}$	$1.53^{2.25}_{1.04}$	972.83/627	$40.84^{40.84}_{40.84}$	$41.03^{41.05}_{41.01}$
9569	-	-	-	-	-	-	-	$40.84^{40.85}_{40.83}$	$40.99^{41.01}_{40.97}$
NGC 4278									
0205010101	$0.03^{0.03}_{0.02}$	-	-	$2.11^{2.14}_{2.08}$	$7.74^{7.95}_{7.54}$	-	844.93/690	$40.71^{40.72}_{40.71}$	$40.71^{40.72}_{40.70}$

Table A.5. (Cont.)

ObsID	N_{H1} (10^{22} cm^{-2})	N_{H2} (10^{22} cm^{-2})	kT (keV)	Γ	$Norm_1$ (10^{-4})	$Norm_2$ (10^{-4})	$\chi^2/d.o.f$	$\log(L_{soft})$ (0.5-2 keV)	$\log(L_{hard})$ (2-10 keV)
(1)	(2)	(3)	(4)	(5)	(6)	(7)	(8)	(9)	(10)
7077					1.15 ^{1.18} _{1.11}			39.89 ^{39.89} _{39.88}	39.86 ^{39.87} _{39.84}
NGC 4494									
0071340301	0.00 ^{0.01} _{0.00}			1.81 ^{1.89} _{1.74}	0.36 ^{0.38} _{0.35}		117.35/86	39.26 ^{39.28} _{39.25}	41.85 ^{42.08} _{41.29}
2079					0.24 ^{0.27} _{0.23}		39.10 ^{39.14} _{39.07}	41.85 ^{42.08} _{41.28}	

Notes. (Col. 1) name and obsID in parenthesis, (Col. 2, 3, 4, 5, 6 and 7) parameters of the best-fit model, (Col. 8) $\chi^2/d.o.f$, and (Col. 9 and 10) soft and hard intrinsic luminosities.

Table A.6. Statistics of the light curves.

Name	ObsID	Energy	$\chi^2/d.o.f$	Prob.(%)	σ_{NXS}^2	$< \sigma_{NXS}^2 >$
(1)	(2)	(3)	(4)	(5)	(6)	(7)
NGC 315	4156	0.5-10	50.2/55	34	<0.0046	
		0.5-2			<0.0086	
		2-10			0.0096 \pm 0.0059	
NGC 1052	0306230101	0.5-10	57.1/49	80	<0.0012	
		0.5-2			<0.0039	
		2-10			<0.0018	
	0553300301	0.5-10	49.5/46	66	<0.0012	
		0.5-2			<0.0037	
		2-10			<0.0016	
	0553300401	0.5-10	39.3/49	16	<0.0011	
		0.5-2			<0.0037	
		2-10			<0.0016	
	5910	0.5-10	48.6/59	17	<0.0046	
		0.5-2			<0.0160	
		2-10			<0.0070	
NGC 2681	2060	0.5-10 (1)	109.8/80	98	<0.0450	< 0.0302
		0.5-10 (2)			<0.0403	
		0.5-2 (1)			<0.0517	< 0.0344
	2061	0.5-10	133.0/78	100	<0.0447	
		0.5-2			<0.0510	
		2-10			<0.5007	
		0.5-10			<0.0357	
NGC 2787	4689	0.5-10	33.4/30	70	<0.0357	
		0.5-2			<0.0464	
		2-10			<0.1732	
NGC 3226	860	0.5-10	51.2/45	76	0.0367 \pm 0.0227	
		0.5-2			0.0838 \pm 0.0649	
		2-10			<0.0784	
NGC 4261	834	0.5-10	35.8/34	62	<0.0063	
		0.5-2			<0.0079	
		2-10			<0.0306	
	9569	0.5-10 (1)	85.7/100	15	<0.0072	< 0.0051
		0.5-10 (2)			<0.0072	
		0.5-2 (1)			<0.0095	< 0.0068
		0.5-2 (2)			<0.0097	

Table A.6. (Cont.)

Name	ObsID	Energy	$\chi^2/d.o.f$	Prob.(%)	σ_{NXS}^2	$\langle \sigma_{NXS}^2 \rangle$
(1)	(2)	(3)	(4)	(5)	(6)	(7)
		2-10 (1)			<0.0285	< 0.0198
		2-10 (2)			<0.0274	
NGC 4278	7077	0.5-10 (1)	124.3/111	82	<0.0076	< 0.0052
		0.5-10 (2)			<0.0070	
		0.5-2 (1)			<0.0093	< 0.0062
		0.5-2 (2)			<0.0083	
		2-10 (1)			<0.0461	< 0.0307
		2-10 (2)			<0.0406	
	7081	0.5-10 (1)	91.4/107	14	<0.0090	< 0.0062
		0.5-10 (2)			<0.0086	
		0.5-2 (1)			<0.0109	< 0.0075
		0.5-2 (2)			<0.0104	
		2-10 (1)			<0.0538	< 0.0361
		2-10 (2)			<0.0482	
	7080	0.5-10	41.0/55	8	<0.0095	
		0.5-2			<0.0116	
		2-10			<0.0573	
NGC 4374	5908	0.5-10	77.8/46	97	0.0089 ± 0.0048	
		0.5-2			0.0094 ± 0.0061	
		2-10			<0.0540	
	6131	0.5-10	38.1/39	49	<0.0278	
		0.5-2			<0.0325	
		2-10			<0.1785	
NGC 4636	0111190701	0.5-10	40.9/56	7	<0.0005	
		0.5-2			<0.0005	
		2-10			0.0278 ± 0.0201	
NGC 4736	0404980101	0.5-10	50.5/39	94	0.0005 ± 0.0003	
		0.5-2			0.0005 ± 0.0004	
		2-10			0.0030 ± 0.0015	
	808	0.5-10	89.64/35	100	0.0082 ± 0.0063	
		0.5-2			0.0137 ± 0.0078	
		2-10			<0.0788	
NGC 5195	13813	0.5-10(1)	247.4/179	100	<0.1059	< 0.0393
		0.5-10 (2)			<0.0672	
		0.5-10 (3)			<0.0631	
		0.5-10 (4)			<0.0709	
		0.5-2 (1)			<0.1544	< 0.0557
		0.5-2 (2)			<0.0957	
		0.5-2 (3)			<0.0876	
		0.5-2 (4)			<0.0950	
		2-10 (1)			<0.4636	< 0.1640
		2-10 (2)			<0.2457	
		2-10 (3)			<0.2805	
		2-10 (4)			<0.2758	
	13812	0.5-10 (1)	231.4/157	100	<0.0626	0.0116 ± 0.0004
		0.5-10 (2)			0.0437 ± 0.0285	
		0.5-10 (3)			<0.0512	
		0.5-2 (1)			<0.0890	0.0189 ± 0.0011
		0.5-2 (2)			0.0764 ± 0.0434	
		0.5-2 (3)			<0.0756	
		2-10 (1)			<0.2172	< 0.1203
		2-10 (2)			<0.2260	

Table A.6. (Cont.)

Name	ObsID	Energy	$\chi^2/d.o.f$	Prob.(%)	σ_{NXS}^2	$\langle \sigma_{NXS}^2 \rangle$	
(1)	(2)	(3)	(4)	(5)	(6)	(7)	
NGC5813	5907	2-10 (3)			<0.1787		
		0.5-10	31.6/48	4	<0.0417		
		0.5-2			<0.0447		
	9517	2-10				<1.1984	
		0.5-10 (1)	100.4/97	61	<0.0415	< 0.0294	
		0.5-10 (2)			<0.0417		
		0.5-2 (1)			<0.0440	< 0.0320	
		0.5-2 (2)			<0.0464		
		2-10 (1)			<0.7487	< 0.6505	
		2-10 (2)			<1.0640		
	12951	0.5-10	73.8/73	55	<0.0487		
		0.5-2			<0.0538		
		2-10			<1.6736		
	12952	0.5-10 (1)	165.7/142	91	<0.0445	< 0.0264	
		0.5-10 (2)			<0.0464		
		0.5-10 (3)			<0.0464		
		0.5-2 (1)			<0.0480	< 0.0284	
		0.5-2 (2)			<0.0494		
		0.5-2 (3)			<0.0498		
		2-10 (1)			<1.0246	< 0.7446	
		2-10 (2)			<1.5137		
		2-10 (3)			<1.2842		
		13253	0.5-10 (1)	129.8/117	80	<0.0482	< 0.0321
0.5-10 (2)				<0.0424			
0.5-2 (1)				<0.0533	< 0.0347		
0.5-2 (2)				<0.0445			
2-10 (1)				<0.6305	< 0.7111		
2-10 (2)				<1.2749			
13255	0.5-10	46.5/42	71	< 0.0487			
	0.5-2			<0.0556			
	2-10			<0.7024			

Notes. (Col. 1) name, (Col. 2) obsID, (Col. 3) energy band in keV, (Cols. 4 and 5) $\chi^2/d.o.f$ and the probability of being variable in the 0.5-10.0 keV energy band of the total light curve, (Col. 6) normalized excess variance, σ_{NXS}^2 , and (Col. 8) the mean value of the normalised excess variance, $\langle \sigma_{NXS}^2 \rangle$, for each light curve and energy band.

Appendix B: Notes and comparisons with previous results for individual objects

B.1. NGC 315

NGC 315 is a radiogalaxy located in the Zwicky cluster 0107.5+3212. It was classified optically as a type 1.9 LINER by Ho et al. (1997), and as an AGN candidate at X-ray frequencies (González-Martín et al. 2009b).

At radio frequencies (*VLBI* and *VLA*) the galaxy shows an asymmetric morphology, with a compact nuclear emission and a one-sided jet (Venturi et al. 1993). The jet can also be observed in X-rays (see Appendix C). Using *VLA* data, Ishwara-Chandra & Saikia (1999) did not find significant variability over a timescale of ~ 12 years.

In X-rays, it was observed twice with *Chandra* in 2000 and 2003 and once with *XMM-Newton* in 2005. Younes et al. (2011) found variations in Γ (from $1.5^{+0.1}$ to $2.1_{-0.2}^{+0.1}$), and a decreasing in the hard luminosity of 53% between 2003 and 2005. They included the emission of the jet in *XMM-Newton* data to derive the nuclear spectral parameters. With the same data set, we obtained very similar individual spectral fittings and luminosities (see Table A.2 and A.3 for *Chandra* data and Table A.4 for the nuclear region in *XMM-Newton* data). However, we do not find spectral variations, since SMF0 was used both for *Chandra* data and when comparing *Chandra* and *XMM-Newton*. The difference found with the results reported by Younes et al. (2011) might be due to the different errors. A large set of X-ray observations would be desirable to obtain conclusive results.

XMM-Newton data were used to study short term variations. From its PSD analysis, González-Martín & Vaughan (2012) did not find them in any of the energy bands (soft, hard, total). From the light curve in the 0.5–10 keV energy band, Younes et al. (2011) reported no variations. We found $\sigma_{NXS}^2 > 0$ at 1.6 σ confidence level in the 2–10 keV energy band, consistent with no variability.

At UV frequencies, Younes et al. (2012) derived the luminosities from the OM onboard *XMM-Newton* with UVW2 and UVM2 filters, that agree with our results. Variability can not be studied since OM data are only available at one epoch.

B.2. NGC 1052

It is the brightest elliptical galaxy in the Cetus I group. Previously classed as a LINER in the pioneering work by Heckman (1980), it was classified optically as a type 1.9 LINER (Ho et al. 1997), and as an AGN candidate at X-ray frequencies (González-Martín et al. 2009b). *VLA* data show a core-dominated and a two-sided jet structure at radio frequencies (Vermeulen et al. 2003).

NGC 1052 was observed twice with *Chandra* and five times with *XMM-Newton*. Long term variability studies are not found in the literature. We find variations due to the nuclear power, $Norm_2$ (49%) and the column density, N_{H2} (31%), both at hard energies, in an eight years period.

González-Martín & Vaughan (2012) studied short term variations from the PSD with *XMM-Newton* data with null results in any of the energy bands. We analysed *Chandra* and *XMM-Newton* light curves and variations were not found. Short term variations were previously studied with other instruments; Guainazzi et al. (2000) studied *BeppoSAX* data and did not find short term variations. The most recent observation in X-rays reported so far is a 100 ks observation taken with *Suzaku* in 2007, the derived spectral characteristics reported by Brenneman et al.

(2009) appear to be similar to those from *XMM-Newton*, which are compatible with the values in González-Martín et al. (2009b), Brightman & Nandra (2011), and this paper (intrinsic luminosity of $\log(L(2-10 \text{ keV})) \sim 41.5$), and no variations along the observation.

In the UV range, Maoz et al. (2005) studied this galaxy with *HST ACS* and found a factor of 2 decrease in the flux of the source between the 1997 data reported by Pogge et al. (2000) and their 2002 dataset. We found a factor of 1.3 UV flux variations using *XMM-OM* data in a seven months period.

B.3. NGC 1961

NGC 1961 is one of the most massive spiral galaxies known (Rubin et al. 1979). It was classified as a type 2 LINER by Ho et al. (1997). *MERLIN* and *EVN* data show a core plus two sided jet structure for this source at radio frequencies (Krips et al. 2007), what makes it a suitable AGN candidate.

This galaxy was observed once with *Chandra* in 2010, and twice with *XMM-Newton* in 2011. X-ray variability from these data was not studied before. We did not find variations in one month period.

No information in the UV is found for this object in the literature.

B.4. NGC 2681

The nucleus of this galaxy was classified optically as a type 1.9 LINER (Ho et al. 1997). Classified as an AGN and as a *Compton-thick* candidate in X-rays (González-Martín et al. 2009b,a), a nuclear counterpart at radio frequencies has not been detected (Nagar et al. 2005).

The source was observed twice with *Chandra* in January and May 2001. Younes et al. (2011) did not find short time scale variations from the analysis of the light curves neither long term variations from the spectral analysis. These results agree with our variability analysis.

At UV frequencies, no variations were found (Cappellari et al. 1999).

B.5. NGC 2787

The nucleus of NGC 2787 is surrounded by diffuse emission extending up to $\sim 30''$ (Terashima & Wilson 2003). It was optically classified as a type 1.9 LINER (Ho et al. 1997), and as an AGN candidate at X-ray frequencies (González-Martín et al. 2009b).

Nagar et al. (2005) detected a radio core with *VLA*, while evidence of a jet structure has not been found in the literature. Flux variations were obtained at 2 and 3.6 cm on timescales of months (Nagar et al. 2002).

In X-rays, this galaxy was observed twice with *Chandra* in 2000 (snapshot) and 2004, and once with *XMM-Newton* in 2004. Younes et al. (2011) found this to be a non-variable object at long timescales after correcting *XMM-Newton* data from contamination of the extranuclear emission in *XMM-Newton* data, we have not performed a simultaneous fit for this object.

From one *Chandra* light curve, Younes et al. (2011) calculated an upper limit of σ_{NXS}^2 with which our value agrees.

No UV data are found in the literature.

B.6. NGC 2841

Ho et al. (1997) optically classified NGC 2841 as a type 2 LINER. It was classified as an AGN candidate at X-ray frequencies by González-Martín et al. (2009b). This galaxy shows some X-ray sources in the surroundings (González-Martín et al. 2009b). A core structure was found with *VLA* by Nagar et al. (2005), without evidence of any jet structure.

NGC 2841 was observed twice with *Chandra* in 1999 (snapshot) and 2004, and once with *XMM-Newton* in 2004. We did not use in the analysis the snapshot *Chandra* data because it does not have enough count rate for the spectral analysis. Moreover, since the extranuclear emission in *Chandra* data contributed with 60% in the 0.5–10.0 keV energy band, we can not analyze the spectral variations in this source. No information on variability is reported in the literature for this source.

B.7. NGC 3226

NGC 3226 is a dwarf elliptical galaxy that is strongly interacting with the type 1.5 Seyfert NGC 3227, located at 2' in projected distance (see Figure C.19 in González-Martín et al. 2009b). NGC 3226 was optically classified by Ho et al. (1997) as a type 1.9 LINER, and as an AGN candidate at X-ray frequencies by González-Martín et al. (2009b). A compact source is detected with *VLA* (Nagar et al. 2005), without evidence of any jet structure.

This galaxy was observed twice with *Chandra* in 1999 and 2001 and four times with *XMM-Newton* from 2000 to 2006. The possible contamination of NGC 3227 avoids the analysis of long term variations. We refer the reader to HG13 for details on this subject.

We analysed one *Chandra* light curve and we obtain $\sigma_{NXS}^2 > 0$ below 2σ , consistent with no short term variations.

UV variations are not found in the literature. We found 11% variations in the UVW1 filter from OM data.

B.8. NGC 3608

NGC 3608 is a member of the Leo II group, which forms a non interacting pair with NGC 3607. It was optically classified as a type 2 LINER (Ho et al. 1997). No hard nuclear point source was detected in *Chandra* images (González-Martín et al. 2009b), thus it was classified in X-rays as a non-AGN candidate, and also it appears to be a *Compton-thick* candidate (González-Martín et al. 2009a). A compact nuclear source at radio frequencies has not been detected (Nagar et al. 2005).

This galaxy was observed once with *Chandra* and twice with *XMM-Newton* in 2000 and 2012. Variability studies are not found at any frequency in the literature. We did not find variations in the 12 years period analyzed.

B.9. NGC 3718

NGC 3718 has a distorted gas and a dusty disc, maybe caused by the interaction with a close companion (Krips et al. 2007). It was optically classified as a type 1.9 LINER (Ho et al. 1997). It shows a point like source in the 4.5–8.0 keV energy band (see Fig. B.1), and therefore we can classify it as an AGN candidate following González-Martín et al. (2009b).

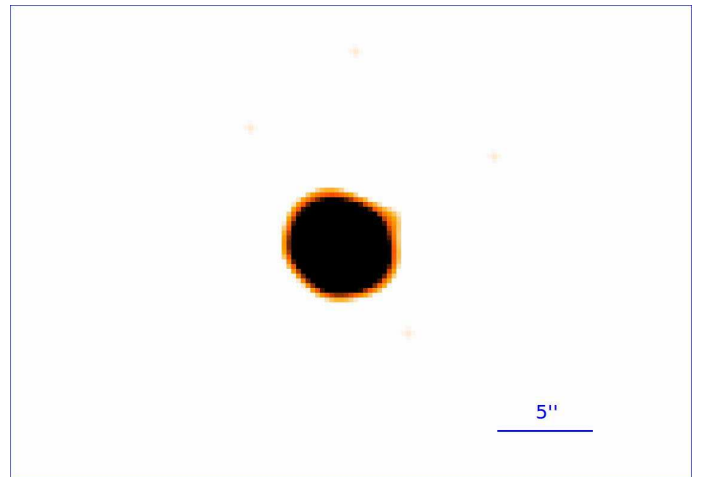


Fig. B.1: *Chandra* image in the 4.5–8.0 keV energy band of NGC 3718, where a point like source can be distinguished.

At radio frequencies, NGC 3718 was observed with the *VLA* by Nagar et al. (2005), and with *MERLIN* at 18 cm by Krips et al. (2007), where it shows a core and a compact jet. Nagar et al. (2002) reported radio variability at 2 cm with *VLA* data, although the result “is not totally reliable”.

In X-rays, this galaxy was observed once with *Chandra* in 1999 and twice with *XMM-Newton* in 2004. Younes et al. (2011) studied all the available data for this object and report it as variable. When jointly fit *Chandra* and *XMM-Newton* data, we found spectral variations in $Norm_2$ (37%).

Younes et al. (2011) did not find short term variations from the analysis of the lightcurves. We did not analyse short term variations because the length of the observations are < 30 ksec.

At UV frequencies, Younes et al. (2012) studied this galaxy with *XMM-Newton* but the nucleus was not detected, so they estimated upper limits for the flux in one epoch.

B.10. NGC 4261

Ho et al. (1997) optically classified this galaxy as a type 2 LINER. González-Martín et al. (2009b) classified it as an AGN candidate at X-ray frequencies. NGC 4261 contains a pair of symmetric kpc-scale jets (Birkinshaw & Davies 1985) and a nuclear disc of dust roughly perpendicular to the radio jet (Ferrarese et al. 1996).

It was observed twice with *Chandra*, in 2000 and 2008, and with *XMM-Newton* in another three epochs from 2001 to 2007. Long term variability studies are not found in the literature. We did not find variations in six years period.

Sambruna et al. (2003) found variations of 3-5 ksec in the 2–10 keV and 0.3–8.0 keV energy bands in the light curve from 2001, and argued in favour of these variations being more related to the inner X-ray jet than to an advection dominated accretion flow (ADAF), since the expected timescale for the light crossing time of an ADAF was ~ 2 orders of magnitude longer than the observed variability timescale. In HG13 we analysed the same observation in the 0.5–10 keV band, and reported it as non variable. However, we notice that $\sigma_{NXS}^2 = 0.109 \pm 0.099$ at 1σ confidence level. In the present paper we did not analyse this light curve since the net exposure time is shorter than 30 ksec. Other light curves were studied. González-Martín & Vaughan (2012) did not find short term variations from the PSD analysis of *XMM-Newton* data. In the present study we analysed two

Chandra observations and we can not confirm rapid variations in this source, since upper limits for the σ_{NXS}^2 were obtained in both cases.

No information from the UV is found in the literature. We found 10% (33%) variation in the UVW1(UVW2) filter.

B.11. NGC 4278

The north-northwest side of NGC 4278 is heavily obscured by large-scale dust-lanes, whose distribution show several dense knots interconnected by filaments (Carollo et al. 1997). It is an elliptical galaxy with a relatively weak, broad H_α line, that made Ho et al. (1997) classify it optically as a type 1.9 LINER. It was classified at X-ray frequencies as an AGN candidate (González-Martín et al. 2009b).

A two-sided jet is observed at radio frequencies with *VLBA* and *VLA* (Giroletti et al. 2005). Nagar et al. (2002) reported radio variability at 2 and 3.6 cm with *VLA* data. However, these results “are not totally reliable”.

In X-rays this galaxy was observed in nine occasions with *Chandra* from 2000 to 2010 and once with *XMM-Newton* in 2004. Brassington et al. (2009) used six *Chandra* observations and found 97 variable sources within NGC 4278, in a 4' elliptical area centered on the nucleus, none of them within the aperture we used for the nuclear extraction. Pellegrini et al. (2012) studied *Chandra* observations of NGC 4278 and found an X-ray luminosity decrease by a factor of ~ 18 between 2005 and 2010. Younes et al. (2010) detected a factor of ~ 3 flux increase on a timescale of a few months and a factor of 5 variation between the faintest and the brightest observations (separated by about three years). We used three of these observations (others were affected by pileup or did not met the minimum count number), our spectral fittings being in good agreement with theirs, although we found weaker variations in luminosities.

Whereas the different *Chandra* observations did not show short timescale variability, during the *XMM-Newton* observation Younes et al. (2010) found a 10% flux increase in few hours. With the same dataset, HG13 obtained a 3% variation in the same time range, the difference being most probably due to the different apertures used for the analysis (10'' vs 25'').

In the UV, Cardullo et al. (2008) found that the luminosity increased a factor of 1.6 in about six months using data from *HST* WFPC2/F218W.

B.12. NGC 4374

NGC 4374 is one of the brightest giant elliptical galaxies in the center of the Virgo cluster. Optically classified as a type 2 LINER (Ho et al. 1997), at X-ray frequencies it is a *Compton-thick* AGN candidate (González-Martín et al. 2009a,b).

At radio frequencies, it shows a core-jet structure, with two-sided jets emerging from its compact core (Xu et al. 2000). Nagar et al. (2002) reported flux variations at 3.6 cm with *VLA*, and variations at 2 cm which “are not fully reliable”.

This galaxy was observed four times with *Chandra*, twice in 2000 (ObsID 401 is a snapshot) and twice in 2005, and once with *XMM-Newton* in 2011. No information about variability in X-ray or UV is found in the literature. Here we report large variations at hard energies (73% in $Norm_2$).

We analysed two *Chandra* light curves, one of them with $\sigma_{NXS}^2 > 0$ below 2σ confidence level, which is compatible with no variations.

B.13. NGC 4494

NGC 4494 is a elliptical galaxy located in the Coma I cloud. It was optically classified as a type 2 LINER (Ho et al. 1997), and at X-rays as an AGN candidate (González-Martín et al. 2009b). The nucleus of this galaxy was not detected in radio with *VLA* data (Nagar et al. 2005).

This galaxy was observed twice with *Chandra* in 1999 (snapshot) and 2001, and once with *XMM-Newton* in 2001. Variability analyses are not found in the literature. We report the source as variable at X-ray frequencies.

B.14. NGC 4636

NGC 4636 was optically classified as a type 1.9 LINER by Ho et al. (1997). At X-rays it does not show emission at hard energies and therefore it was classified as a non-AGN candidate (González-Martín et al. 2009b). It was also classified as a *Compton-thick* candidate (González-Martín et al. 2009a).

At radio frequencies, it shows a compact core with *VLA* data (Nagar et al. 2005). Recently, Giacintucci et al. (2011) found bright jets at radio frequencies. No variations were found at 2 cm with *VLA* data (Nagar et al. 2002).

This galaxy was observed four times with *Chandra* data between 1999 and 2003, and three times with *XMM-Newton* between 2000 and 2001. O’Sullivan et al. (2005) studied the X-ray morphology of the galaxy and suggest that it can be the result of a past AGN that is actually quiescent. Long term variations were not found in the present analysis.

González-Martín & Vaughan (2012) did not find short term variations from the analysis of *XMM-Newton* light curves. From one *XMM-Newton* light curve, we found $\sigma_{NXS}^2 > 0$ at 1.4σ confidence level. We did not find long term variations.

No UV variability studies are found in the literature. Our analysis let us conclude that it is variable at UV frequencies.

B.15. NGC 4736

NGC 4736 is a Sab spiral galaxy, member of the Canes Venatici I (CVn I) Cloud (de Vaucouleurs 1975). Optically classified as a type 2 LINER (Ho et al. 1997), it is an AGN candidate at X-ray frequencies (González-Martín et al. 2009b). Nagar et al. (2005) reported an unresolved nuclear source at its nucleus, using 0.15'' resolution *VLA* data, without evidence of any jet structure.

This galaxy was observed three times with *Chandra* between 2000 and 2008 and three times with *XMM-Newton* between 2002 and 2006. No long term variability information is found in the literature. In the present work we did not find any variation in four years period.

It harbors a plethora of discrete X-ray sources in and around its nucleus (see Appendix C). Eracleous et al. (2002) studied *Chandra* data from 2000. They found a very dense cluster of ten discrete sources in the innermost 400×400 pc of the galaxy. They studied the brightest four sources (namely X-1 to X-4), and found that spectra are well described by a single power law with photon indices in the range 1.1–1.8, and 2–10 keV luminosities between $4 - 9 \times 10^{39}$ erg s^{-1} . They also studied short timescale variability from the analysis of the light curves. They estimated the normalised excess variance ($\sigma^2 = 0.06 \pm 0.04$) of the nucleus of NGC 4736 (X-2), and reported it as variable. The other sources also showed short-term variations (see Table 5 in Eracleous et al. 2002). They argued that there is no evidence for the presence of an AGN, and concluded that this LINER spectrum could be the result either from a current or

recent starburst or from an AGN. However, they noted that X-2 is the only source with an UV counterpart, detected by *HST*. González-Martín et al. (2009b) assigned X-2 to the nucleus of the galaxy, since it coincides with the 2MASS near-IR nucleus within $0.82''$.

By studying *BeppoSAX* and *ROSAT* data, Pellegrini et al. (2002) excluded variations of the 2–10 keV flux larger than $\sim 50\%$ on time scales of the order of one day. Comparing data from both instruments, they did not find variations between 1995 and 2000. They concluded that the X-ray emission is due to a recent starburst in NGC 4736. However, they mentioned that an extremely low luminosity AGN could still be present, though, due to the presence of a compact non-thermal radio source coincident with an X-ray faint central point source.

González-Martín & Vaughan (2012) studied the PSD of the *XMM*–Newton data from 2006 and found no short term variations.

We analysed *Chandra* and *XMM*–Newton light curves. Variations were found but in all cases below 2σ confidence level, in agreement with Eracleous et al. (2002).

At UV frequencies, Maoz et al. (2005) found long term variations between 1993 and 2003, the nucleus being 2.5 times brighter in 2003. From the OM data, we found variations of 66% in the U filter between 2002 and 2006.

B.16. NGC 5195

NGC 5195 is tidally interacting with a companion SB0 galaxy NGC 5194 (M51). It was optically classified as a type 2 LINER by Ho et al. (1997). It shows a point like source in the 4.5–8.0 keV energy band (see Fig. B.2), and therefore we can classify it as an AGN candidate following González-Martín et al. (2009b). A radio counterpart was found by Ho & Ulvestad (2001) with *VLA* data at 6 and 20 cm, without any jet indications.

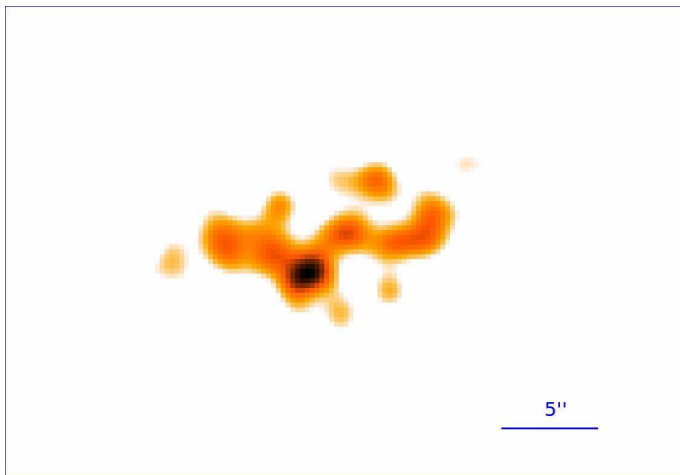


Fig. B.2: *Chandra* image of NGC 5195 in the 4.5–8.0 keV energy band, where a point like source can be distinguished.

This source was observed eight times with *Chandra* between 2000 and 2012, and five times with *XMM*–Newton between 2003 and 2011. Terashima & Wilson (2004) studied *Chandra* data from 2000 and 2001 and found neither long term, nor short term variability in the full, soft, nor hard energy bands. Since the *Chandra* observations from 2000 and 2001 were rejected from our sample because of the low number counts, we can not com-

pare our spectral fittings with theirs. However, our estimation of the luminosity in *Chandra* data agrees with their results. We found this object to be variable on long timescales, whereas short term variations were not detected.

At UV frequencies, no references are found in the literature. We found variations in the UVW1 filter.

B.17. NGC 5813

NGC 5813 is one of the galaxies in the group catalogue by de Vaucouleurs (1975), with NGC 5846 being the brightest member of the group. It was classified as a type 2 LINER by Ho et al. (1997). The X-ray morphology is extremely diffuse, with very extended emission at softer energies and without emission above 4 keV, what made González-Martín et al. (2009b) classify it as a non-AGN candidate. It was also classified as *Compton*-thick candidate (González-Martín et al. 2009a). At radio frequencies, it shows a compact core (Nagar et al. 2005) and a jet-like structure (Randall et al. 2011).

This source was observed nine times with *Chandra* between 2005 and 2011, and three times with *XMM*–Newton between 2005 and 2009. Variability studies at X-ray and UV frequencies are not reported in the literature. We did not find either long term or short term variations in X-rays. UV variations were found in the UVW1 filter.

B.18. NGC 5982

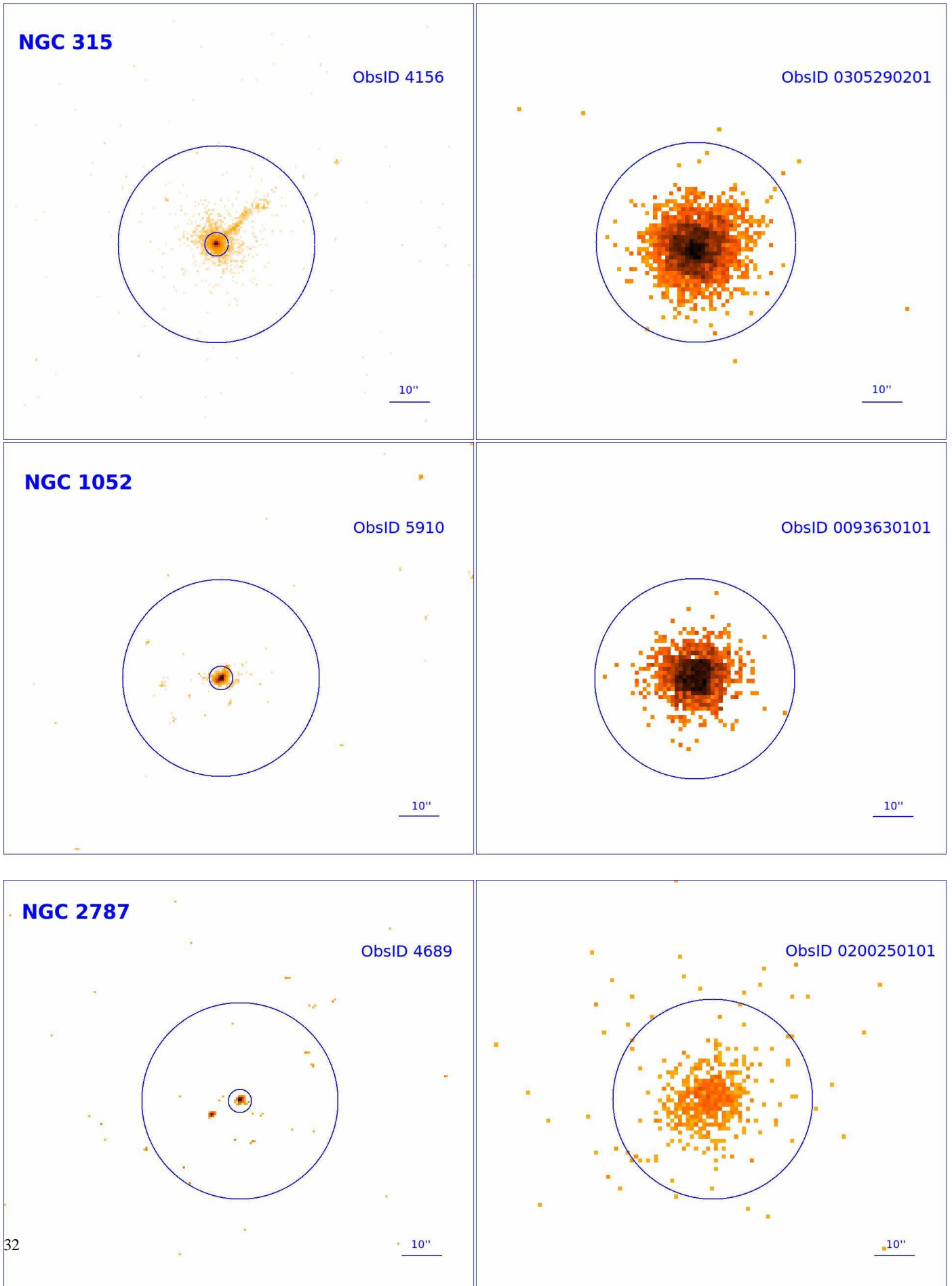
NGC 5982 is the brightest galaxy in the LGG 402 group, which is composed by four members (Garcia 1993). Recently, Vrtilik et al. (2013) using *GMRT* 610 MHz observations found a compact radio core in the position of the source, indicating an AGN-like object; jets were not detected.

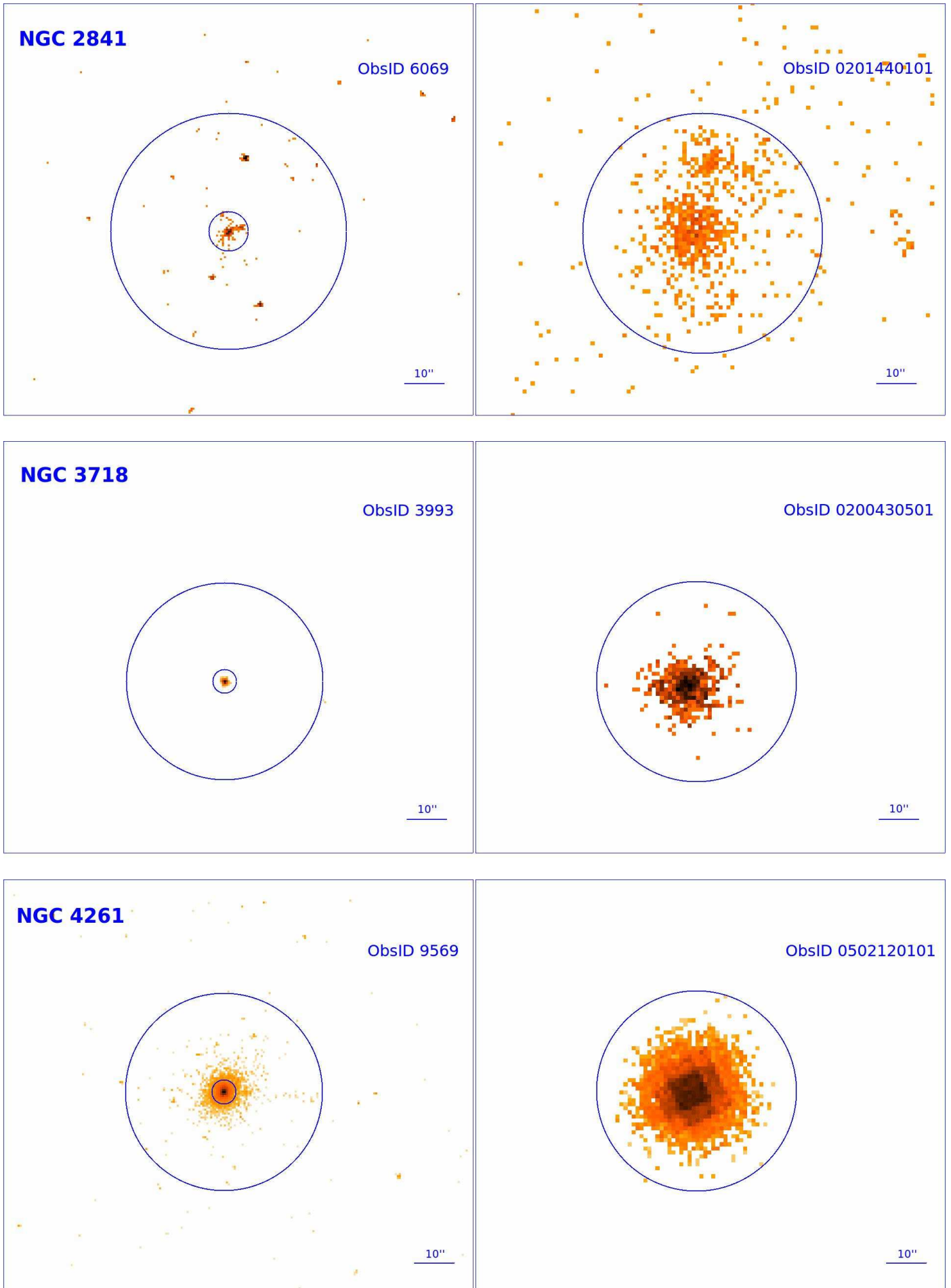
This galaxy was observed twice with *XMM*–Newton in 2011 and 2012. Variability studies are not reported in the literature. We found variations in the nuclear power (50%) in a one year period, whereas UV variations were not found.

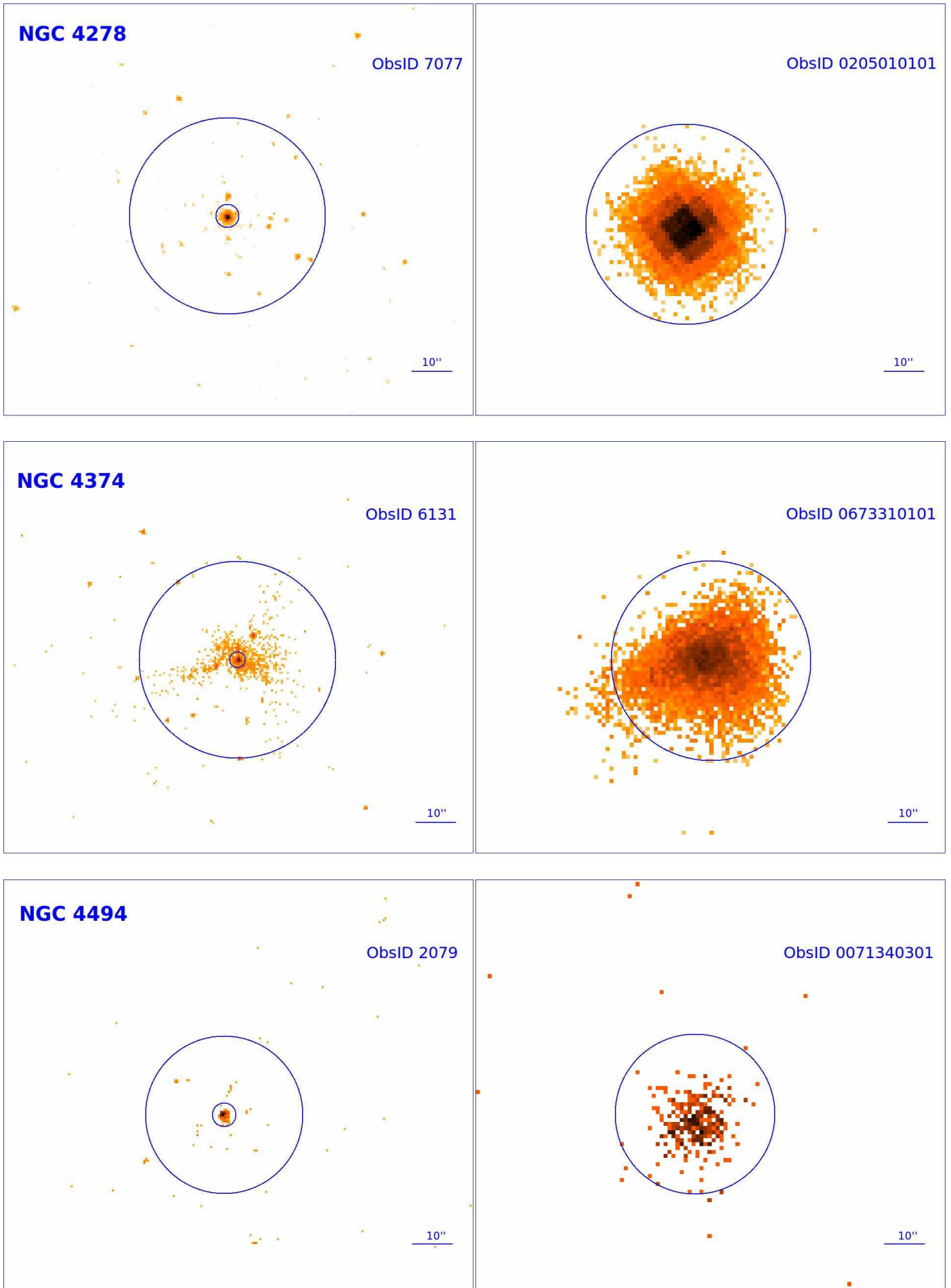
Appendix C:

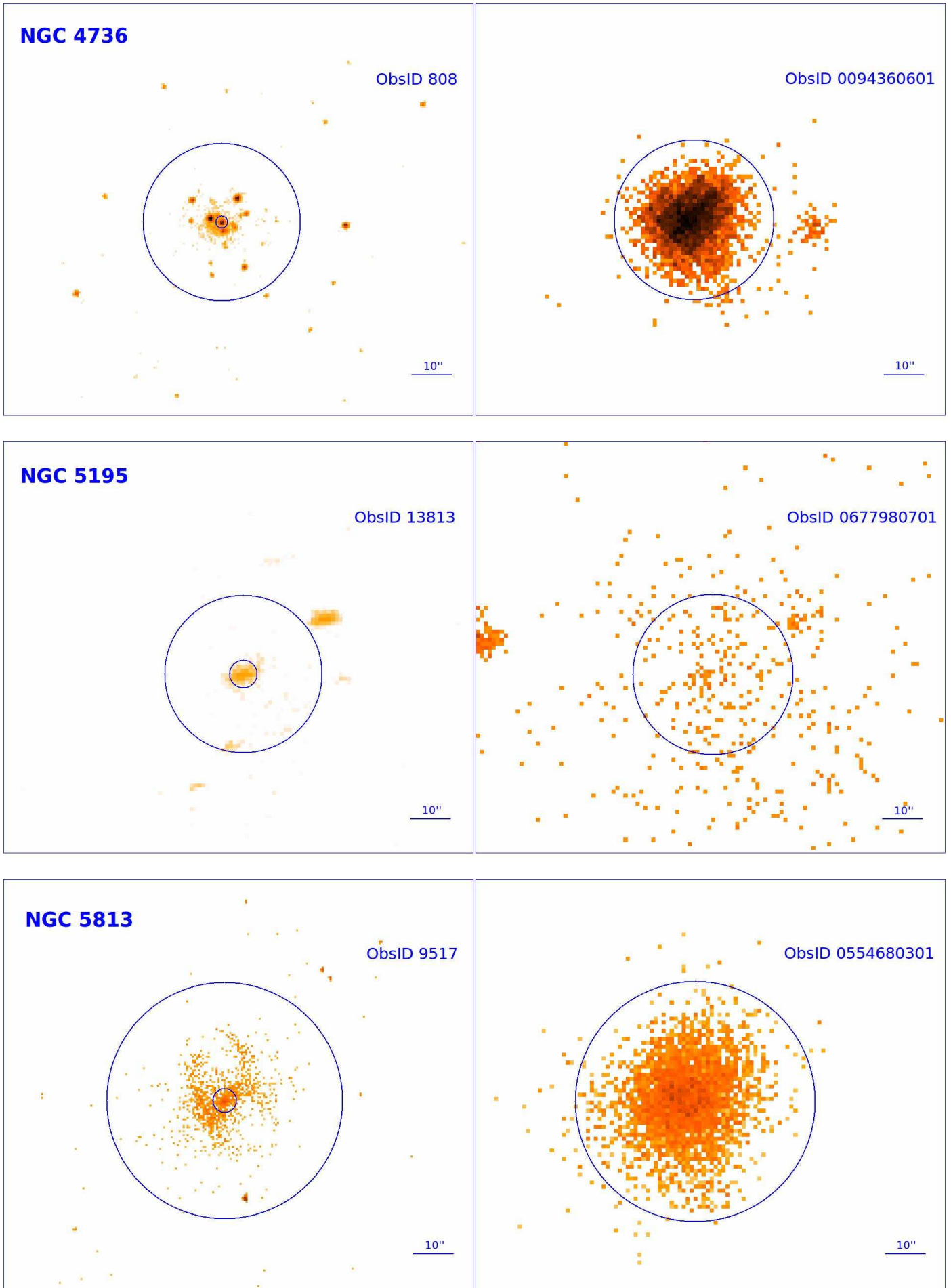
In this appendix we present the images from *Chandra* (left) and *XMM*–Newton (right) that were used to compare the spectra from these two instruments in the 0.5–10 keV band. Big circles represent *XMM*–Newton apertures. Small circles in the figures to the left represent the nuclear extraction aperture used with *Chandra* observations (see Table A.1). In all cases, the gray levels extend from twice the value of the background dispersion to the maximum value at the center of each galaxy.

Fig. C.1: Images for *Chandra* data (left) and *XMM-Newton* data (right) for the sources in the 0.5-10 keV band. Big circles represent *XMM-Newton* datas apertures. Small circles in the figures to the left represent the nuclear extraction aperture used with *Chandra* observations (see Table A.1).









Appendix D: Light curves

In this appendix the plots corresponding to the light curves are provided. Three plots per observation are presented, corresponding to soft (left), hard (middle), and total (right) energy bands. Each light curve has a minimum of 30 ksec (i.e., 8 hours) exposure time, whereas long light curves are divided in segments of 40 ksec (i.e., 11 hours). Each segment is enumerated in the title of the light curve. Count rates versus time continuous are represented. The solid line represent the mean value and dashed lines $\pm 1\sigma$ from the average.

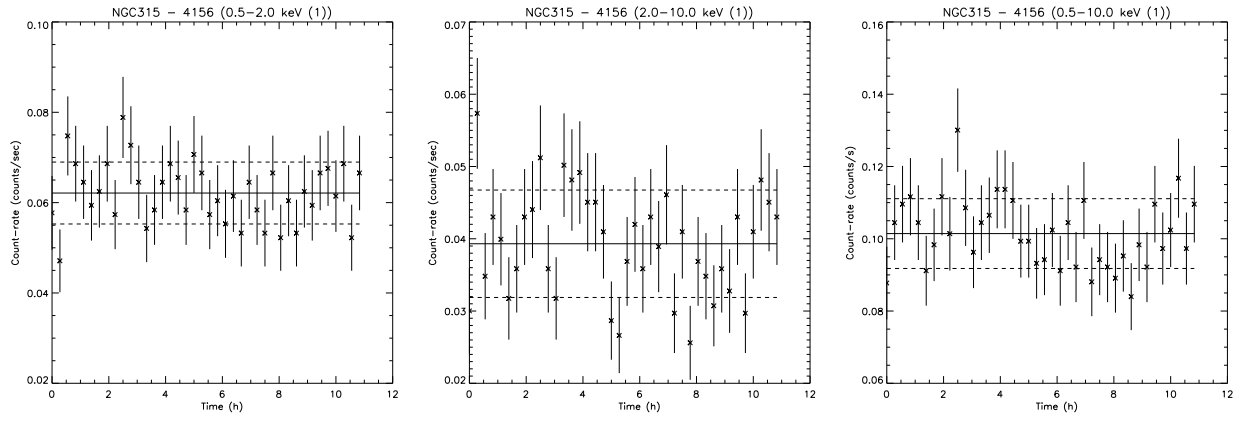


Fig. D.1: Light curves of NGC 315 from *Chandra* data.

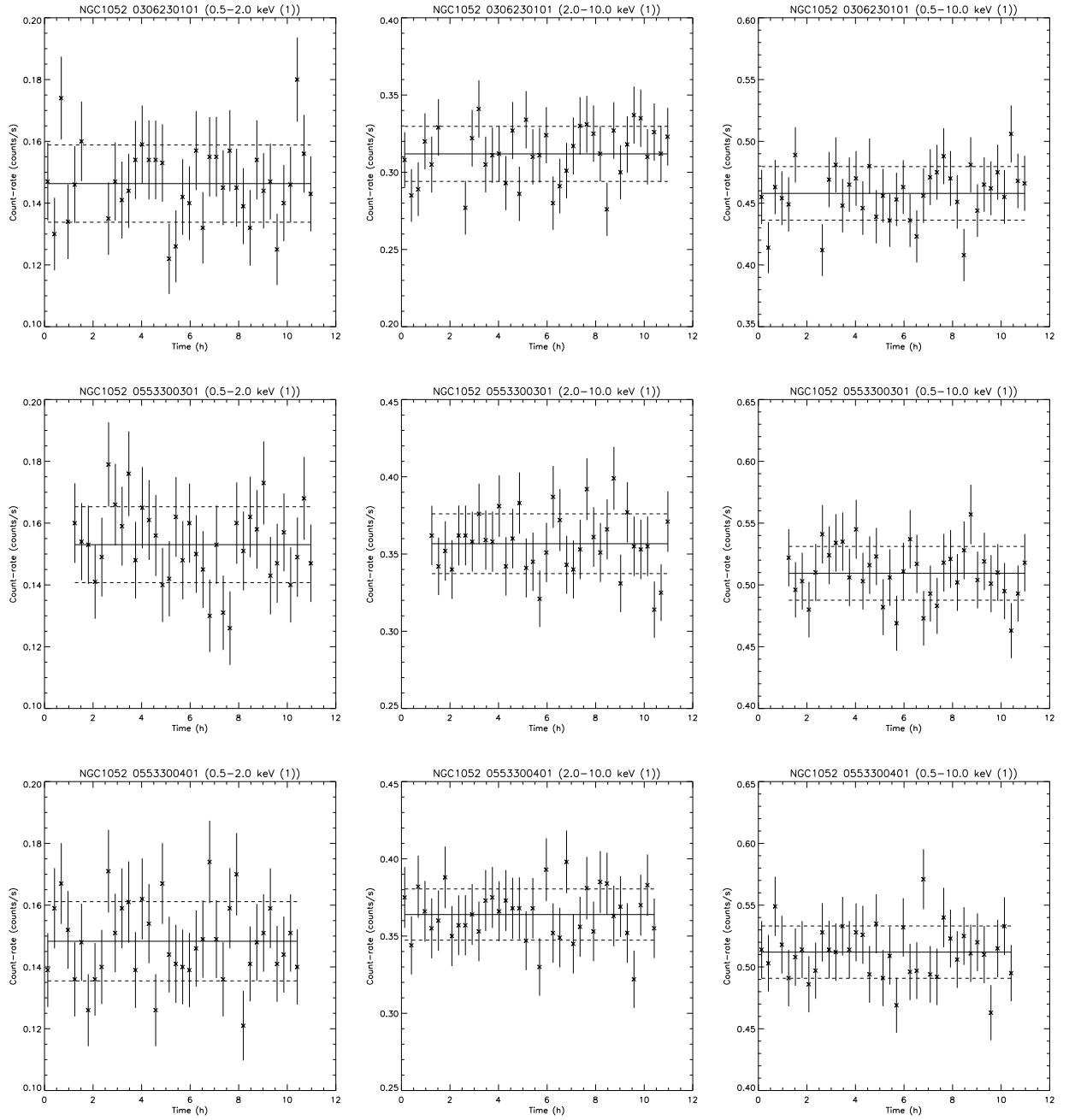


Fig. D.2: Light curves of NGC 1052 from *XMM*–*Newton* data.

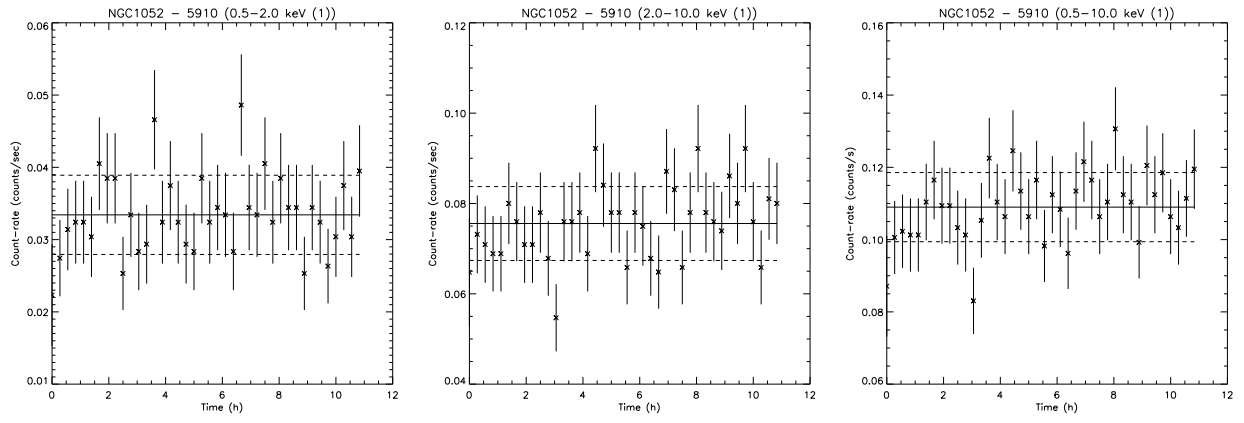


Fig. D.3: Light curves of NGC 1052 from *Chandra* data.

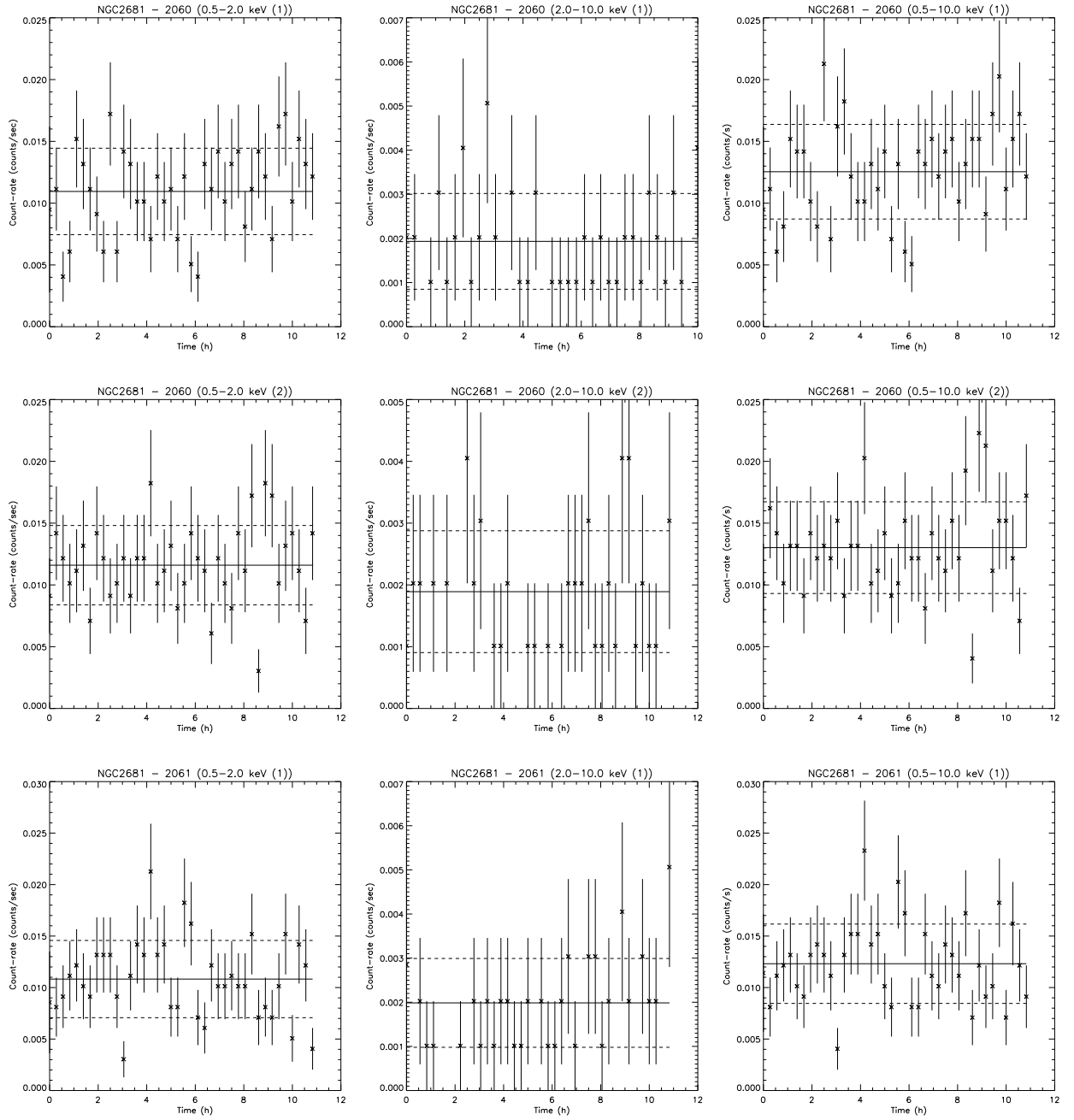


Fig. D.4: Light curves of NGC 2681 from *Chandra* data. Note that ObsID. 2060 is divided in two segments.

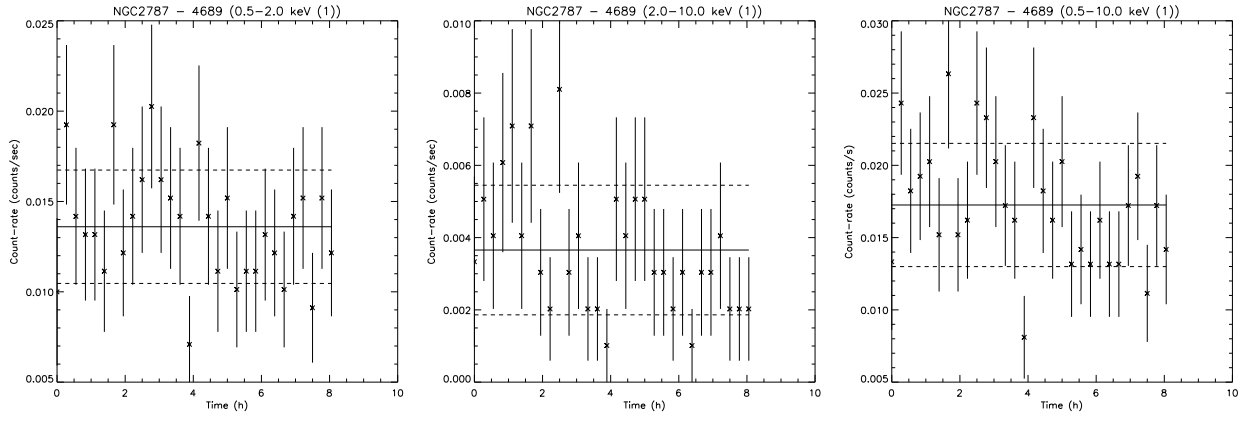


Fig. D.5: Light curves of NGC 2787 from *Chandra* data.

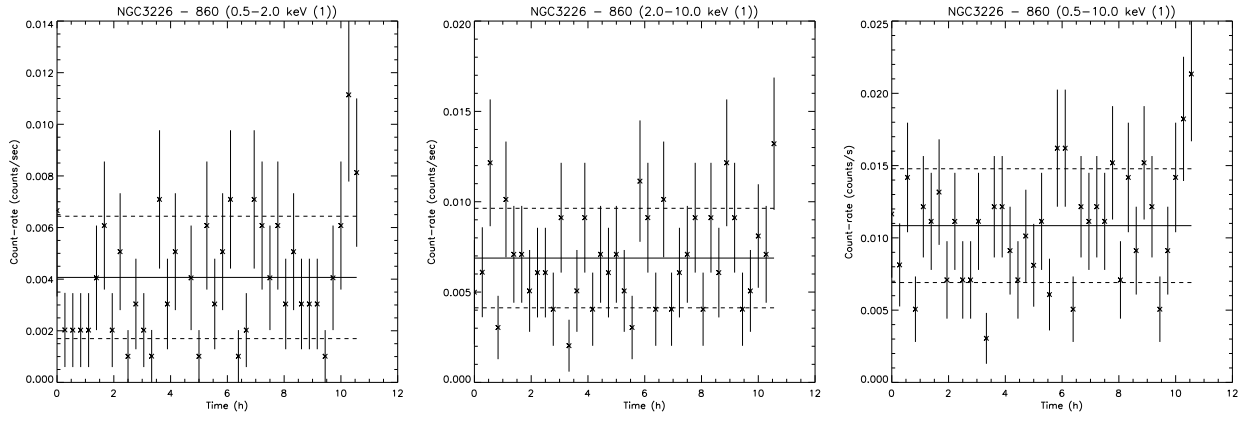


Fig. D.6: Light curves of NGC 3226 from *Chandra* data.

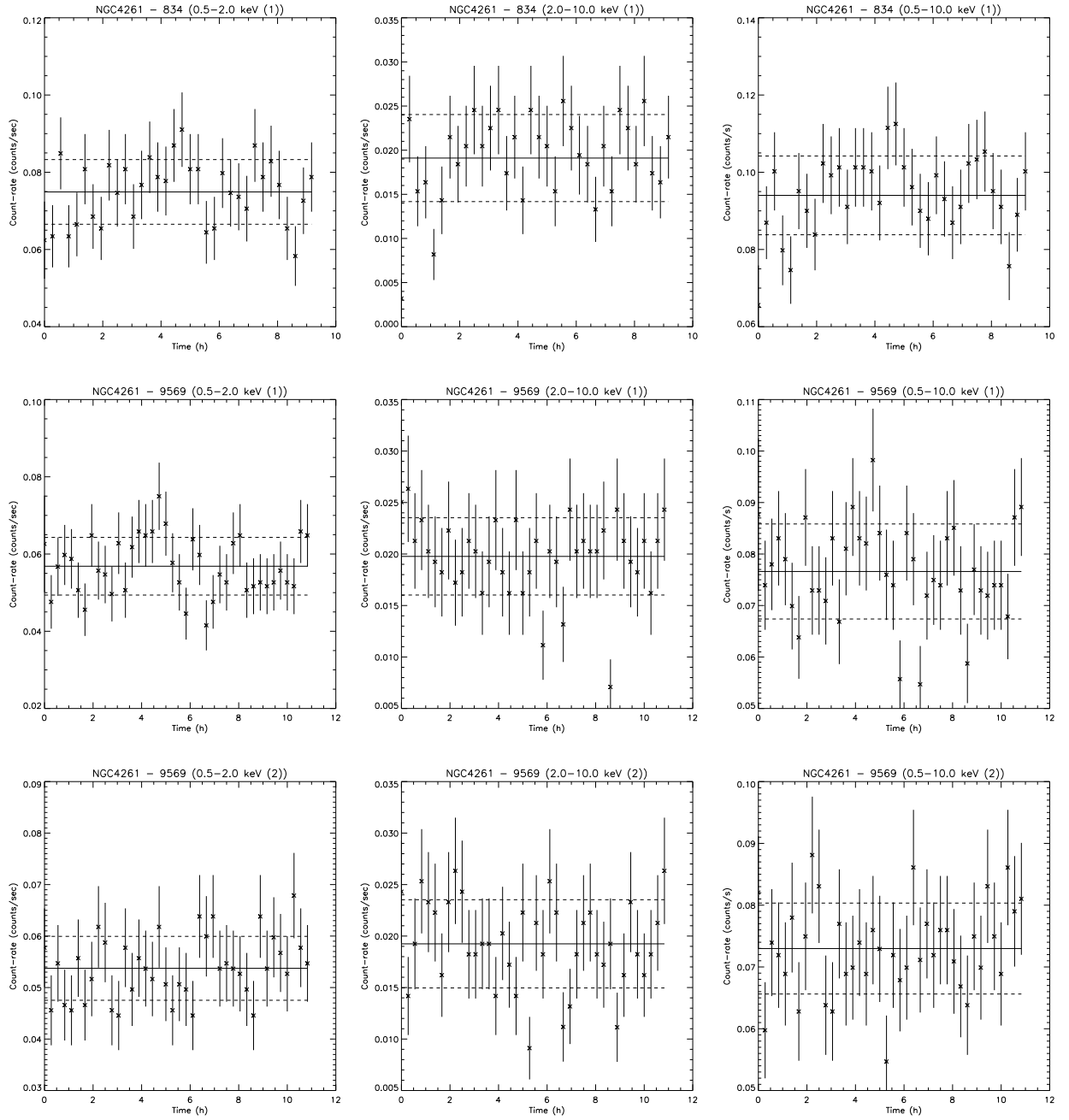


Fig. D.7: Light curves of NGC 4261 from *Chandra* data. Note that ObsID. 9569 is divided in two segments.

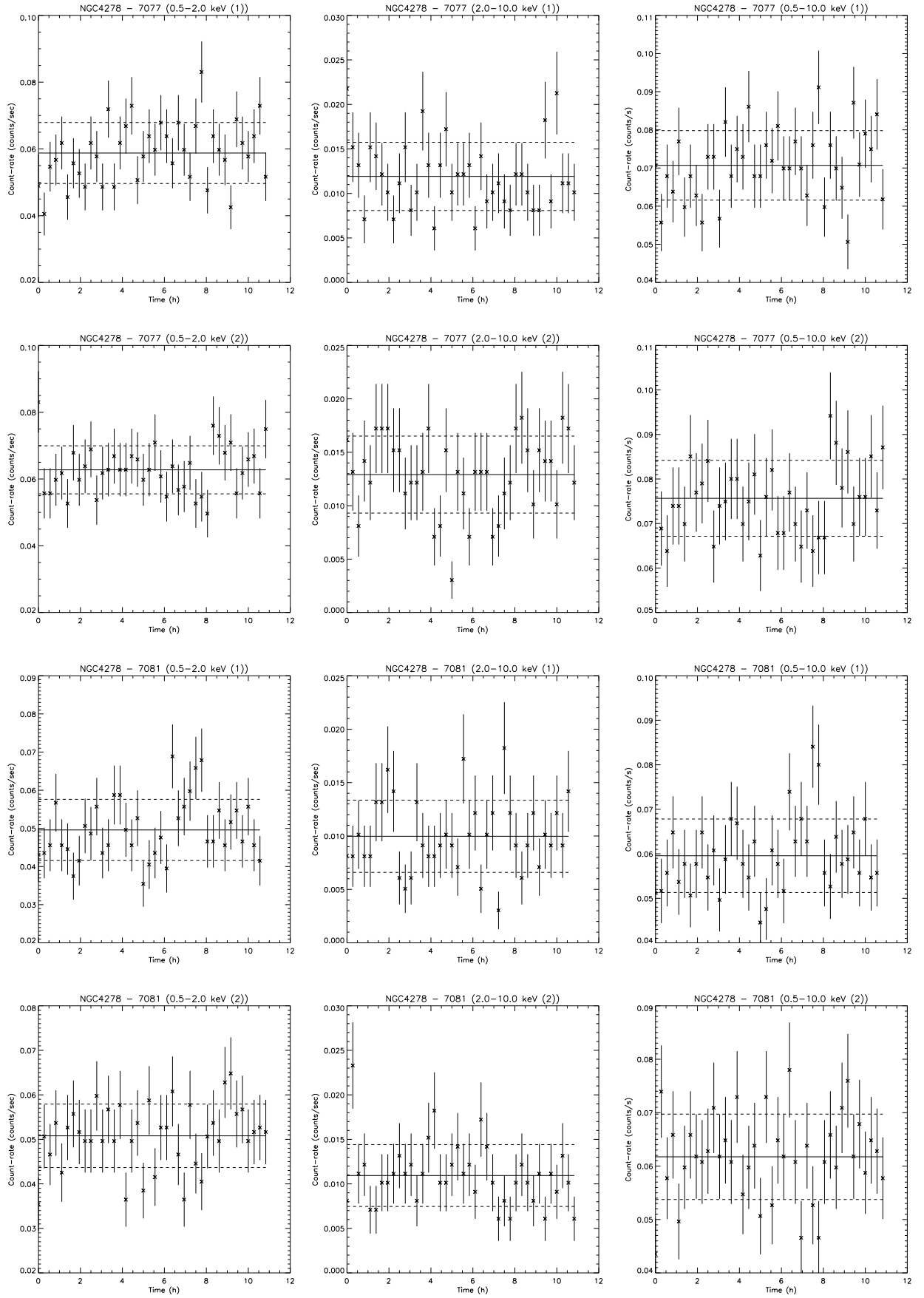


Fig. D.8: Light curves of NGC 4278 from *Chandra* data. Note that ObsID. 7077 and 7081 are divided in two segments.

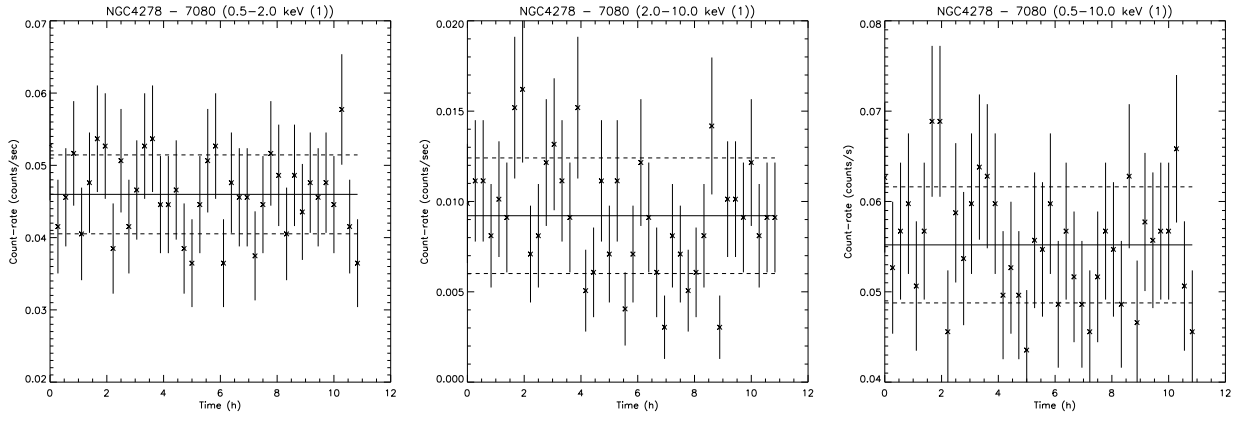


Fig. D.8: (Cont.)

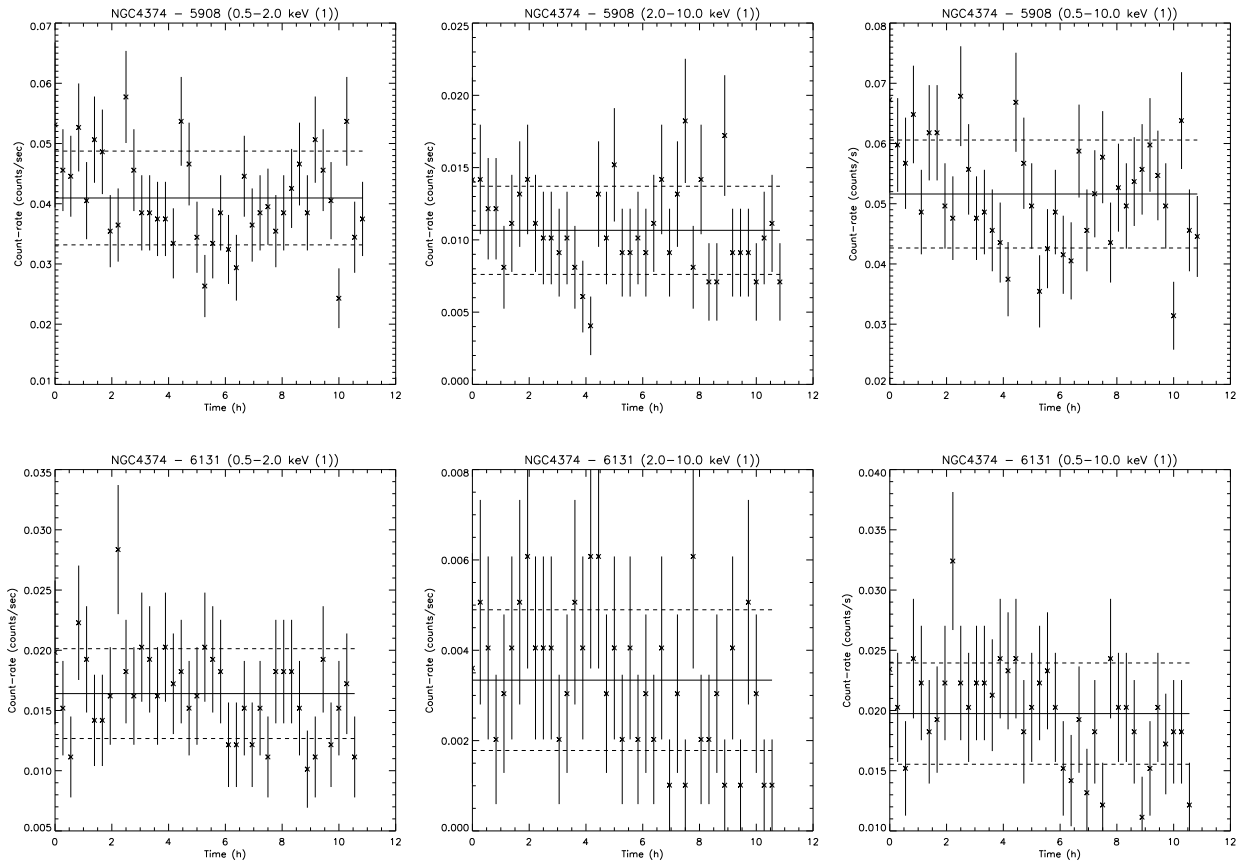


Fig. D.9: Light curves of NGC 4374 from *Chandra* data.

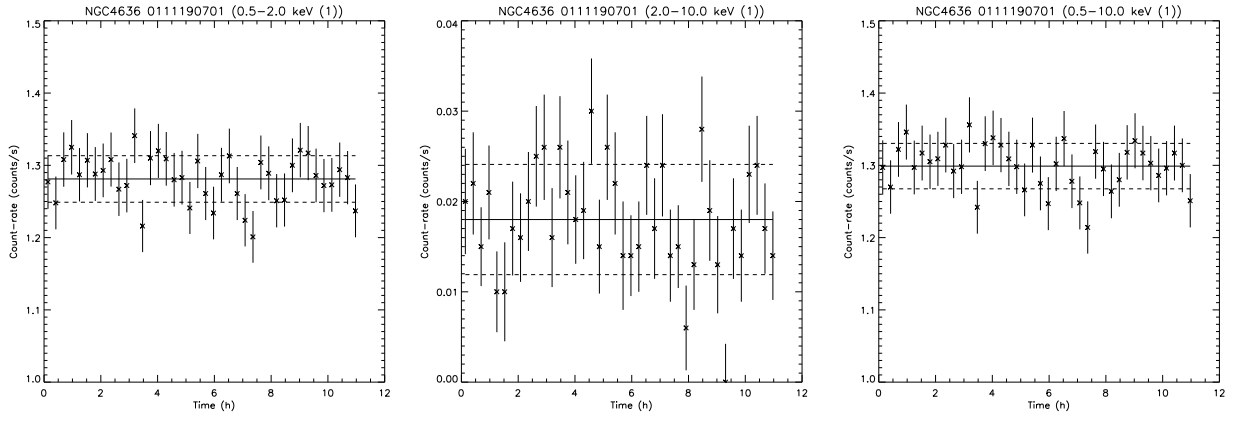


Fig. D.10: Light curves of NGC 4636 from *XMM*–*Newton* data.

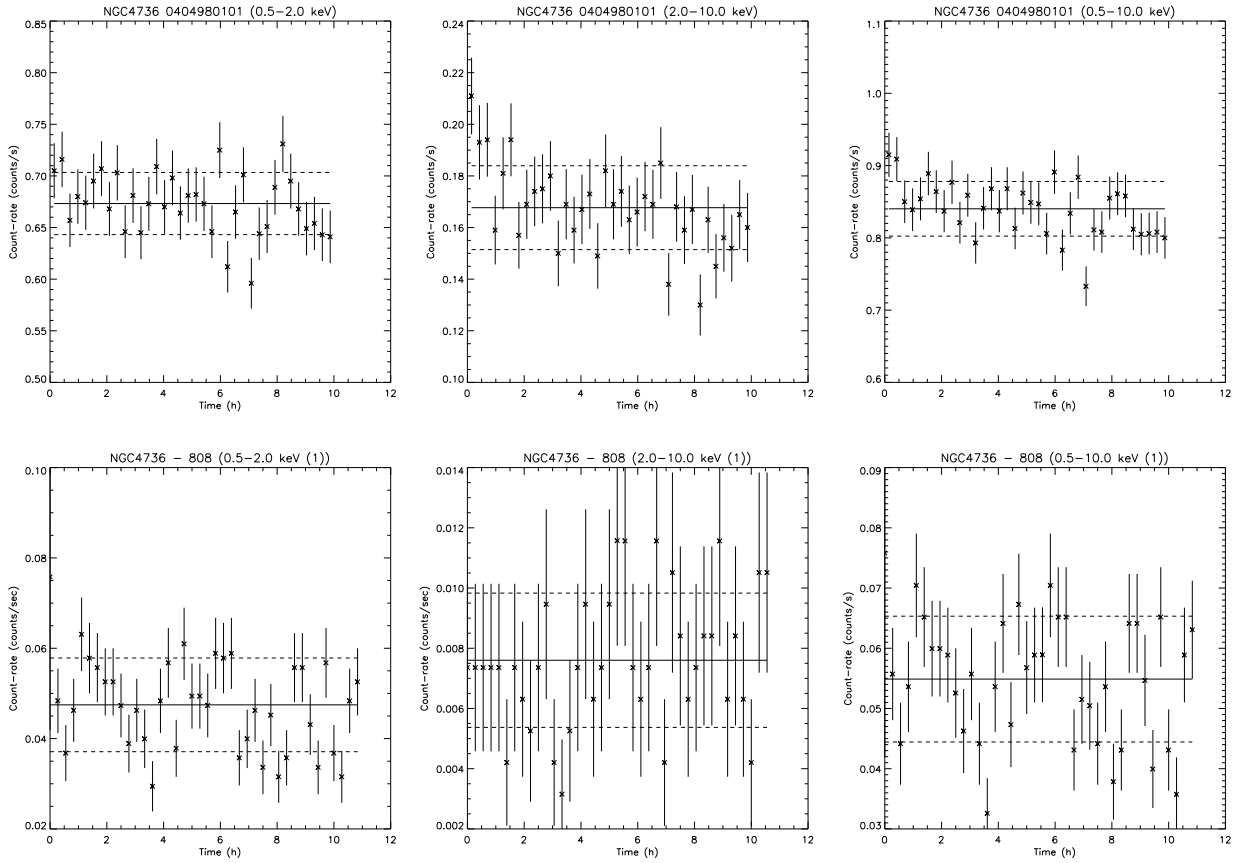


Fig. D.11: Light curves of NGC 4736 from *XMM*–*Newton* (up) and *Chandra* (down) data.

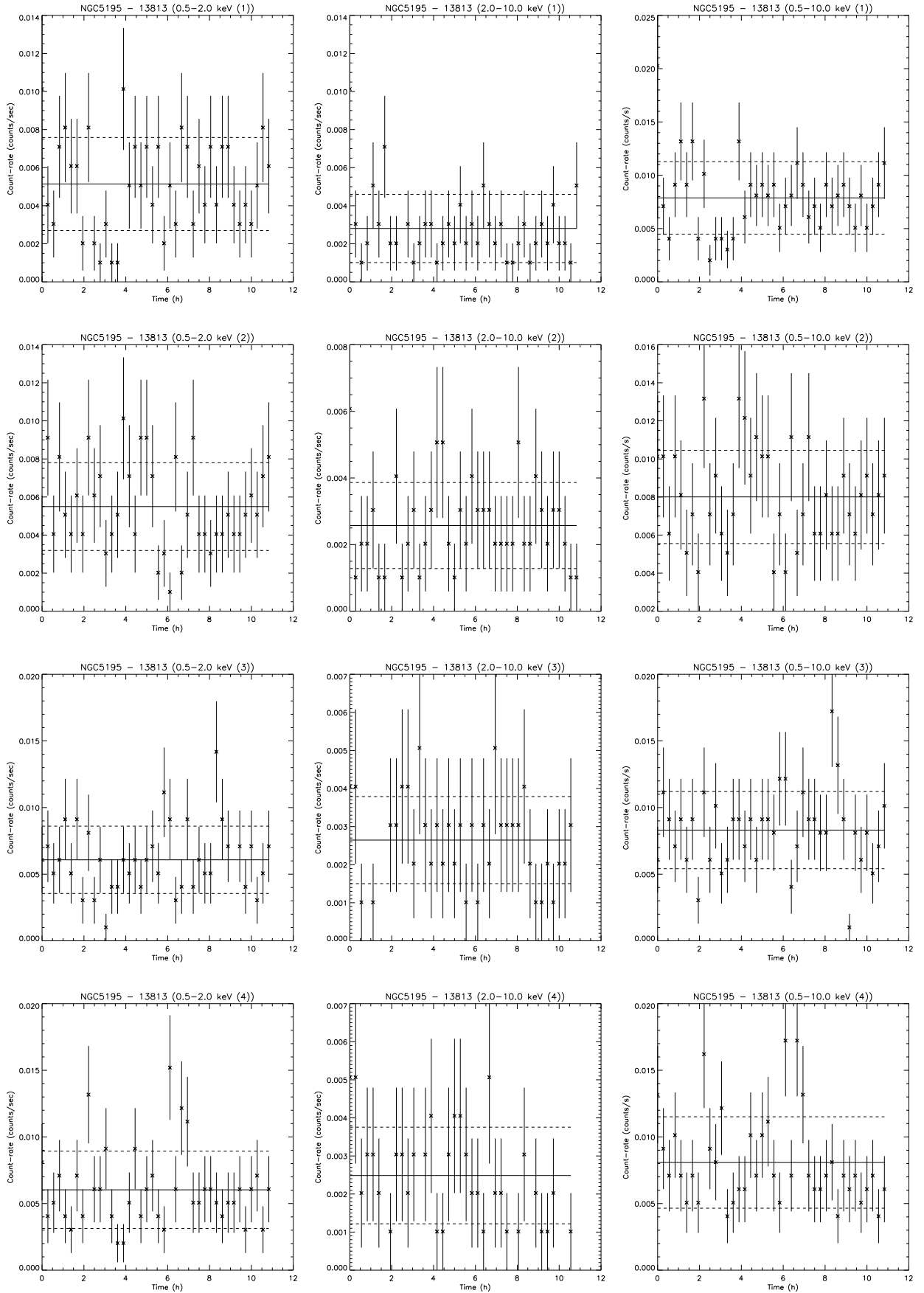


Fig. D.12: Light curves of NGC 5195 from *Chandra* data. Note that ObsID. 13813 is divided in four segments and ObsID. 13812 in three segments.

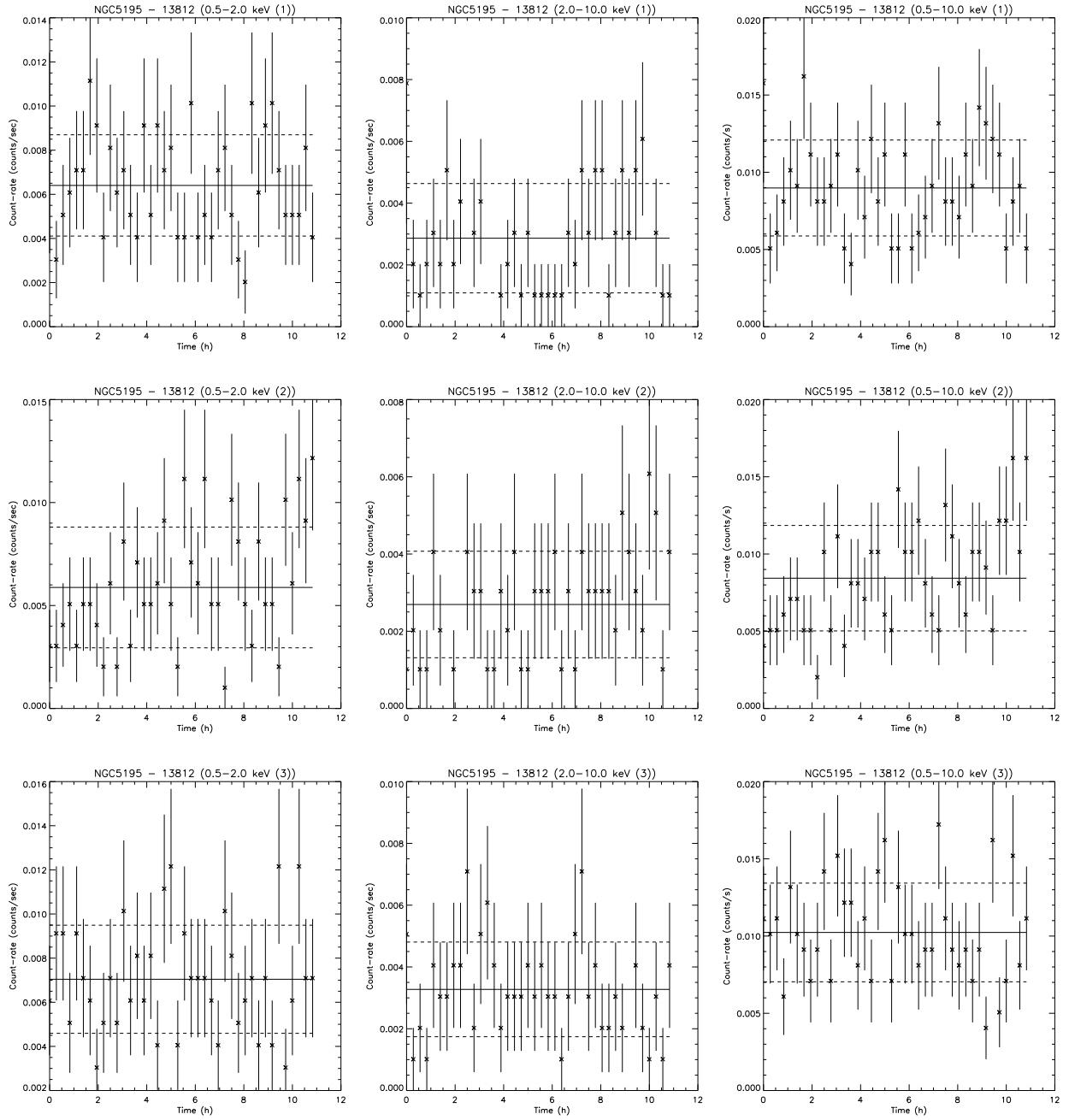


Fig. D.12: (Cont.)

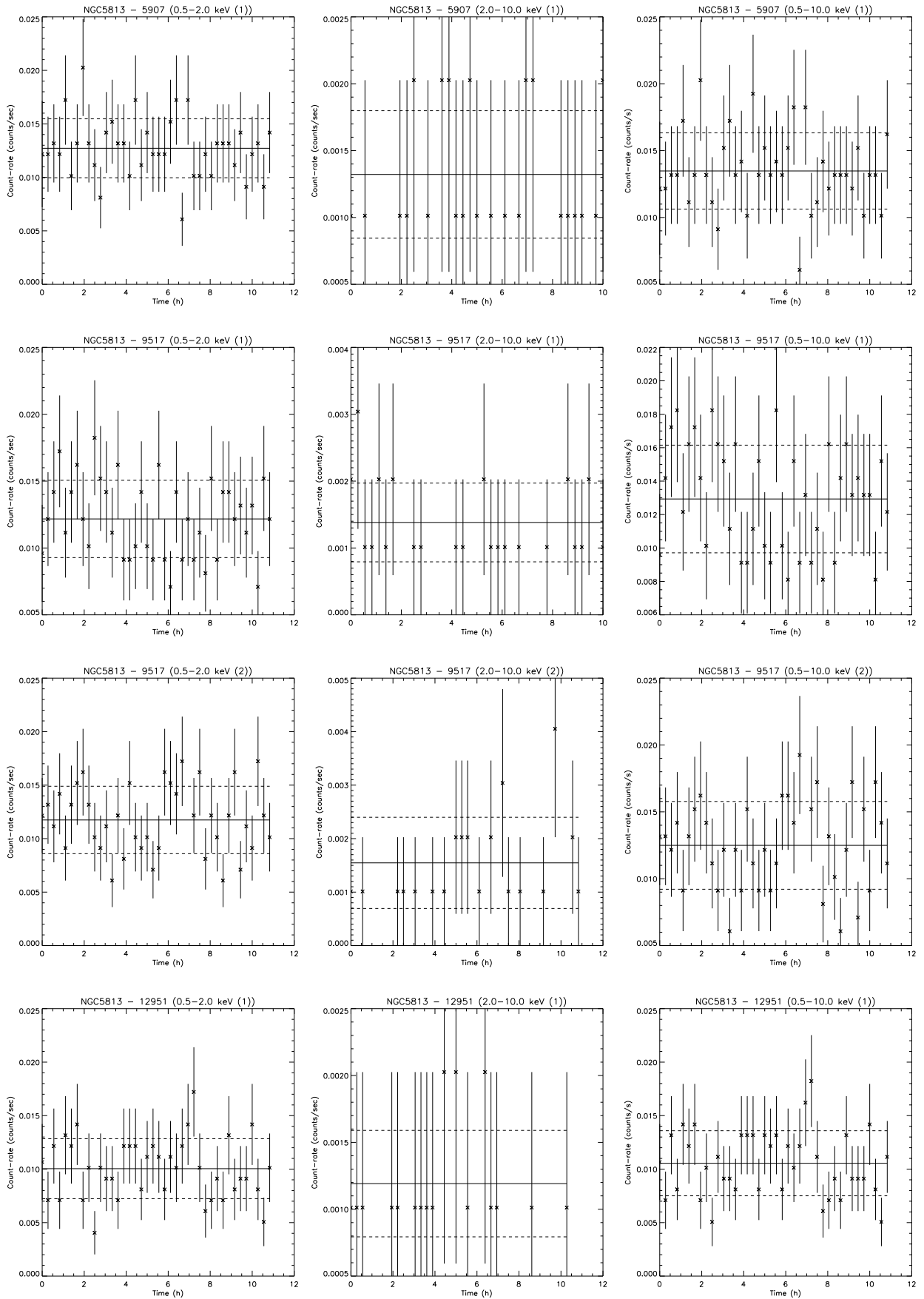


Fig. D.13: Light curves of NGC 5813 from *Chandra* data. Note that ObsID. 9517 and 13253 are divided in two segments

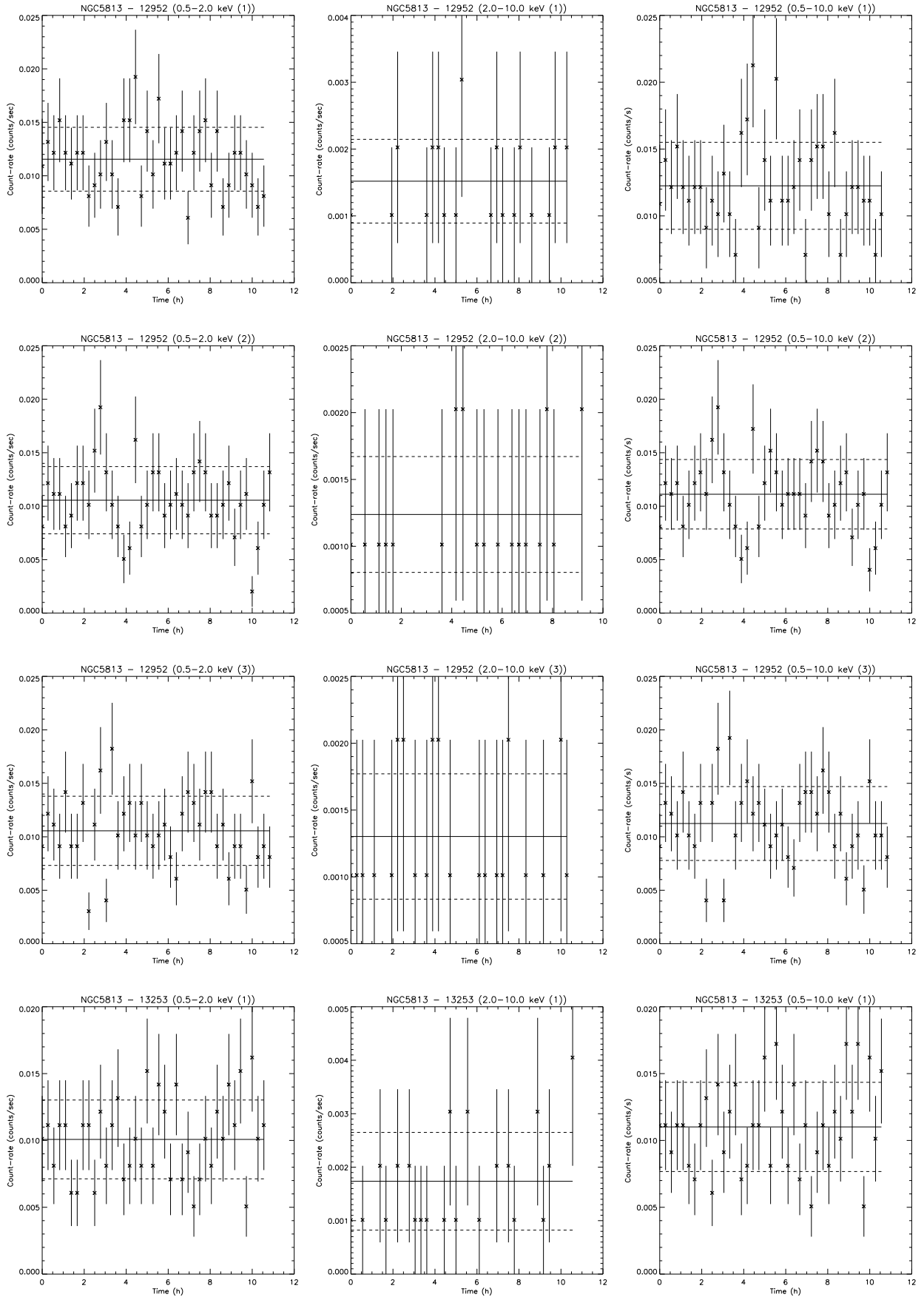


Fig. D.13: (Cont.)

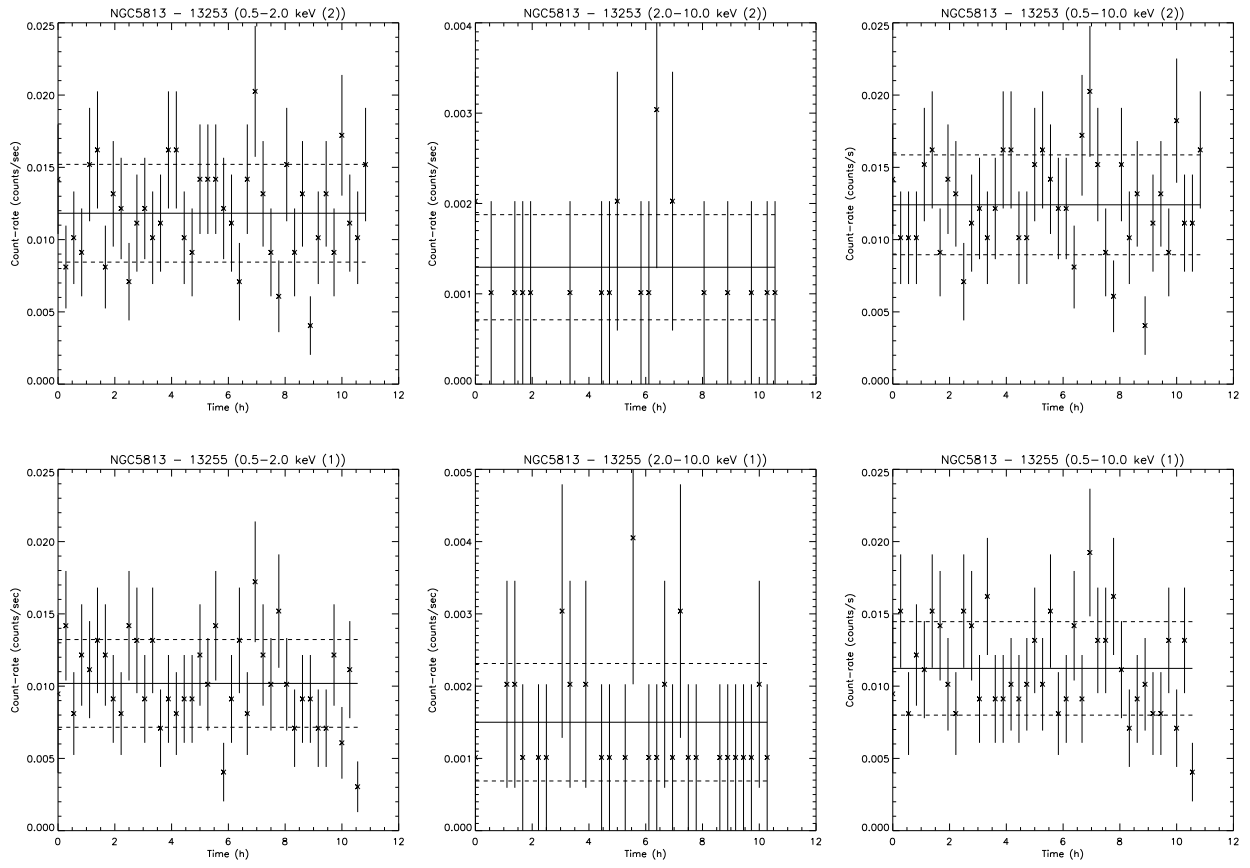


Fig. D.13: (Cont.)